Ing. DAN DRAGOMIR-DĂESCU

APLICAȚII ALE SENSIBILITĂȚII SISTEMELOR DINAMICE.
Analiza dinamică a plăcilor compozite și a plăcilor compozite inteligente pentru detectarea defectelor structurale.

TEZĂ DE DOCTORAT

CONDUCĂTOR ȘTIINȘIFIC

Prof. univ. dr. ing. BRÎNDEU LIVIU

Membru corespondent al Academiei de Științe Tehnice din România

2001

UNIVERSITY "POLITEHNICA" OF TIMIŞOARA
FACULTATY OF MECHANICS
DEPARTMENT OF MECHANICS AND VIBRATION

Eng. DAN DRAGOMIR-DĂESCU

APPLICATION OF DYNAMICAL SYSTEM SENSITIVITY.
Dynamical Analysis of Composite Plates and Smart Composite Plates
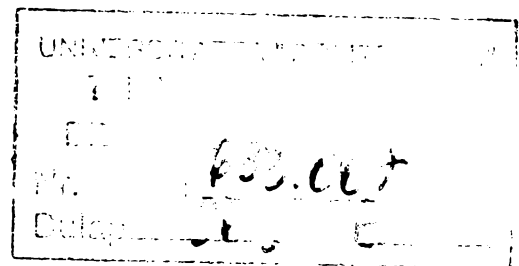for Structural Damage Detection.

DOCTORAL THESIS

SCIENTIFIC ADVISOR

Prof. univ. dr. ing. BRÎNDEU LIVIU
Fellow member of
Romanian Technical Science Academy

2001

ABSTRACT

In designing with composites, it is important to take into consideration imperfections such as delaminations. The presence of delaminations in a composite structure can cause degradation in the structure performance. The focus of the present work is on modeling and analysis of composite and smart composite plates with delaminations. Adaptive composite structures are capable to actively respond to environment changes. Piezoelectric actuation is the most used concept in adaptive structures due to dynamic control capabilities over a large range of frequencies. Essential to the implementation of these smart structures with defects are accurate and efficient modeling techniques. Identification of damage in a composite based structure is also important. This thesis addresses each of these important topics.

A refined higher order theory model is used to analyze the dynamic response of delaminated composite and smart composite plates. Actuators are used to control the plate shape. The theory accurately captures the transverse shear deformation through the thickness of the composite laminate while satisfying stress free boundary conditions on the free surfaces. The theory is extended to incorporate the presence of delaminations. Continuity conditions are imposed on delamination lateral boundary. The model is implemented using the finite element method utilizing an induced strain approach for computational efficiency. This allows general laminate geometries and boundary conditions to be analyzed. Specifically, the effect of delaminations on the dynamic behavior of the composite is studied.

Dynamic results using the higher order theory are correlated with available experimental data. Comparisons, including delaminations, are also made with a general purpose finite element code. Agreement is very good. Additional results demonstrate the utility of the developed theory to study delaminated composites with or without piezoelectric actuation.

Several damage index criteria are used to characterize the damage in composite and smart composite plates. Published damage index criteria are analyzed and modified in the context of the present theory. A new strain based damage index is defined. Robustness of each index is verified in the presence of noise. The results demonstrate that the new index is the most reliable and robust in detecting delaminations.

Respectfully dedicated to the

memory of

my beloved father

Mihai Dragomir

ACKNOWLEDGMENTS

I would like to thank my advisor committee members Prof. Dr. Liviu Brindeu and Prof. Dr. Titus Cioara, for guidance and support throughout the completion of this thesis. I am indebted to my friend Dr. Adrian G. Radu for his support.

Finally I wish to thank Dr. Aditi Chattopadhyay and Dr. Brian Sanders for supporting part of this work.

TABLE OF CONTENTS

BUPT

LIST OF TABLES

x

LIST OF FIGURES

xi

BUPT

1. Introduction

1.1 Structural Modeling

Smart composite materials offer the potential for designing structures which are both light in weight and possess adaptive control capabilities for shape correction and vibration control. In designing with composites, it is important to take into consideration imperfections, such as delamination, that are often pre-existing or are generated by external impact forces during the service life. The existence of delamination can significantly alter the dynamic response of smart composite structures (Chattopadhyay and Seeley, 1997).

Several mathematical models have been reported in the literature for the analysis of beams and plates with piezoelectric sensing/actuation. The classical theory-based approach was introduced by Crawley and Anderson (1989) to investigate such problems with thin beams. This was followed by the first order Mindlin type analyses (Chandrashekara and Agarwal, 1993) and the expensive layer-wise theories (Robbins and Reddy, 1993). A hybrid theory has also been reported by Mitchell and Reddy (1995).

It is well known that refined higher order theories are capable of capturing the transverse shear deformation through the thickness quite accurately (Chattopadhyay and Gu, 1994). These theories are applicable for laminates of thicker construction and have been shown to be useful in modeling smart composite laminates (Chattopadhyay and Seeley, 1997). Finite element based solution procedures are practical since real

geometry and boundary conditions can be investigated (Chandrashekara and Agarwal, 1993, Seeley and Chattopadhyay, 1996).

A significant amount of research has also been performed in modeling delamination in composites. Although three dimensional approaches (Yang and He, 1994) are more accurate than two dimensional theories (Pavier and Clark, 1996), their implementation can be very expensive for practical applications. The layer-wise approach introduced by Barbero and Reddy (1991) is an alternative since it is capable of modeling displacement discontinuities. However, the computational effort increases with the number of plies. A refined higher order theory developed by Chattopadhyay and Gu (1994), has been shown to be both accurate and efficient in modeling delamination in composite plates and shells of moderately thick construction. This theory has also been shown to agree well with both elasticity solutions (Chattopadhyay and Gu, 1996) and experimental results (Gu and Chattopadhyay, 1996).

1.2   Delamination detection

Preliminary research has also been conducted on the use of smart materials in detecting pre-existing delaminations by Keilers and Chang (1995). However, the mathematical model used in this work is simply classical theory based approach, which exclude the transverse shear effects. As much as 50% deviation in structural response has been reported in thick constructions (Chattopadhyay and Gu, 1994, Barbero and Redy, 1991). Recently, Chattopadhyay and Seeley (1998) introduced the higher order

theory in the analysis of adaptive composite plates in the presence of debonding between the laminate and the actuator. It was shown that the presence of debonding significantly alters the dynamic response.

The presence of delaminations in a composite structure can cause significant degradation in the structural performance. Many techniques have been developed to locate defects in such structures and this work considers only those based on vibration methods. Cawley and Adams (1980) and Williams et all. (1997) used the changes in natural frequencies of a structure to quantify damage. Lew (1997) presented a damage detection technique based on transfer function parameter changes. Keilers and Chang (1995) proposed an experimental delamination detection procedure using built in piezoelectrics. An approach based on mode shapes was first introduced by Pandey et al. in 1991. While noting that the mode shapes alone or in combination with changes in natural frequencies are not sufficient to detect the position and size of defects in various structures, they proposed the use of curvature mode shapes in detecting damage in a beam. The curvature is obtained from mode shapes using Laplace's finite difference equation. It was shown that the absolute difference in the curvature mode shapes between the healthy and the damaged beams is a better indicator of damage location compared to the absolute difference in the displacement mode shapes.

Ratcliffe and Bagaria (1998) improved the above technique using a gapped smoothing technique. They observed that Laplace's equation enhances irregularities such as measurement noise and proposed that the curvature should be locally smoothed. In their approach, for a composite beam with a through the width delamination, a third order polynomial was used to locally describe the curvature. This procedure uses the

assumption that the damage is strictly located in a very small zone, considering the damage discrete rather than continuous.

The objective of the current research is to develop a mathematical model for the analysis of delaminated smart composite laminates using a refined higher order theory. The theory is implemented using the finite element method. The model, also carefully accounts for the distributed nature of delaminations and actuators in the primary structure. Since actuators are modeled, the relationship between the applied electric field and the strain is based on an induced strain approach.

Four damage index criteria are used in an attempt to characterize delaminated composite and smart composite plates. Two published criteria, MAC and COMAC indices (Harris, 1996), are modified in the context of the present theory. The new defined indices, MSAC and COMSAC are computed in the present work in terms of strain rather than in terms of modal vectors. A third damage index is developed by modifying the existing gapped smoothing technique index introduced by Ratcliffe and Bagaria (1998). In the case when investigating plates, it is easier to measure strains than bidimensional curvature. Therefore, the modified index is also computed using strain distribution. Finally, a new index is defined. The inplane modal strains of the delaminated structure are compared with those of a similar healthy structure. This new index is expected to be more reliable and robust in locating delaminations in composite and smart composite plates

2. Mathematical Modeling

2.1 Fundamental Concepts in Laminate Theory

2.1.1 Constitutive Equations

For an orthotropic material in the local system of coordinates the constitutive equations can be written as

$$\begin{Bmatrix} \sigma_1 \\ \sigma_2 \\ \sigma_3 \\ \sigma_4 \\ \sigma_5 \\ \sigma_6 \end{Bmatrix} = \begin{bmatrix} Q_{11} & Q_{12} & Q_{13} & 0 & 0 & 0 \\ Q_{12} & Q_{22} & Q_{23} & 0 & 0 & 0 \\ Q_{13} & Q_{23} & Q_{33} & 0 & 0 & 0 \\ 0 & 0 & 0 & 2Q_{44} & 0 & 0 \\ 0 & 0 & 0 & 0 & 2Q_{55} & 0 \\ 0 & 0 & 0 & 0 & 0 & 2Q_{66} \end{bmatrix} \left(\begin{Bmatrix} \varepsilon_1 \\ \varepsilon_2 \\ \varepsilon_3 \\ \varepsilon_4 \\ \varepsilon_5 \\ \varepsilon_6 \end{Bmatrix} - \begin{Bmatrix} \Lambda_1 \\ \Lambda_2 \\ \Lambda_3 \\ 0 \\ 0 \\ 0 \end{Bmatrix} \right) \qquad (2.1.1)$$

where σ_i and ε_i (i=1,2,...,6) are the stresses and strains, respectively, (Vinson and Sierakowski, 1987) and Λ_i (i=1,2,3) are the induced strains due to piezoelectric actuation.

The constitutive equations, in the structural frame, can be expressed as follows

$$\begin{Bmatrix} \sigma_x \\ \sigma_y \\ \sigma_z \\ \sigma_{yz} \\ \sigma_{xz} \\ \sigma_{xy} \end{Bmatrix} = \overline{\mathbf{Q}} \begin{Bmatrix} \varepsilon_x - \Lambda_x \\ \varepsilon_y - \Lambda_y \\ \varepsilon_z - \Lambda_z \\ \varepsilon_{yz} \\ \varepsilon_{xz} \\ \varepsilon_{xy} - \Lambda_{xy} \end{Bmatrix} \qquad (2.1.2)$$

where the stiffness matrix

$$\overline{\mathbf{Q}} = \begin{bmatrix} \overline{Q}_{11} & \overline{Q}_{12} & \overline{Q}_{13} & 0 & 0 & 2\overline{Q}_{16} \\ \overline{Q}_{12} & \overline{Q}_{22} & \overline{Q}_{23} & 0 & 0 & 2\overline{Q}_{26} \\ \overline{Q}_{13} & \overline{Q}_{23} & \overline{Q}_{33} & 0 & 0 & 2\overline{Q}_{36} \\ 0 & 0 & 0 & 2\overline{Q}_{44} & 2\overline{Q}_{45} & 0 \\ 0 & 0 & 0 & 2\overline{Q}_{45} & 2\overline{Q}_{55} & 0 \\ \overline{Q}_{16} & \overline{Q}_{26} & \overline{Q}_{36} & 0 & 0 & 2\overline{Q}_{66} \end{bmatrix} \tag{2.1.3}$$

is obtained from coordinate transformation (Vinson and Sierakowski, 1987).

Assuming ε_z to be negligible across the thickness of the plate, Eqs. 2.1.2 can be written, for the kth laminae of the plate as follows (Fig. 2.1).

$$\left\{ \begin{matrix} \sigma_x \\ \sigma_y \\ \sigma_{xy} \end{matrix} \right\}_k = \begin{bmatrix} \overline{Q}_{11} & \overline{Q}_{12} & 2\overline{Q}_{16} \\ \overline{Q}_{12} & \overline{Q}_{22} & 2\overline{Q}_{26} \\ \overline{Q}_{16} & \overline{Q}_{26} & 2\overline{Q}_{66} \end{bmatrix}_k \left\{ \begin{matrix} \varepsilon_x - \Lambda_x \\ \varepsilon_y - \Lambda_y \\ \varepsilon_{xy} - \Lambda_{xy} \end{matrix} \right\}_k \tag{2.1.4}$$

$$\left\{ \begin{matrix} \sigma_{yz} \\ \sigma_{xz} \end{matrix} \right\}_k = \begin{bmatrix} 2\overline{Q}_{44} & 2\overline{Q}_{45} \\ 2\overline{Q}_{45} & 2\overline{Q}_{55} \end{bmatrix}_k \left\{ \begin{matrix} \varepsilon_{yz} \\ \varepsilon_{xz} \end{matrix} \right\}_k \tag{2.1.5}$$

The above decomposition is very useful in the solution procedure since it decomposes the problem into two smaller subproblems in terms of stresses and strains.
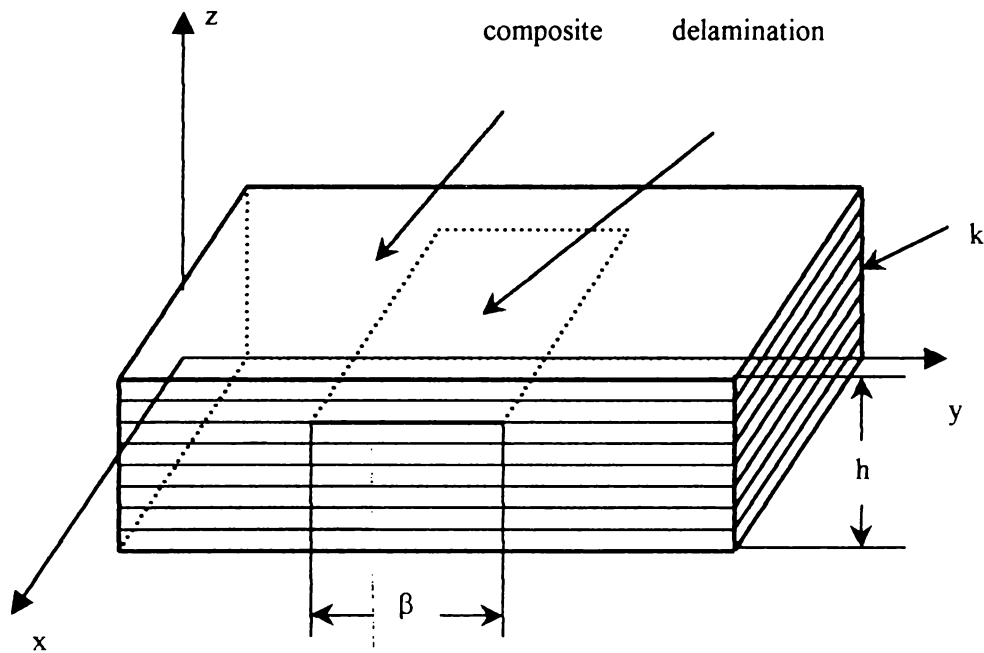
Figure. 2.1.   Composite plate with delamination.

2.1.2   Kinematic Equations

A higher order displacement field is used to model the kinematics of deformation. The inplane displacements (u and v) are assumed to have cubic variations through the laminate thickness and the out of plane deformation (w) is assumed to be independent of thickness.

$$u(x,y,z,t) = u_0(x,y,t) + z\left[-\frac{\partial w_0}{\partial x} + \alpha(x,y,t)\right] + z^2\varphi(x,y,t) + z^3\theta(x,y,t)$$

$$v(x,y,z,t) = v_0(x,y,t) + z\left[-\frac{\partial w_0}{\partial y} + \beta(x,y,t)\right] + z^2\psi(x,y,t) + z^3\eta(x,y,t) \qquad (2.1.6)$$

$$w(x,y,z,t) = w_0(x,y,t)$$

where u_0, v_0 and w_0 are the displacements of an arbitrary point (x,y,0) at the laminate midplane, α and β are additional rotation functions while φ, θ, ψ and η are higher order

functions. In the hypothesis of small deformations, the strain-displacement relations are written as follows.

$$\varepsilon_x = \frac{\partial u}{\partial x}$$

$$\varepsilon_y = \frac{\partial v}{\partial y}$$

$$\varepsilon_z = \frac{\partial w}{\partial z}$$

$$\varepsilon_{yz} = \frac{1}{2}\left(\frac{\partial v}{\partial z} + \frac{\partial w}{\partial y}\right) = \frac{1}{2}\gamma_{yz}$$

$$\varepsilon_{xz} = \frac{1}{2}\left(\frac{\partial u}{\partial z} + \frac{\partial w}{\partial y}\right) = \frac{1}{2}\gamma_{xz}$$

$$\varepsilon_{xy} = \frac{1}{2}\left(\frac{\partial u}{\partial y} + \frac{\partial v}{\partial x}\right) = \frac{1}{2}\gamma_{xy}$$

(2.1.7)

The displacement field defined in Eqs. 2.1.6 does not satisfy the shear stress free boundary conditions. Therefore, it is necessary to impose these conditions as follows

$$\sigma_{yz}(x,y,\pm\frac{h}{2},t) = \sigma_{xz}(x,y,\pm\frac{h}{2},t) = 0$$

(2.1.8)

where h is the thickness of the plate (Fig. 2.1).

For orthotropic laminate, these conditions are equivalent to

$$\varepsilon_{yz}(x,y,\pm\frac{h}{2},t) = \varepsilon_{xz}(x,y,\pm\frac{h}{2},t) = 0$$

(2.1.9)

The displacement field (Eqs. 2.1.15), then reduces to the following form

$$u(x,y,z,t) = u_0(x,y,t) + z\left[-\frac{\partial w_0}{\partial x} + \alpha(x,y,t)\right] - \frac{4z^3}{3h^2}\alpha(x,y,t)$$

$$v(x,y,z,t) = v_0(x,y,t) + z\left[-\frac{\partial w_0}{\partial y} + \beta(x,y,t)\right] - \frac{4z^3}{3h^2}\beta(x,y,t)$$

(2.1.10)

$$w(x,y,z,t) = w_0(x,y,t)$$

where α and β are shear correction functions. It is to be noted that this higher order displacement field uses the same number of unknown functions (u_0, v_0, w_0, α and β) as the first order displacement field while being able to model the strain-displacement relations with quadratic and cubic polynomials as shown below

$$\varepsilon_1 = \varepsilon_1^0 + z\varepsilon_1^1 + z^3\varepsilon_1^3$$
$$\varepsilon_2 = \varepsilon_2^0 + z\varepsilon_2^1 + z^3\varepsilon_2^3$$
$$\varepsilon_4 = \varepsilon_4^0 + z^2\varepsilon_4^2 \qquad\qquad (2.1.11)$$
$$\varepsilon_5 = \varepsilon_5^0 + z^2\varepsilon_5^2$$
$$\varepsilon_6 = \varepsilon_6^0 + z\varepsilon_6^1 + z^3\varepsilon_6^3$$

where the index convention (1=x, 2=y, 3=z, 4=yz, 5=xz and 6=xy) is used for simplicity

and

$$\varepsilon_1^0 = \frac{\partial u_0}{\partial x}, \qquad \varepsilon_1^1 = -\frac{\partial^2 w_0}{\partial x^2} + \frac{\partial \alpha}{\partial x}, \qquad \varepsilon_1^3 = C_1\frac{\partial \alpha}{\partial x}$$

$$\varepsilon_2^0 = \frac{\partial v_0}{\partial y}, \qquad \varepsilon_2^1 = -\frac{\partial^2 w_0}{\partial y^2} + \frac{\partial \beta}{\partial y}, \qquad \varepsilon_2^3 = C_1\frac{\partial \beta}{\partial y}$$

$$\varepsilon_6^0 = \frac{\partial u_0}{\partial y} + \frac{\partial v_0}{\partial x}, \quad \varepsilon_6^1 = -2\frac{\partial^2 w_0}{\partial x\,\partial y} + \frac{\partial \alpha}{\partial y} + \frac{\partial \beta}{\partial x}, \quad \varepsilon_1^3 = C_1\left(\frac{\partial \alpha}{\partial y} + \frac{\partial \beta}{\partial x}\right) \quad (2.1.12)$$

$$\varepsilon_4^0 = \beta(x,y,t), \qquad \varepsilon_4^2 = C_2\,\beta(x,y,t)$$

$$\varepsilon_5^0 = \alpha(x,y,t), \qquad \varepsilon_5^2 = C_2\,\alpha(x,y,t)$$

$$C_1 = -\frac{4}{3h^2}, \qquad C_2 = -\frac{4}{h^2} \qquad\qquad (2.1.13)$$

From the above equations, it must also be noted that both first order and third order displacement fields introduce two additional unknown functions, (α and β) compared to classical laminates plate theory while greatly improve the accuracy. The first order displacement field assumes a constant distribution of shear strain through the thickness resulting in the use of empirical shear correction factors in numerical

implementations. The third order displacement field models a quadratic distribution of shear strain over the thickness of the plate while satisfying the boundary conditions.

2.1.3 Hamilton's Principle

In variational form, Hamilton's principle is expressed as follows

$$\delta\Pi = \int_{t_1}^{t_2}\left(\delta K - \delta U + \delta W\right)dt = 0 \tag{2.1.14}$$

where δK is the variation of kinetic energy, δU is the variation of strain energy and δW is infinitesimal work done by external loads in a virtual displacement compatible with system constraints. The displacement field must be a continuously differentiable function of position and time. The first term in Eq. 2.1.14 can be written as follows.

$$\delta\Pi_K = \int_{t_1}^{t_2}\int_V \rho\,\delta\dot{\overline{\mathbf{u}}}^T\,\dot{\overline{\mathbf{u}}}\,dV\,dt \tag{2.1.15}$$

Switching the order of integration, integrating by parts with respect to time t, and switching back the order of integration, yields the following

$$\partial\Pi_K = -\int_{t_1}^{t_2}\int_V \rho\,\delta\overline{\mathbf{u}}^T\,\ddot{\overline{\mathbf{u}}}\,dV\,dt \tag{2.1.16}$$

where

$$\overline{\mathbf{u}}(x,y,z,t) = \begin{Bmatrix} u(x,y,z,t) \\ v(x,y,z,t) \\ w(x,y,z,t) \end{Bmatrix} \tag{2.1.17}$$

In the above (x,y,z) is the position vector of an arbitrary point in the structure, u, v and w are the actual displacements of the point (x,y,z) in x, y and z directions respectively. Hamilton's principle is rewritten in the following form

$$\delta\Pi = \int_{t_1}^{t_2}\left(\int_V \rho\,\delta\overline{\mathbf{u}}^T\,\ddot{\overline{\mathbf{u}}}\,dV + \int_V \delta\varepsilon^T\,\sigma\,dV - \int_V \delta\overline{\mathbf{u}}^T\,\mathbf{p}(x,y,z,t)dV\right)dt = 0 \qquad (2.1.18)$$

where p is the applied load vector and ρ is the mass density function.

Kinetic Energy

The displacement field can be written in the following simplified form

$$u(x,y,z,t) = u_0^0(x,y,t) + u_0^1(x,y,t)z + u_0^3(x,y,t)z^3$$
$$v(x,y,z,t) = v_0^0(x,y,t) + v_0^1(x,y,t)z + v_0^3(x,y,t)z^3 \qquad (2.1.19)$$
$$w(x,y,z,t) = w_0^0(x,y,t)$$

where

$$u_0^0(x,y,t) = u_0(x,y,t)$$
$$u_0^1(x,y,t) = -\frac{\partial w_0}{\partial x} + \alpha(x,y,t)$$
$$u_0^3(x,y,t) = C_1\alpha(x,y,t)$$
$$v_0^0(x,y,t) = v_0(x,y,t) \qquad (2.1.20)$$
$$v_0^1(x,y,t) = -\frac{\partial w_0}{\partial y} + \beta(x,y,t)$$
$$v_0^3(x,y,t) = C_1\beta(x,y,t)$$
$$w_0^0(x,y,t) = w_0(x,y,t)$$

The quantity C_1 is defined in Eqs. 2.1.13. The variation of the kinetic energy is expressed as follows

$$\delta K = \int_V \rho\,\delta\overline{\mathbf{u}}^T\,\ddot{\overline{\mathbf{u}}}\,dV = \int_A\int_{-\frac{h}{2}}^{\frac{h}{2}}\rho\,\delta\overline{\mathbf{u}}^T\,\ddot{\overline{\mathbf{u}}}\,dz\,dA \qquad (2.1.21)$$

where the volume integral is split into two, one double integral over the area of the plate and a simple integral in z direction.

The inner integral can be expressed as follows

$$J_m = \delta \overline{U}^T J_\rho \ddot{\overline{U}} \tag{2.1.22}$$

where

$$\overline{U} = \left\{ u_0^0 \quad u_0^1 \quad u_0^3 \quad v_0^0 \quad v_0^1 \quad v_0^3 \quad w_0^0 \right\}^T \tag{2.1.23}$$

$$J_\rho = \begin{bmatrix} J_{11} & O_{3x3} & O_{3x1} \\ O_{3x3} & J_{11} & O_{3x1} \\ O_{1x3} & O_{1x3} & J_0 \end{bmatrix} \tag{2.1.24}$$

$$J_{11} = \begin{bmatrix} J_0 & J_1 & J_3 \\ J_1 & J_2 & J_4 \\ J_3 & J_4 & J_6 \end{bmatrix} \tag{2.1.25}$$

and

$$J_k = \int_{-\frac{h}{2}}^{\frac{h}{2}} \rho z^k \, dz = \frac{1}{k+1} \sum_{r=1}^{n_l} \rho(r)(h_{r+1}^{k+1} - h_r^{k+1}) \tag{2.1.26}$$

In Eq. 2.1.26, h_r, ($r=1,\ldots,n_l$) are the z coordinates of all laminae interfaces in the plate, n_l is the number of laminae and $\rho(r)$, ($r=1,\ldots n_l$) is the mass density distribution over the thickness of the plate, $k=0,1,2,3,4,6$. Using the above notations (Eqs. 2.1.22-26) the variation of kinetic energy can be expressed as follows.

$$\delta K = \int_A J_m \, dA = \int_A \delta \overline{U}^T J_\rho \ddot{\overline{U}} \, dA \tag{2.1.27}$$

Equation 2.1.27 is used in the Finite Element implementation to derive the element mass matrix.

Strain Energy

The variation of strain energy, neglecting the strain in z direction, can be written as

$$\delta U = \int_V \delta \varepsilon_{ij} \, \sigma_{ij} \, dV = \int_V \left(\delta \varepsilon_1 \sigma_1 + \delta \varepsilon_2 \sigma_2 + \delta \varepsilon_6 \sigma_6 + \delta \varepsilon_4 \sigma_4 + \delta \varepsilon_5 \sigma_5 \right) dV \tag{2.1.28}$$

For convenience, the above integral is decomposed into two parts.

$$\delta U_b = \int_V \left(\delta \varepsilon_1 \sigma_1 + \delta \varepsilon_2 \sigma_2 + \delta \varepsilon_6 \sigma_6 \right) dV \tag{2.1.29}$$

$$\delta U_s = \int_V \left(\delta \varepsilon_4 \sigma_4 + \delta \varepsilon_5 \sigma_5 \right) dV \tag{2.1.30}$$

The stress-strain relations, as expressed in Eqs.2.1.4-5, are considered in the case where induced strain is produced due to inverse piezoelectric effect. In this case, the induced inplane shear strain vanishes. The following form is obtained for the integral in Eq. 2.1.29.

$$
\begin{aligned}
\delta U_b = \int_V (\, & \delta \varepsilon_1 \overline{Q}_{11} \varepsilon_1 + \delta \varepsilon_1 \overline{Q}_{12} \varepsilon_2 + \delta \varepsilon_1 \overline{Q}_{16} \varepsilon_6 \\
& + \delta \varepsilon_2 \overline{Q}_{12} \varepsilon_1 + \delta \varepsilon_2 \overline{Q}_{22} \varepsilon_2 + \delta \varepsilon_2 \overline{Q}_{26} \varepsilon_6 \\
& + \delta \varepsilon_6 \overline{Q}_{16} \varepsilon_1 + \delta \varepsilon_6 \overline{Q}_{26} \varepsilon_2 + \delta \varepsilon_6 \overline{Q}_{16} \varepsilon_6) \, dV \\
- \int_V (\, & \delta \varepsilon_1 \overline{Q}_{11} \Lambda_1 + \delta \varepsilon_1 \overline{Q}_{12} \Lambda_2 + \delta \varepsilon_2 \overline{Q}_{12} \Lambda_1 \\
& + \delta \varepsilon_2 \overline{Q}_{22} \Lambda_2 \delta \varepsilon_6 \overline{Q}_{16} \Lambda_1 + \delta \varepsilon_6 \overline{Q}_{26} \Lambda_6) \, dV
\end{aligned}
\tag{2.1.31}
$$

The first integral in Eqs.2.1.31 can be decomposed into two parts, one in xy plane and the other in z direction, resulting in the following expression

$$\delta U_b^1 = \int_A I_b \, dA \tag{2.1.32}$$

where

$$
\begin{aligned}
I_b = \int_{-\frac{h}{2}}^{\frac{h}{2}} (\, & \delta \varepsilon_1 \overline{Q}_{11} \varepsilon_1 + \delta \varepsilon_1 \overline{Q}_{12} \varepsilon_2 + \delta \varepsilon_x \overline{Q}_{16} \varepsilon_6 \\
& + \delta \varepsilon_2 \overline{Q}_{12} \varepsilon_1 + \delta \varepsilon_2 \overline{Q}_{22} \varepsilon_2 + \delta \varepsilon_2 \overline{Q}_{26} \varepsilon_6 \\
& + \delta \varepsilon_6 \overline{Q}_{16} \varepsilon_1 + \delta \varepsilon_6 \overline{Q}_{26} \varepsilon_2 + \delta \varepsilon_6 \overline{Q}_{16} \varepsilon_6) \, dz
\end{aligned}
\tag{2.1.33}
$$

The above integral can be expressed in the following vector-matrix form

$$I_b = \delta \overline{\varepsilon}_b^{\ T} \mathbf{I}_{Q_b} \overline{\varepsilon}_b \tag{2.1.34}$$

where

$$\overline{\varepsilon}_b = \left\{\varepsilon_1^0 \quad \varepsilon_1^1 \quad \varepsilon_1^3 \quad \varepsilon_2^0 \quad \varepsilon_2^1 \quad \varepsilon_2^3 \quad \varepsilon_6^0 \quad \varepsilon_6^1 \quad \varepsilon_6^3\right\}^T \tag{2.1.35}$$

$$\mathbf{I}_{Q_b} = \begin{bmatrix} \mathbf{I}_{Q_{11}} & \mathbf{I}_{Q_{12}} & \mathbf{I}_{Q_{16}} \\ \mathbf{I}_{Q_{12}} & \mathbf{I}_{Q_{22}} & \mathbf{I}_{Q_{26}} \\ \mathbf{I}_{Q_{16}} & \mathbf{I}_{Q_{26}} & \mathbf{I}_{Q_{66}} \end{bmatrix} \tag{2.1.36}$$

$$\mathbf{I}_{Q_{ij}} = \begin{bmatrix} I_0^{ij} & I_1^{ij} & I_3^{ij} \\ I_1^{ij} & I_2^{ij} & I_4^{ij} \\ I_3^{ij} & I_4^{ij} & I_6^{ij} \end{bmatrix} \tag{2.1.37}$$

and

$$I_k^{ij} = \int_{-\frac{h}{2}}^{\frac{h}{2}} \overline{Q}_{ij}\, z^k \, dz = \frac{1}{k+1} \sum_{r=1}^{n_l} \overline{Q}_{ij}(r)\left(h_{r+l}^{k+1} - h_r^{k+1}\right) \tag{2.1.38}$$

In Eqs. 2.1.37-38 $\overline{Q}_{ij}(r)$ (i,j= 1,2,6, i<j, k=0,1,2,3,4,6, r=1,...,n_l) is the discrete stiffness distribution across the thickness of the laminate.

The second integral in Eq.2.1.31 yields the piezoelectric force due to piezoelectric actuation and can be expressed as follows

$$\delta U_b^2 = \int_A I_p \, dA \tag{2.1.39}$$

where

$$\begin{aligned} I_p = \int_{-\frac{h}{2}}^{\frac{h}{2}} (&\delta\varepsilon_1 \overline{Q}_{11}\Lambda_1 + \delta\varepsilon_1 \overline{Q}_{12}\Lambda_2 + \delta\varepsilon_2 \overline{Q}_{12}\Lambda_1 \\ &+ \delta\varepsilon_2 \overline{Q}_{22}\Lambda_2 + \delta\varepsilon_6 \overline{Q}_{16}\Lambda_1 + \delta\varepsilon_6 \overline{Q}_{26}\Lambda_6)\, dz \end{aligned} \tag{2.1.40}$$

Since $\Lambda_x=\Lambda_1$ and $\Lambda_y=\Lambda_2$ are nonzero only in the piezoelectric layers, the integral in z direction must be computed only in those layers. In the following derivations the induced strain is computed as follows

$$\Lambda_x = \Lambda_1 = \begin{cases} d_{31}E_3, & z \in \left[-\dfrac{h}{2}, -\dfrac{h}{2}+t_p\right] \\ d_{31}(-E_3), & z \in \left[\dfrac{h}{2}-t_p, \dfrac{h}{2}\right] \end{cases}$$

$$\Lambda_y = \Lambda_2 = \begin{cases} d_{32}E_3, & z \in \left[-\dfrac{h}{2}, -\dfrac{h}{2}+t_p\right] \\ d_{32}(-E_3), & z \in \left[\dfrac{h}{2}-t_p, \dfrac{h}{2}\right] \end{cases}$$

(2.1.41)

Considering surface bonded actuators in bimorph configuration, the integral in Eq. 2.1.40 can be performed and expressed in the following form.

$$I_p = \delta \bar{\varepsilon}_b^T \mathbf{I}_d E_3(t)$$

(2.1.42)

where $\bar{\varepsilon}_b$ is expressed in Eq. 2.1.35, $E_3(t)$ is the applied electric field in z direction and $\mathbf{I}_d$ is expressed by equations as follows

$$\mathbf{I}_d = \left\{ I_{d_0}^1 \quad I_{d_1}^1 \quad I_{d_3}^1 \quad I_{d_0}^2 \quad I_{d_1}^2 \quad I_{d_3}^2 \quad I_{d_0}^6 \quad I_{d_1}^6 \quad I_{d_3}^6 \right\}^T$$

(2.1.43)

where

$$I_{d_0}^1 = (I_0^{inf} - I_0^{sup})(Q_{p_{12}}d_{31} + Q_{p_{22}}d_{32})$$

$$I_{d_1}^1 = (I_1^{inf} - I_1^{sup})(Q_{p_{12}}d_{31} + Q_{p_{22}}d_{32})$$

$$I_{d_3}^1 = (I_3^{inf} - I_3^{sup})(Q_{p_{12}}d_{31} + Q_{p_{22}}d_{32})$$

$$I_{d_0}^2 = (I_0^{inf} - I_0^{sup})(Q_{p_{12}}d_{31} + Q_{p_{22}}d_{32})$$

$$I_{d_1}^2 = (I_1^{inf} - I_1^{sup})(Q_{p_{12}}d_{31} + Q_{p_{22}}d_{32})$$

(2.1.44)

$$I_{d_3}^2 = (I_3^{inf} - I_3^{sup})(Q_{p_{12}}d_{31} + Q_{p_{22}}d_{32})$$

$$I_{d_0}^6 = (I_0^{inf} - I_0^{sup})(Q_{p_{16}}d_{31} + Q_{p_{26}}d_{32})$$

$$I_{d_1}^6 = (I_1^{inf} - I_1^{sup})(Q_{p_{16}}d_{31} + Q_{p_{26}}d_{32})$$

$$I_{d_3}^6 = (I_3^{inf} - I_3^{sup})(Q_{p_{16}}d_{31} + Q_{p_{26}}d_{32})$$

and

$$I_0^{inf} = \int_{-\frac{h}{2}}^{-\frac{h}{2}+t_p} dz = t_p$$

$$I_1^{inf} = \int_{-\frac{h}{2}}^{-\frac{h}{2}+t_p} z\,dz = \frac{1}{2}\left[\left(-\frac{h}{2}+t_p\right)^2 - \frac{h^2}{4}\right]$$

$$I_3^{inf} = \int_{-\frac{h}{2}}^{-\frac{h}{2}+t_p} z^3\,dz = \frac{1}{4}\left[\left(-\frac{h}{2}+t_p\right)^4 - \frac{h^4}{16}\right] \qquad (2.1.45)$$

$$I_0^{sup} = \int_{\frac{h}{2}-t_p}^{\frac{h}{2}} dz = t_p$$

$$I_1^{sup} = \int_{\frac{h}{2}-t_p}^{\frac{h}{2}} z\,dz = \frac{1}{2}\left[\frac{h^2}{4} - \left(\frac{h}{2}-t_p\right)^2\right]$$

$$I_3^{sup} = \int_{\frac{h}{2}-t_p}^{\frac{h}{2}} z^3\,dz = \frac{1}{4}\left[\frac{h^4}{16} - \left(\frac{h}{2}-t_p\right)^4\right]$$

Usually, piezoelectric materials are considered isotropic, therefore, the constants Q_{p16}, and Q_{p26} are zero and $Q_{p11}=Q_{p22}$. For isotropic materials all the material properties are invariant with respect to material reference frame such that $d_{31}=d_{32}$ and $\Lambda_x=\Lambda_y$. The above considerations are used in the numerical implementation of the piezoelectric force vector.

Finally, the variation of the strain energy due to transverse shear effect can be computed from Eq. 2.1.30 using Eqs. 2.1.5, as follows.

$$\delta U_s = \int_V \left(\delta\varepsilon_4 Q_{44}\varepsilon_4 + \delta\varepsilon_4 Q_{45}\varepsilon_5 + \delta\varepsilon_5 Q_{45}\varepsilon_4 + \delta\varepsilon_5 Q_{55}\varepsilon_5 \right) dV \qquad (2.1.46)$$

Decomposing the integral in Eq. 2.1.46 into two parts, one in the xy plane and the other in z direction,

$$\delta U_s = \int_A I_s \, dA \qquad (2.1.47)$$

where

$$I_s = \int_{-\frac{h}{2}}^{\frac{h}{2}} \left(\delta\varepsilon_4 Q_{44}\varepsilon_4 + \delta\varepsilon_4 Q_{45}\varepsilon_5 + \delta\varepsilon_5 Q_{45}\varepsilon_4 + \delta\varepsilon_5 Q_{55}\varepsilon_5 \right) \qquad (2.1.48)$$

In a vector-matrix form,

$$I_s = \delta\overline{\varepsilon}_s^{\ T} \mathbf{I}_{Q_s} \overline{\varepsilon}_s \qquad (2.1.49)$$

where

$$\overline{\varepsilon}_s = \left\{ \delta\varepsilon_4^0 \quad \delta\varepsilon_4^2 \quad \delta\varepsilon_5^0 \quad \delta\varepsilon_5^2 \right\} \qquad (2.1.50)$$

$$\mathbf{I}_{Q_s} = \begin{bmatrix} \mathbf{I}_{Q_{44}} & \mathbf{I}_{Q_{45}} \\ \mathbf{I}_{Q_{45}} & \mathbf{I}_{Q_{55}} \end{bmatrix} \qquad (2.1.51)$$

$$\mathbf{I}_{Q_{ii}} = \begin{bmatrix} I_0^{ij} & I_2^{ij} \\ I_2^{ij} & I_4^{ij} \end{bmatrix} \qquad (2.1.52)$$

and

$$I_k^{ij} = \int_{-\frac{h}{2}}^{\frac{h}{2}} \overline{Q}_{ij} \, z^k \, dz = \frac{1}{k+1} \sum_{r=1}^{n_1} \overline{Q}_{ij}(r) \left(h_{r+1}^{k+1} - h_r^{k+1} \right) \qquad (2.1.53)$$
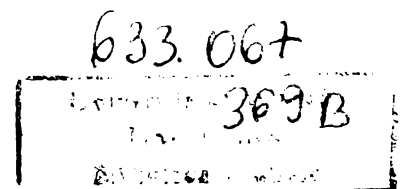
In Eqs. 2.1.52-53 it is assumed that k=0,2,4 and i,j=4,5, i<j. The transverse shear strain energy (U_s) and the classical term energy (U_b) are used in the numerical implementation in computing the structural stiffness.

External Work Done

The work done by external forces in a virtual displacement compatible with system constraints is represented by the last term in Eq. 2.1.18. This general form accounts for volume external forces. For common structures however, the forces are surface distributed therefore, the integral over the volume V is replaced by a surface integral over the area A. The computation of work done is made for the latest case. The work done in a virtual displacement $\delta\overline{\mathbf{u}}$ can be written as follows

$$\delta W = \int_A \delta\overline{\mathbf{u}}^T \mathbf{p}(x, y, z, t)\, dA \tag{2.1.54}$$

where

$$\mathbf{p}(x, y, z, t) = \left\{ p_x(x, y, z, t) \quad p_y(x, y, z, t) \quad p_z(x, y, z, t) \right\}^T \tag{2.1.55}$$

is the distributed load vector and $\delta\overline{\mathbf{u}} = \{\delta u(x,y,z,t) \quad \delta v(x,y,z,t) \quad \delta w(x,y,z,t)\}^T$ is the virtual displacement corresponding to the displacement field in equation 2.1.17. Further, from relations 2.1.19-20 the displacement field ($\overline{\mathbf{u}}$) is related to the vector of intermediate unknowns ($\overline{\mathbf{U}}$) as follows

$$\overline{\mathbf{u}} = \mathbf{L}_W \overline{\mathbf{U}} \tag{2.1.56}$$

where $\mathbf{L}_W$ is an operator matrix formed with the z coordinate of the application points of distributed external force.

$$\mathbf{L}_W = \begin{bmatrix} 1 & z_p & z_p^3 & 0 & 0 & 0 & 0 \\ 0 & 0 & 0 & 1 & z_p & z_p^3 & 0 \\ 0 & 0 & 0 & 0 & 0 & 0 & 1 \end{bmatrix} \tag{2.1.57}$$

In the above equation z_p, the z coordinate of the application point, is measured from the midplane of the plate. Now, the work done is computed as follows.

$$\delta W = \int_A \delta \overline{\mathbf{U}}^T \mathbf{L}_W^T \mathbf{p}(x, y, z, t) \, dA \tag{2.1.58}$$

The work done is used in the next chapter in computing the element force vector due to external loads.

2.2 Continuity Conditions

For a plate with delaminations, the structure is decomposed into three distinct regions as in Fig. 2.2. There are denoted D_1 for the undelaminated part, D_2, the region above delamination and D_3 for the region below delamination. The higher order displacement field is independently applied to each region (Seeley, 1997).

$$u_i(x, y, z, t) = u_{0i}(x, y, t) + (z - c_i)\left[-\frac{\partial w_{0i}}{\partial x} + \alpha_i(x, y, t) \right] - \frac{4(z - c_i)^3}{3h_i^2}\alpha_i(x, y, t)$$

$$v_i(x, y, z, t) = v_{0i}(x, y, t) + (z - c_i)\left[-\frac{\partial w_{0i}}{\partial y} + \beta_i(x, y, t) \right] - \frac{4(z - c_i)^3}{3h_i^2}\beta_i(x, y, t) \tag{2.2.1}$$

$$w_i(x, y, z, t) = w_{0i}(x, y, t)$$

where c_i are the z coordinates of the midplanes of each region, h_i are the local thicknesses and the index $i = 1, 2, 3$ represents the three regions.

Additional conditions are necessary to assure the continuity of the displacement field and its derivatives, on the delamination interface S. In a general form the continuity conditions at S are expressed as follows.

$$u_1(x,y,z,t) = u_i(x,y,z,t)$$

$$v_1(x,y,z,t) = v_i(x,y,z,t)$$

$$w_1(x,y,z,t) = w_i(x,y,z,t)$$

$$\frac{\partial^r u_1}{\partial x^n \partial y^m} = \frac{\partial^r u_i}{\partial x^n \partial y^m}$$

$$\frac{\partial^r v_1}{\partial x^n \partial y^m} = \frac{\partial^r v_i}{\partial x^n \partial y^m}$$

$$\frac{\partial^r w_1}{\partial x^n \partial y^m} = \frac{\partial^r w_i}{\partial x^n \partial y^m}$$
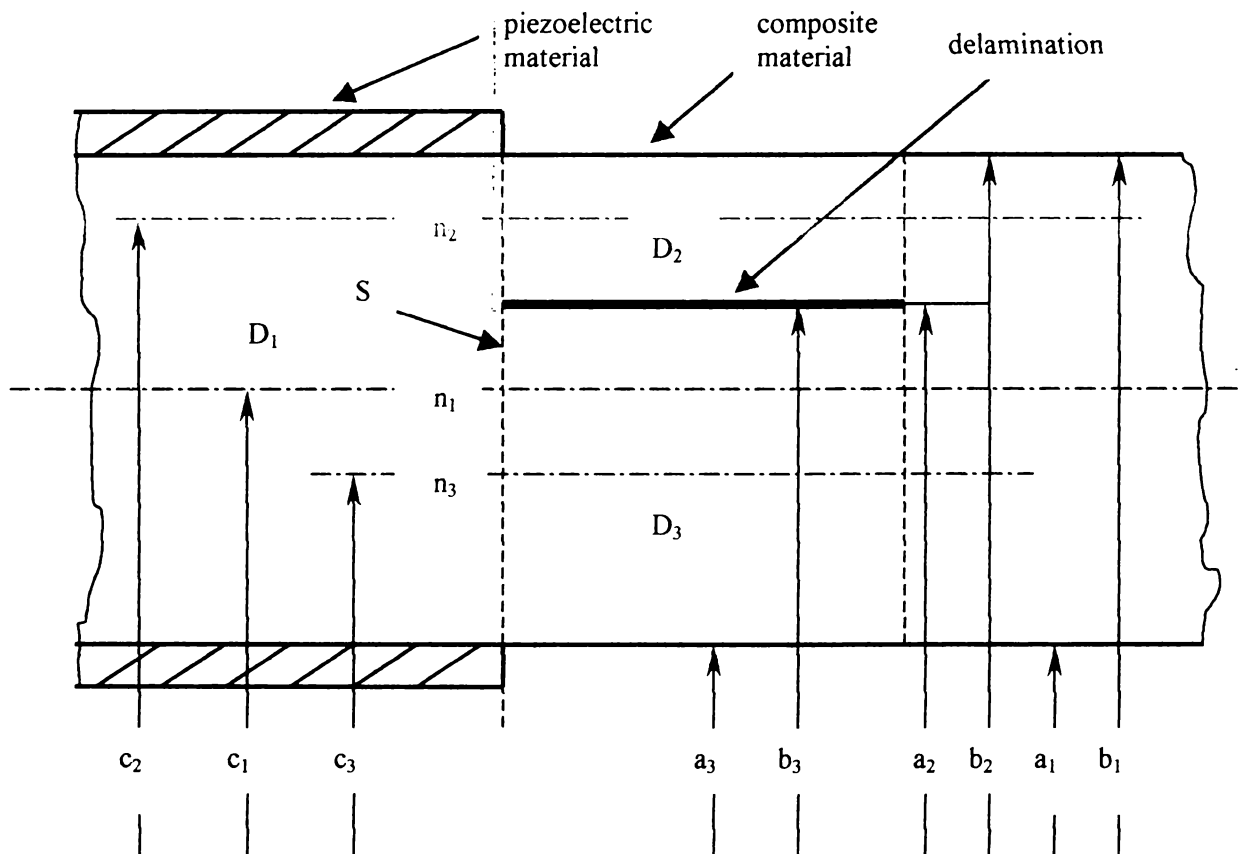
$$(2.2.2)$$

Figure 2.2.   Delaminated composite plate with actuators.

In the above equation i=2,3 represent the delaminated regions, and r denotes the required order of continuity, r=m+n, m,n=0,1,...,r. Since the theory developed is

implemented using the Finite Element Method (FEM), the continuity of displacement is imposed at the midplane of each delaminated region corresponding to nodal location in FEM. This case requires C^0 continuity of u and v with respect to inplane coordinates x and y, C^1 continuity of u and v with respect to z and C^2 continuity of w with respect to x and y, Equations 2.2.2 can be written as follows.

$$u_i = u_{0i} = u_{01} + (c_i - c_1)\left(-\frac{\partial w_{01}}{\partial x} + \alpha_1\right) - \frac{4}{3h_1^2}(c_i - c_1)^3 \alpha_1$$

$$v_i = v_{0i} = v_{01} + (c_i - c_1)\left(-\frac{\partial w_{01}}{\partial y} + \alpha_1\right) - \frac{4}{3h_1^2}(c_i - c_1)^3 \beta_1$$

$$\alpha_i = \left[1 - \frac{4}{h_1^2}(c_i - c_1)^2\right]\alpha_1$$

$$\beta_i = \left[1 - \frac{4}{h_1^2}(c_i - c_1)^2\right]\beta_1$$

(2.2.3)

$$w_{0i} = w_{01}$$

$$\frac{\partial w_{0i}}{\partial x} = \frac{\partial w_{01}}{\partial x}$$

$$\frac{\partial w_{0i}}{\partial y} = \frac{\partial w_{01}}{\partial y}$$

$$\frac{\partial^2 w_{0i}}{\partial x^2} = \frac{\partial^2 w_{01}}{\partial x^2}$$

$$\frac{\partial^2 w_{0i}}{\partial y^2} = \frac{\partial^2 w_{01}}{\partial y^2}$$

$$\frac{\partial^2 w_{0i}}{\partial x \partial y} = \frac{\partial^2 w_{01}}{\partial x \partial y}$$

Equations (2.2.2-3) can be tailored requiring the necessary degree of continuity of unknown functions for a specific FEM implementation. This is discussed in chapter 3.

3. Numerical Implementation

The finite element implementation of the equations of motion describing a smart composite plate in the presence of delaminations, is described in the following sections. This approach allows the modeling of arbitrary geometry and boundary conditions. The unknown functions are the displacements u, v and w and the shear correction functions α and β. Isoparametric interpolation is used for the inplane displacements u and v and the functions α and β, while cubic interpolation is used for the out of plane displacement, w (Reddy, 1993).

3.1   Stiffness Properties

The elemental stiffness is composed of two terms, one due to inplane strains (ε_1, ε_2 and ε_6) and the other due to transverse shear effects (ε_4 and ε_5). The contribution of the shear strains is particularly important for thick plates. Some details of these computations are presented next.

3.1.1   Stiffness Due to Inplane Effects

Equations 2.1.12 can be expressed in the local system of coordinates in a matrix-vector form as follows.

$$\overline{\varepsilon}_b = \mathbf{L}_{b\xi}\overline{\mathbf{u}}_\xi \tag{3.1.1}$$

where $\overline{\varepsilon}_b$ is the strain vector expressed as follows

$$\overline{\epsilon}_b = \left\{ \varepsilon_1^0 \quad \varepsilon_1^1 \quad \varepsilon_1^3 \quad \varepsilon_2^0 \quad \varepsilon_2^1 \quad \varepsilon_2^3 \quad \varepsilon_6^0 \quad \varepsilon_6^1 \quad \varepsilon_6^3 \right\}_\xi^T \tag{3.1.2}$$

$\mathbf{L}_{b\xi}$ is a matrix differential operator.

$$\mathbf{L}_{b\xi} = \begin{bmatrix} \dfrac{1}{a}\dfrac{\partial}{\partial\xi} & 0 & 0 & 0 & 0 \\ 0 & \dfrac{1}{a}\dfrac{\partial}{\partial\xi} & 0 & 0 & -\dfrac{1}{a^2}\dfrac{\partial^2}{\partial\xi^2} \\ 0 & C_1\dfrac{1}{a}\dfrac{\partial}{\partial\xi} & 0 & 0 & 0 \\ 0 & 0 & \dfrac{1}{b}\dfrac{\partial}{\partial\eta} & 0 & 0 \\ 0 & 0 & 0 & \dfrac{1}{b}\dfrac{\partial}{\partial\eta} & -\dfrac{1}{b^2}\dfrac{\partial^2}{\partial\eta^2} \\ 0 & 0 & 0 & C_1\dfrac{1}{b}\dfrac{\partial}{\partial\eta} & 0 \\ \dfrac{1}{b}\dfrac{\partial}{\partial\eta} & 0 & \dfrac{1}{a}\dfrac{\partial}{\partial\xi} & 0 & 0 \\ 0 & \dfrac{1}{b}\dfrac{\partial}{\partial\eta} & 0 & \dfrac{1}{a}\dfrac{\partial}{\partial\xi} & -\dfrac{2}{ab}\dfrac{\partial^2}{\partial\xi\partial\eta} \\ 0 & C_1\dfrac{1}{b}\dfrac{\partial}{\partial\eta} & 0 & C_1\dfrac{1}{a}\dfrac{\partial}{\partial\xi} & 0 \end{bmatrix} \tag{3.1.3}$$

and

$$\overline{\mathbf{u}}_\xi = \left\{ u_0(\xi,\mu) \quad \alpha(\xi,\mu) \quad v_0(\xi,\mu) \quad \alpha(\xi,\mu) \quad w_0(\xi,\mu) \right\} \tag{3.1.4}$$

In the above equations coordinates $\xi=(\xi,\eta)$ correspond to a point in the reference element and $\mathbf{u}_\xi$ is the vector of unknown functions (Reddy, 1993).

The unknown displacement functions are now expressed in terms of the nodal variables. Using the appropriate interpolation functions the following relationship is obtained.

$$\overline{\mathbf{u}}_\xi = \sum_{i=1}^{4} \mathbf{N}_i \mathbf{w}_i^e \tag{3.1.5}$$

$$w_i^e = \left\{ u_{0i} \quad \alpha_i \quad v_{0i} \quad \beta_i \quad w_{0i} \quad \frac{\partial w_{0i}}{\partial x} \quad \frac{\partial w_{0i}}{\partial y} \quad \frac{\partial^2 w_{0i}}{\partial x \partial y} \right\}^T \tag{3.1.6}$$

$$N_i = \begin{bmatrix} H_i & 0 & 0 & 0 & 0 & 0 & 0 & 0 \\ 0 & H_i & 0 & 0 & 0 & 0 & 0 & 0 \\ 0 & 0 & H_i & 0 & 0 & 0 & 0 & 0 \\ 0 & 0 & 0 & H_i & 0 & 0 & 0 & 0 \\ 0 & 0 & 0 & 0 & N_{1i} & a N_{2i} & b N_{3i} & ab N_{4i} \end{bmatrix} \tag{3.1.7}$$

where $i=1,\ldots,4$ refers to the nodes of each element, $N=[N_1, N_2, N_3, N_4]$ is a 5x32 shape function matrix and $w^e = \left\{ w_1^{e^T} \quad w_2^{e^T} \quad w_3^{e^T} \quad w_4^{e^T} \right\}^T$ is the 32x1 element nodal unknowns vector. In Eq. 3.1.7 H_i ($i=1,\ldots,4$) are bilinear interpolation functions while N_{ij} ($i,j=1,\ldots4$) are Hermite cubic functions. The resulting finite element comprises 32 unknowns variables. The strain is related to the nodal displacements using Eqs. 3.1.1 and 3.1.5 as follows.

$$\overline{\varepsilon}_b = B_b w^e \tag{3.1.8}$$

where

$$B_b = L_{b\xi} N = \begin{bmatrix} B_{b1} & B_{b2} & B_{b3} & B_{b4} \end{bmatrix} \tag{3.1.9}$$

and

$$\mathbf{B}_{bi} = \begin{bmatrix} \frac{1}{a}H_{i,\xi} & 0 & 0 & 0 & 0 & 0 & 0 & 0 \\ 0 & \frac{1}{a}H_{i,\xi} & 0 & 0 & -\frac{1}{a^2}N_{1i,\xi\xi} & -\frac{1}{a}N_{2i,\xi\xi} & -\frac{b}{a^2}N_{3i,\xi\xi} & -\frac{b}{a}N_{4i,\xi\xi} \\ 0 & C_1\frac{1}{a}H_{i,\xi} & 0 & 0 & 0 & 0 & 0 & 0 \\ 0 & 0 & \frac{1}{b}H_{i,\eta} & 0 & 0 & 0 & 0 & 0 \\ 0 & 0 & 0 & \frac{1}{b}H_{i,\eta} & -\frac{1}{b^2}N_{1i,\eta\eta} & -\frac{a}{b^2}N_{2i,\eta\eta} & -\frac{1}{b}N_{3i,\eta\eta} & -\frac{a}{b}N_{4i,\eta\eta} \\ 0 & 0 & 0 & C_1\frac{1}{b}H_{i,\eta} & 0 & 0 & 0 & 0 \\ \frac{1}{b}H_{i,\eta} & 0 & \frac{1}{a}H_{i,\xi} & 0 & 0 & 0 & 0 & 0 \\ 0 & \frac{1}{b}H_{i,\eta} & 0 & \frac{1}{a}H_{i,\xi} & -\frac{2}{ab}N_{1i,\xi\eta} & -\frac{2}{b}N_{2i,\xi\eta} & -\frac{2}{a}N_{3i,\xi\eta} & -2N_{4i,\xi\eta} \\ 0 & C_1\frac{1}{b}H_{i,\eta} & 0 & C_1\frac{1}{a}H_{i,\xi} & 0 & 0 & 0 & 0 \end{bmatrix}$$

$$(3.1.10)$$

In Eqs. 3.2.3 and 3.2.10, C_1 is a constant defined in Eqs. 2.1.13 and a shorthand convention for derivatives is used: $f_{,\xi} = \partial f/\partial\xi$, etc.

The element stiffness matrix due to inplane strains is computed next. From Eqs. 2.1.32, 2.1.34-38 and relations 3.1.7-10, the variation of inplane strain energy can be expressed as

$$\delta U_b^e = \int_{-1}^{1}\int_{-1}^{1} \delta\mathbf{w}^e\, \mathbf{B}_b^T\, \mathbf{I}_{Q_b}\, \mathbf{B}_b\, \mathbf{w}^e\, ab\, d\xi\, d\eta = \delta\mathbf{w}^e\, \mathbf{k}_b^e\mathbf{w}^e \qquad (3.1.11)$$

where the stiffness matrix, $\mathbf{k}_b^e$, is obtained through the following numerical integration.

$$\mathbf{k}_b^e = \int_{-1}^{1}\int_{-1}^{1} \mathbf{B}_b^T\, \mathbf{I}_{Q_b}\, \mathbf{B}_b\, ab\, d\xi\, d\eta \cong ab\sum_{r=1}^{n}\sum_{s=1}^{n} w_{tr}w_{ts}\mathbf{B}_b^T(\xi_r,\eta_r)\mathbf{I}_{Q_b}\mathbf{B}_b(\xi_r,\eta_r) \qquad (3.1.12)$$

In the above equation $\mathbf{I}_{Qb}$ is expressed in relations 2.1.36-38, n is the number of Gauss points, w_{tr} and w_{ts} are weights (Reddy, 1993) and a and b are the dimensions of the plate element.

3.1.2 Stiffness Due to Transverse Effects

The variation of strain energy due to shear deformation was derived in Eqs. 2.1.47-53. Further, from Eqs. 2.1.12-13 the shear strains can be expressed in terms of the unknown functions as follows.

$$\bar{\varepsilon}_s = \mathbf{L}_{s_\xi} \bar{\mathbf{u}}_\xi \tag{3.1.13}$$

where $\mathbf{u}_\xi$ is given by Eq. 3.1.4 and $\bar{\varepsilon}_s$ and $\mathbf{L}_{s\xi}$ are defined by the following relations

$$\bar{\varepsilon}_s = \left\{ \varepsilon_4^0 \quad \varepsilon_4^2 \quad \varepsilon_5^0 \quad \varepsilon_5^2 \right\}^{\mathrm{T}} \tag{3.1.14}$$

and

$$\mathbf{L}_{s\xi} = \begin{bmatrix} 0 & 0 & 0 & 1 & 0 \\ 0 & 0 & 0 & C_2 & 0 \\ 0 & 1 & 0 & 0 & 0 \\ 0 & C_2 & 0 & 0 & 0 \end{bmatrix} \tag{3.1.15}$$

In Eq. 3.1.15, C_2 is a constant defined in Eqs. 2.1.13. Using the relation between the unknown functions and the nodal variables (Eq. 3.1.5) the transverse strains can be further related to the nodal unknowns as follows.

$$\bar{\varepsilon}_s = \mathbf{B}_s \mathbf{w}^e \tag{3.1.16}$$

where $\mathbf{w}^e$ is the 32x1 nodal unknowns vector and $\mathbf{B}_s$ is defined as

$$\mathbf{B}_s = \mathbf{L}_s \mathbf{N} = \begin{bmatrix} \mathbf{B}_{s1} & \mathbf{B}_{s2} & \mathbf{B}_{s3} & \mathbf{B}_{s4} \end{bmatrix} \tag{3.1.17}$$

where

$$\mathbf{B}_{si} = \begin{bmatrix} 0 & 0 & 0 & H_i & 0 & 0 & 0 & 0 \\ 0 & 0 & 0 & C_2H_i & 0 & 0 & 0 & 0 \\ 0 & H_i & 0 & 0 & 0 & 0 & 0 & 0 \\ 0 & C_2H_i & 0 & 0 & 0 & 0 & 0 & 0 \end{bmatrix} \tag{3.1.18}$$

From Eqs. 2.1.47, 2.1.49-2.1.53 and 3.1.16 the variation of potential energy due to shear effects can be written as

$$\delta U_s = \int_{-1}^{1} \int_{-1}^{1} \delta \mathbf{w}^e \, \mathbf{B}_s^T \, \mathbf{I}_{Q_s} \, \mathbf{B}_s \, \mathbf{w}^e \, ab \, d\xi \, d\eta = \delta \mathbf{w}^e \, \mathbf{k}_s^e \mathbf{w}^e \tag{3.1.19}$$

where the stiffness matrix $\mathbf{k}_s^e$ is computed through numerical integration as follows.

$$\mathbf{k}_s^e = \int_{-1}^{1} \int_{-1}^{1} \mathbf{B}_s^T \, \mathbf{I}_{Q_s} \, \mathbf{B}_s \, ab \, d\xi \, d\eta \cong ab \sum_{r=1}^{n} \sum_{s=1}^{n} w_{tr} w_{ts} \mathbf{B}_s^T(\xi_r, \eta_r) \mathbf{I}_{Q_s} \mathbf{B}_s(\xi_r, \eta_r) \tag{3.1.20}$$

The matrix $\mathbf{I}_{Qs}$ is defined in Eqs. 2.1.51-53.

Finally the element stiffness matrix ($\mathbf{k}^e$) is the summation of the two matrices

$$\mathbf{k}^e = \mathbf{k}_b^e + \mathbf{k}_s^e \tag{3.1.21}$$

The derivation of the inertia element matrix is presented, next.

3.2 Inertia Properties

In section 2.1.3, the variation of the kinetic energy was defined in Eqs. 2.1.21-26 in terms seven intermediate unknowns (Eqs. 2.1.20). Now, it is necessary to relate the intermediate unknowns in terms of the nodal unknowns. From equations 2.1.20 and the derivatives transformation one obtains an operator equation as follows.

$$\overline{\mathbf{U}}_\xi = \mathbf{L}_{m\xi} \overline{\mathbf{u}}_\xi \tag{3.2.1}$$

where

$$\mathbf{L}_{m\xi} = \begin{bmatrix} 1 & 0 & 0 & 0 & 0 \\ 0 & 1 & 0 & 0 & -\dfrac{1}{a}\dfrac{\partial}{\partial\xi} \\ 0 & C_1 & 0 & 0 & 0 \\ 0 & 0 & 1 & 0 & 0 \\ 0 & 0 & 0 & 1 & -\dfrac{1}{b}\dfrac{\partial}{\partial\eta} \\ 0 & 0 & 0 & C_1 & 0 \\ 0 & 0 & 0 & 0 & 1 \end{bmatrix}$$ (3.2.2)

is the inertia differential operator which acts on the unknown functions vector (Eq. 3.1.4). From Eqs 3.2.1 and 3.1.5 the intermediate unknown vector is expressed in terms of element nodal variables as follows

$$\overline{U}_\xi = \mathbf{B}_m \mathbf{w}^e$$ (3.2.3)

where

$$\mathbf{B}_m = \begin{bmatrix} \mathbf{B}_{m1} & \mathbf{B}_{m2} & \mathbf{B}_{m3} & \mathbf{B}_{m4} \end{bmatrix}$$ (3.2.4)

$$\mathbf{B}_{mi} = \begin{bmatrix} H_i & 0 & 0 & 0 & 0 & 0 & 0 & 0 \\ 0 & H_i & 0 & 0 & -\dfrac{1}{a}N_{1i,\xi} & -N_{2i,\xi} & -\dfrac{b}{a}N_{3i,\xi} & -bN_{4i,\xi} \\ 0 & C_1 H_i & 0 & 0 & 0 & 0 & 0 & 0 \\ 0 & 0 & H_i & 0 & 0 & 0 & 0 & 0 \\ 0 & 0 & 0 & H_i & -\dfrac{1}{b}N_{1i,} & -\dfrac{a}{b}N_{2i,\eta} & -N_{3i,\eta} & -aN_{4i,\eta} \\ 0 & 0 & 0 & C_1 H_2 & 0 & 0 & 0 & 0 \\ 0 & 0 & 0 & 0 & N_{1i} & aN_{2i} & bN_{3i} & abN_{4i} \end{bmatrix}$$ (3.2.5)

The inertia matrix is obtained from the variation of kinetic energy for an element, as shown in Eqs. 2.1.21-26 and Eqs. 3.2.3-5 as follows

$$\delta K^e = -\int_{-1}^{1}\int_{-1}^{1} \delta\mathbf{w}^{e^T}\mathbf{B}_m^T \mathbf{J}_\rho \mathbf{B}_m \ddot{\mathbf{w}}^e \, ab\,d\xi\,d\eta = -\delta\mathbf{w}^{e^T}\mathbf{m}^e\ddot{\mathbf{w}}^e$$ (3.2.6)

where $\mathbf{m}^e$ is computed again using Gauss-Legendre quadrature.

$$\mathbf{m}^e = ab \int_{-1}^{1}\int_{-1}^{1} \mathbf{B}_m^T \mathbf{J}_\rho \mathbf{B}_m \ d\xi d\eta \cong ab \sum_{r=1}^{n}\sum_{s=1}^{n} w_{tr} w_{ts} \mathbf{B}_m^T(\xi_r,\eta_s)\mathbf{J}_\rho \mathbf{B}_m(\xi_r,\eta_s) \qquad (3.2.7)$$

3.3 Load Vectors

The loads on a smart structure comprise the forces due to piezoelectric actuation and external forces. In the following sections the derivation of the force vectors and their FEM implementation are discussed.

3.3.1 Piezoelectric Force Vector

The force vector due to piezoelectric actuation can be computed from the variation of strain energy, more precisely the second term in Eq. 2.1.31. As shown in section 2.1.3, for a composite plate with surface bonded piezoelectric actuators, in bimorph configuration the variation of strain energy is given in Eqs. 2.1.39-45. Considering equations 2.1.39 and 2.1.41-42 in conjunction with Eq. 3.1.8 this can be written as follows

$$\delta U_b^2 = \int_{-1}^{1}\int_{-1}^{1} \delta \mathbf{w}^e \mathbf{B}_b^T \mathbf{I}_d E_3(t) ab \, d\xi \, d\eta = \delta \mathbf{w}^e \mathbf{f}_p^e E_3(t) \qquad (3.3.1)$$

where the piezoelectric force vector, $\mathbf{f}_p^e$, due to unit electric field is obtained by a numerical quadrature

$$\mathbf{f}_p^e = \int_{-1}^{1}\int_{-1}^{1} \mathbf{B}_b^T \mathbf{I}_d ab d\xi \, d\eta \cong ab \sum_{r=1}^{n}\sum_{s=1}^{n} w_{tr} w_{ts} \mathbf{B}_b^T(\xi_r,\eta_s) \mathbf{I}_d \qquad (3.3.2)$$

where $\mathbf{B}_b$ is defined in Eqs. 3.2.4-5 and $\mathbf{I}_d$ is given by relations 2.1.43-45. It must be noted that in the presence of delamination, in a zone covered by piezoelectric actuators, equations 2.1.44 must be modified to account for unimorph configuration in the damaged zone. The details are presented in section 3.5.

3.3.2 External Force Vector

Equation 2.1.58, in chapter 2, shows the work done by a distributed force in a virtual displacement compatible with system constraints. The intermediate unknowns vector $\overline{\mathbf{U}}_\xi$ is related with the nodal displacement vector through Eqs. 3.2.3 such that the work done for an element can be written as follows

$$\delta W = \int_{-1}^{1}\int_{-1}^{1} \delta\mathbf{w}^{e^T} \mathbf{B}_m^T \mathbf{L}_W^T \mathbf{p}(\xi,\eta,t)\, ab\, d\xi\, d\eta = \delta\mathbf{w}^{e^T}\mathbf{f}^e \qquad (3.3.3)$$

where $\delta\mathbf{w}^e$ is the virtual displacement in terms of nodal variables and $\mathbf{f}^e$ is the element force vector derived from external loads. Using Gauss-Legendre numerical quadrature,

$$\mathbf{f}^e = \int_{-1}^{1}\int_{-1}^{1} \mathbf{B}_m^T \mathbf{L}_W^T\, \mathbf{p}(\xi,\eta,t) = ab\sum_{r=1}^{n}\sum_{s=1}^{n} \mathbf{w}_{tr}\mathbf{w}_{ts}\mathbf{B}_m^T(\xi_r,\eta_s,t)\mathbf{L}_W^T\, \mathbf{p}(\xi_r,\eta_s) \qquad (3.3.4)$$

Care should be made in the assembling process to asses the appropriate load applied to various elements of the smart composite plate.

3.4 Implementation of Continuity Conditions

The presence of delaminations alters both the static and dynamic behavior of a smart composite plate reducing the stiffness and increasing the strain in the damaged zone. Because the laminate is divided into several domains, accounting for the presence of delaminations, the continuity of the displacement field at the delamination lateral boundary is enforced. It is important that the numerical (discrete) implementation of these boundary conditions is accurate.

3.4.1 Nodal Transformation

The continuity conditions of the displacement field at the delamination interface was discussed in section 2.2. These continuity conditions are consistent with the higher order theory and are based on the kinematic equations 2.2.1. They can be tailored for any specific FEM implementation. In Eqs. 2.2.3, a specific condition requiring continuity at the midplanes of each sublaminate for different unknown functions was presented. In this section a new method of imposing continuity conditions, numerically consistent with FEM implementation, is presented. The necessary continuity is assured at the nodes of each element on delamination lateral boundary S, Fig. 3.1. As will be shown, this approach significantly reduces the size of the stiffness and inertia matrices compared to penalty approach (Seeley and Chattopadhyay, 1998) or Lagrange multipliers method.
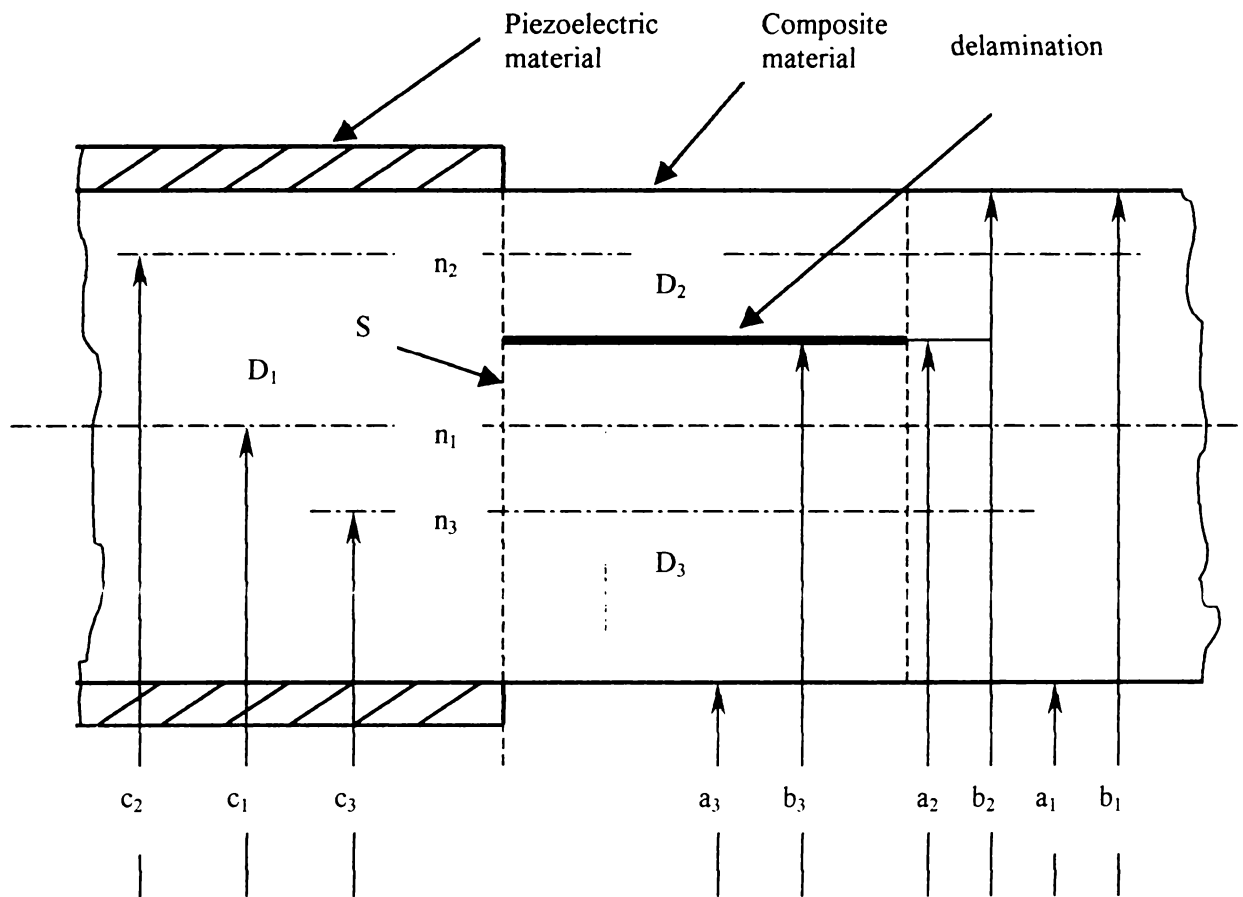
Figure 3.1. Smart composite plate geometry.

As expressed in Eqs. 2.2.3, C^0 continuity is necessary for the unknown functions u_0, v_0, α and β, C^1 continuity is necessary for w_0 and in addition the continuity of the mixed derivative $\partial^2 w_0/\partial x\, \partial y$ is also required. These continuity conditions, imposed at the nodes on S of elements in both top and bottom sublaminates (Fig. 3.1), can be expressed as

$$\mathbf{w}_{n_i} = \mathbf{T}_i\, \mathbf{w}_{n_1} \qquad\qquad (3.4.1)$$

where $\mathbf{w}_{n_1}$ and $\mathbf{w}_{n_i}$ (i=2,3), the nodal unknowns of the undelaminated region and the delaminated region respectively, are as follows.

$$\mathbf{w}_{n1} = \{u_{01} \quad \alpha_1 \quad v_{01} \quad \beta_1 \quad w_{01} \quad w_{01,x} \quad w_{01,y} \quad w_{01,xy}\}^T \tag{3.4.2}$$

$$\mathbf{w}_{ni} = \{u_{0i} \quad \alpha_i \quad v_{0i} \quad \beta_i \quad w_{0i} \quad w_{0i,x} \quad w_{0i,y} \quad w_{0i,xy}\}^T \tag{3.4.3}$$

The transformation matrix, which relates the unknowns in the undelaminated region to those in the delaminated sublaminates is expressed as follows.

$$\mathbf{T}_i = \begin{bmatrix} 1 & c_i - c_1 - \dfrac{4(c_i - c_1)^3}{3h_1^2} & 0 & 0 & 0 & -(c_i - c_1) & 0 & 0 \\ 0 & 1 - \dfrac{4(c_i - c_1)^2}{h_1^2} & 0 & 0 & 0 & 0 & 0 & 0 \\ 0 & 0 & 1 & c_i - c_1 - \dfrac{4(c_i - c_1)^3}{3h_1^2} & 0 & 0 & -(c_i - c_1) & 0 \\ 0 & 0 & 0 & 1 - \dfrac{4(c_i - c_1)^2}{h_1^2} & 0 & 0 & 0 & 0 \\ 0 & 0 & 0 & 0 & 1 & 0 & 0 & 0 \\ 0 & 0 & 0 & 0 & 0 & 1 & 0 & 0 \\ 0 & 0 & 0 & 0 & 0 & 0 & 1 & 0 \\ 0 & 0 & 0 & 0 & 0 & 0 & 0 & 1 \end{bmatrix}$$

$$\tag{3.4.4}$$

Typically, the above transformation is applied to two or three nodes on the interface S of the elements on the top or bottom sublaminates. It eliminates the need for nodes of type n_2 or n_3 s in Figure 3.1 modifying the element matrices.
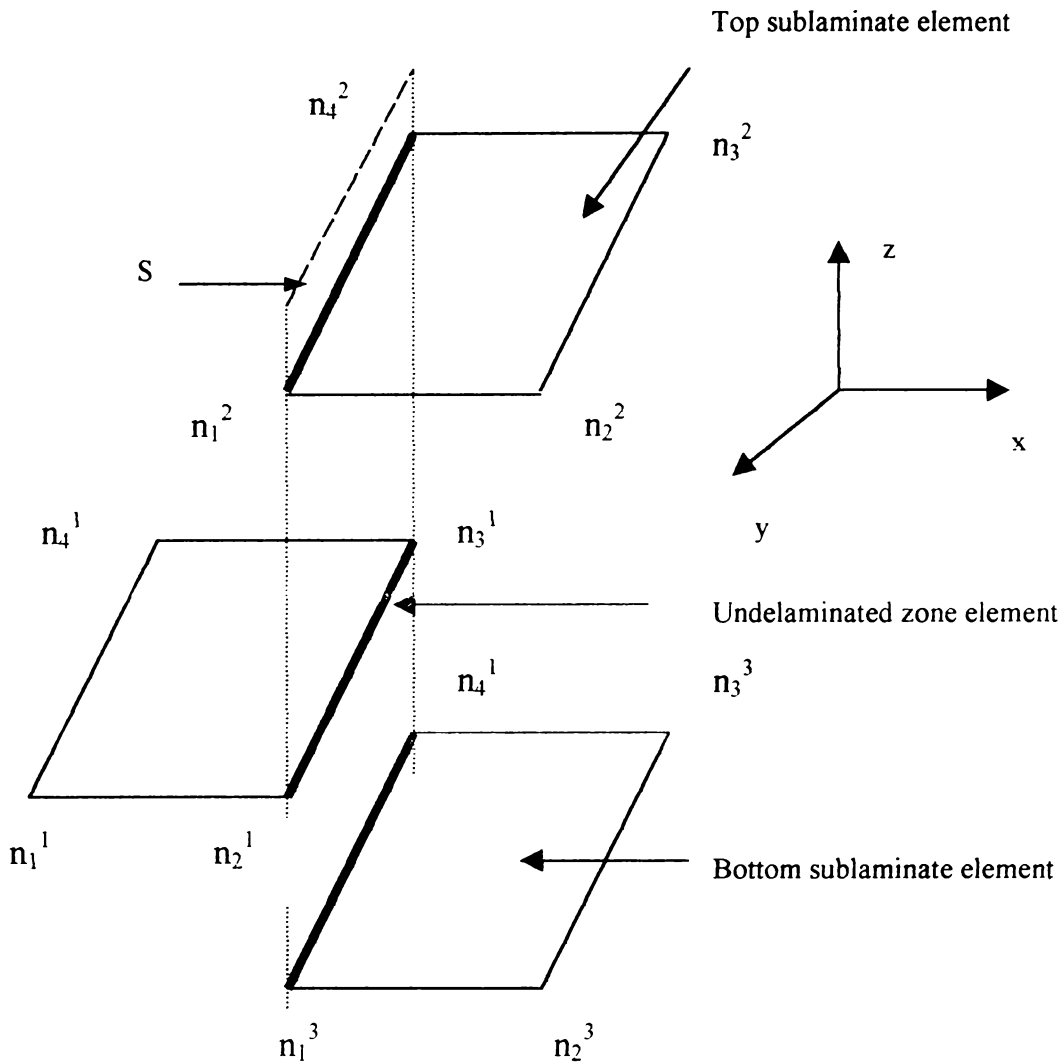
Figure 3.2. Transformation of nodes on S.

3.4.2   Element Transformation

For elements on the two sublaminates, with nodes on the delamination lateral interface S as shown in Fig. 3.2, the transformation in Eqs. 3.4.1-4 is applied for each node belonging to S. This transformation is then used to express the kinetic and potential energies of those elements with respect to the nodes in the undelaminated zone. The invariance of the energy leads to modifications of the corresponding element matrices,

thereby eliminating unnecessary nodes. Thus, the size of the assembled inertia and stiffness matrices is drastically reduced.

For the case shown in Fig. 3.2 the nodal unknowns of the delaminated zone elements (top and bottom sublaminates, denoted by D_2 and D_3 in Fig. 3.1), are expressed in terms of nodal unknowns of undelaminated zone (denoted by D_1 in Fig. 3.1) as follows.

$$
\begin{aligned}
\mathbf{w}_{n_1^2} &= \mathbf{T}_2 \mathbf{w}_{n_2^1}, & \mathbf{w}_{n_4^2} &= \mathbf{T}_2 \mathbf{w}_{n_3^1} \\
\mathbf{w}_{n_1^3} &= \mathbf{T}_3 \mathbf{w}_{n_2^1}, & \mathbf{w}_{n_4^3} &= \mathbf{T}_3 \mathbf{w}_{n_3^1}
\end{aligned}
\qquad \vdots \qquad (3.4.5)
$$

In a matrix-vector form, the above relations can be written as

$$
\mathbf{w}_{old}^e = \left\{ \begin{array}{c} \mathbf{w}_{n_1^i} \\ \mathbf{w}_{n_2^i} \\ \mathbf{w}_{n_3^i} \\ \mathbf{w}_{n_4^i} \end{array} \right\} = \mathbf{Y}_{1i} \left\{ \begin{array}{c} \mathbf{w}_{n_2^1} \\ \mathbf{w}_{n_3^1} \\ \mathbf{w}_{n_3^1} \\ \mathbf{w}_{n_3^1} \end{array} \right\} = \mathbf{Y}_{1i}\, \mathbf{w}_{new}^e \qquad (3.4.6)
$$

where i=2,3 corresponds to elements in zones D_2 and D_3, respectively. The element transformation matrix $\mathbf{Y}_{1i}$ is given by a 32x32 matrix in the following blockwise form

$$
\mathbf{Y}_{1i} = \begin{bmatrix} \mathbf{T}_i & \mathbf{O} & \mathbf{O} & \mathbf{O} \\ \mathbf{O} & \mathbf{I} & \mathbf{O} & \mathbf{O} \\ \mathbf{O} & \mathbf{O} & \mathbf{I} & \mathbf{O} \\ \mathbf{O} & \mathbf{O} & \mathbf{O} & \mathbf{T}_i \end{bmatrix} \qquad (3.4.7)
$$

where $\mathbf{I}$ is the 8x8 unity matrix and $\mathbf{O}$ is the 8x8 null matrix.

The kinetic and potential energies can be written in two forms, first using the element node unknowns vector (denoted by 'old') and second the transformed vectors (denoted by 'new'). From this equivalence, results the element matrices with respect to the new system of coordinates.

$$K_i^e = \frac{1}{2} {\mathbf{w}_{old_i}^e}^T \mathbf{m}_{old_i}^e \mathbf{w}_{old_i}^e = \frac{1}{2} {\mathbf{w}_{new_i}^e}^T \mathbf{m}_{new_i}^e \mathbf{w}_{new_i}^e$$

$$U_i^e = \frac{1}{2} {\mathbf{w}_{old_i}^e}^T \mathbf{k}_{old_i}^e \mathbf{w}_{old_i}^e = \frac{1}{2} {\mathbf{w}_{new_i}^e}^T \mathbf{k}_{new_i}^e \mathbf{w}_{new_i}^e \qquad (3.4.8)$$

From Eqs 3.4.8 and 3.4.6, the modified element matrices are computed as follows.

$$\mathbf{m}_{new_i}^e = \mathbf{Y}_{li}^T \mathbf{m}_{old_i}^e \mathbf{Y}_{li}$$

$$\mathbf{k}_{new_i}^e = \mathbf{Y}_{li}^T \mathbf{k}_{old_i}^e \mathbf{Y}_{li} \qquad (3.4.9)$$

In the reverse case when going from the damaged zone to the healthy zone, Eqs. 3.4.9 are accordingly changed resulting into the following form

$$\mathbf{m}_{new_i}^e = \mathbf{Z}_{il}^T \mathbf{m}_{old_i}^e \mathbf{Z}_{il}$$

$$\mathbf{k}_{new_j}^e = \mathbf{Z}_{il}^T \mathbf{k}_{old_i}^e \mathbf{Z}_{il} \qquad (3.4.10)$$

where the new transformation matrices, $\mathbf{Z}_{il}$, affect different nodes of elements in the zone of delamination.

$$\mathbf{Z}_{il} = \begin{bmatrix} \mathbf{I} & \mathbf{O} & \mathbf{O} & \mathbf{O} \\ \mathbf{O} & \mathbf{T}_i & \mathbf{O} & \mathbf{O} \\ \mathbf{O} & \mathbf{O} & \mathbf{T}_i & \mathbf{O} \\ \mathbf{O} & \mathbf{O} & \mathbf{O} & \mathbf{I} \end{bmatrix} \qquad (3.4.11)$$

Finally, the element force vectors are transformed as follows

$$\mathbf{f}_{new_i}^e = \mathbf{Y}_{li}^T \mathbf{f}_{old_i}^e \qquad (3.4.12)$$

when going from the healthy to the damaged zones. When going from the damaged to the healthy zone, these take the following form.

$$\mathbf{f}_{new_i}^e = \mathbf{Z}_{il}^T \mathbf{f}_{old_i}^e \qquad (3.4.13)$$

3.4.3   Element Properties in Delamination Zone

The inertia and stiffness matrices and the external load vector for the sublaminates in the delaminated zone are computed using the procedure described in sections 3.1-3. It considers the appropriate stacking sequence of layers in the sublaminates. It must be noted, that the integrals in z direction are performed only over the layers belonging to each sublaminate. The total thickness is appropriately used. Then, using the procedure presented in sections 3.4.1-3 the continuity conditions are imposed to change the element properties for the global finite element mesh only for elements with nodes on S.

One important difference occurs in computing the force vector due to piezoelectric actuation. If the elements in the delaminated zone have piezoelectric active layers separated by a delamination, the assumption of bimorph configuration is violated. In this case, each element in both top and bottom sublaminates must be modeled using unimorph behavior. The piezoelectric force vector still can be computed using Eqs. 2.1.39-45 with the difference that either I_i^{inf} for the top sublaminate elements or I_i^{sup} for the bottom sublaminate elements must be set to zero in Eqs. 2.1.44. The remaining computations remain unchanged as expressed in Eq. 3.3.2. In the calculation of the inertia and stiffness matrices and the external load vector, the total thickness of the sublaminates in the damaged zone is used. For elements with nodes on the delamination lateral boundary S, the piezoelectric force vector is modified using equations 3.4.12 or 3.4.13.

In the case of elements with three nodes on S, the transformation matrices $\mathbf{Y}_{1i}$ and $\mathbf{Z}_{i1}$ must be modified by replacing submatrices $\mathbf{I}$ on the main block-diagonal for each

node on S, with either T_2 or T_3. The element nodes not belonging to S are not affected. This means that a 8x8 identity matrix **I** appears in those positions.

3.5   Assembly Procedure

An assembly procedure is developed to appropriately designate the inertia, stiffness and load properties to each node of the global mesh while accounting for the contributions from adjacent elements sharing that node. Various types of elements can have contribution to a single node. These include contribution from healthy laminate elements, healthy elements with piezoelectric actuators in bimorph configuration, elements in the top and bottom sublaminates and delaminated elements with piezoelectric actuators in unimorph configuration.

The corresponding nodal unknowns of elements in the delaminated zone which belong to the delamination lateral boundary are transformed, as shown in section 3.4, to the nodal unknowns of the healthy structure in the global mesh. The transformation is applied to the smaller element matrices or vectors and the resulting matrix or vector is added in the assembly process. Thus, the size of the global inertia and stiffens matrices is significantly reduced. For multiple delaminations, as much as 70-80% saving in both storage requirements and CPU time is obtained.

The assembled system of ordinary differential equations, describing the dynamics of a smart composite plate with actuators and possible delaminations is written in the following form.

$$\mathbf{M}\ddot{\mathbf{q}} + \mathbf{K}\mathbf{q} = \mathbf{F} + \mathbf{F}_p \tag{3.5.1}$$

where $\mathbf{M}$ is the global inertia matrix, $\mathbf{K}$ is the global stiffness matrix, $\mathbf{F}$ is the external load vector and $\mathbf{F}_p$ is the piezoelectric force vector.

4. Damage Detection Techniques

4.1 Introduction

A delamination technique based on mode shapes was introduced by Pandey et al. in 1991. They proposed the use of curvature mode shapes in detecting damage in a beam. The curvature is obtained from mode shapes using Laplace's finite difference equation

$$C_i = w_i^{"} = \frac{w_{i+1} - 2w_i + w_{i-1}}{h^2} \qquad (4.1.1)$$

where w is the modal displacement, h is the stepsize of the finite difference mesh and index i denotes the location where curvature is computed. The authors reported that the absolute difference in the curvature mode shapes, between the healthy and the damaged beam, is a better indicator of damage location compared to the absolute difference in the displacement mode shapes.

Ratcliffe and Bagaria (1998) modified the above procedure using a gapped technique and proposed that the curvature should be locally smoothed. In their approach, for a composite beam with a through the width delamination a third order polynomial was used to describe the curvature. The gapped cubic calculated for the *i*th element of the curvature C_i, at position x_i along the beam, was defined as

$$p(x_i) = a_0 + a_1 x_i + a_2 x_i^2 + a_3 x_i^3 \qquad (4.1.2)$$

The coefficients a_0, a_1, a_2 and a_3 are determined using curvature elements C_{i-2}, C_{i-1}, C_{i+1} and C_{i+2}. The curvature C_i of the *i*th element is not included (gapped) in the calculation of

the third order polynomial. A damage index δ_i is calculated for the *i*th position on the beam as follows:

$$\delta_i = [p(x_i) - C_i]^2 \qquad (4.1.3)$$

In Eq. 4.1.3, the right-hand side is squared to reduce the effect of numerical errors or measurement noise. Separate gapped cubic polynomials and damage index values are determined for each grid point in turn. The above procedures uses the assumption that the damage is strictly located in a very small zone, considering the damage to be discrete rather than continuous. However, results are not presented for cases where the defect is spread over a larger zone such as is the case with delaminations. Even the meshsize used in this work is not refined enough in the delamination zone.

Other methods have also been proposed to characterize defects in structures. The modal vector consistency method uses a set of measures based on mode shapes (Harris, 1996). In this procedure a *modal assurance criterion* (MAC), is defined as a scalar constant which is a measure of consistency between a given modal vector and a reference modal vector, is defined as follows.

$$MAC_{crk} = \frac{\left| \psi_c^{k^H} \psi_r^k \right|^2}{\left(\psi_c^{k^H} \psi_c^k \right)\left(\psi_r^{k^H} \psi_r^k \right)} \qquad (4.1.4)$$

The comparison is made between reference modal vector *r* and the compared modal vector *c* for the *k*th eigenvector. Superscript H stands for the hermitian conjugate of a vector. The modal assurance criterion takes on values from 0, representing no consistent correspondence, to 1 representing a consistent correspondence. Based on this approach,

if the modal vectors truly exhibit a consistent relationship, the modal assurance criterion should approach unity.

Another modal assurance criterion is the *coordinate modal assurance criterion* (COMAC) (Harris, 1996). This measure is used to identify the degrees of freedom with the largest influence in a low value of MAC. A set of pairs of corresponding modal vectors is used to define COMAC as follows

$$COMAC_i = \frac{\left| \sum_{k=1}^{N} \psi_i^k \phi_i^k \right|^2}{\sum_{r=1}^{N} \psi_i^k \overline{\psi}_i^k \sum_{r=1}^{N} \phi_i^k \overline{\phi}_i^k} \qquad (4.1.5)$$

where ψ_i^k is the modal coefficient associated with the ith degree of freedom and kth modal vector from one set of modal vectors and ϕ_i^k is the modal coefficient associated with the ith degree of freedom and kth modal vector from the second set of modal vectors. The summation is extended over N modes of interest. Only those modes that match between the two sets are included in the computation.

4.2   Strain Based Delamination Detection Techniques

Delamination detection in a smart composite structure is in some respects different from any other damage detection technique. First of all, the delamination cannot be treated as a punctual or discrete damage. A refined modeling procedure must be employed to account for the presence of delamination as a continuous defect, even in the case when the delaminated zone is small. Also, from an experimental point of view a

comprehensive set of measurements must be performed to better characterize the changes in both static and dynamic parameters with and without delaminations. This should be followed by an accurate mathematical treatment of the experimental data.

Second, the presence of actuators induces discontinuities in both geometry and material properties of the structure. Large jumps in mechanical parameters such as strain, appear in the actuator zones. These jumps are misleading, especially in the case when a delamination is present and contribute to extra jumps.

Third, a composite structure is highly anisotropic. Therefore, minor changes appear in the natural frequencies and displacement mode shapes for relatively large delaminations. Researchers have observed less than 2-3% changes in the fundamental frequency with delamination area up to 20% of the composite structure (Shen and Graddy, 1991). This is a result of the strong coupling between different types of displacements and forces in the composite structure when the delamination breaks the continuity and the possible symmetry in the thickness direction.

Fourth, the previous research in delamination modeling and detection techniques for composites or smart composite structures used classical laminate theory or first order laminate theory. As shown by Chattopadhyay et al. (1998) and Dragomir-Daescu et al. (1998) the higher order theory is able to accurately model even thick composite structures. The contribution of the transverse effects is very important in the computation of natural frequencies for thick composites. Both the classical theory and first order theory largely overpredict the natural frequencies especially for higher natural frequencies. They also overestimate the higher eigenfrequencies when delaminations are present in the composite.

Finally, the presence of multiple delaminations was never accurately described. It is known that multiple small delaminations could produce similar changes in modes and natural frequencies as a single larger delamination.

In order to have multiple characterization of delamination, the previous criteria (MAC and COMAC) are modified to account for modal strains instead of modal displacements. It was observed by Chattopadhyay et al. (1998) that the strain is a more appropriate measure of delamination than classical mode shapes. Also, the gapped smoothing technique of Ratcliffe and Bagaria (1998) is extended to a two dimensional method suited for smart composite plates. The method is also modified to account for strains instead of curvatures. This is due to the following reasons. First, it is difficult to measure the curvature mode shapes for plates and second the Laplace's equation used to find the curvature from the mode shape amplifies both small numerical errors and experimental noise. The strain is also easily measured in experimental work using a variety of methods starting from strain gauge techniques, piezoelectric sensor measurements and more sophisticated Moiré's techniques and laser scanning.

The new *modal strain assurance criterion* (MSAC) is defined as a scalar measure of consistency between the modal strain of the healthy structure and the modal strain of the damaged structure. It also takes on values between 0-1. A good correlation of modal strains representing consistency is suggested by a value approaching unity.

$$\text{MSAC}_{rk} = \frac{\left(\sum_{m=1}^{m_{max}} \sum_{l=1}^{l_{max}} \left(\varepsilon_{ml}^{rk} \right) \left(\varepsilon_{ml}^{rk} \right)_{del} \right)^2}{\sum_{m=1}^{m_{max}} \sum_{l=1}^{l_{max}} \left(\varepsilon_{ml}^{rk} \right)^2 \sum_{m=1}^{m_{max}} \sum_{l=1}^{l_{max}} \left(\varepsilon_{ml}^{rk} \right)_{del}^2} \tag{4.2.1}$$

The summation in Eq. 4.2.1 is extended over the $(m_{max} \times l_{max})$ elements in the plate for both the healthy and the damaged structures (denoted by subscript 'del'). In Eq. 4.2.1, k is the mode of interest and index r=1,2,6 accounts for the appropriate inplane strain. Subscript indices m and l denote the element position in the plate (Fig. 4.1). This index is expected to give better indication of mode consistency because the absolute differences between modal strains of the healthy structure and the damaged structure are larger than the corresponding differences between modal displacements.

An extension of the modal strain assurance criterion is the *coordinate modal strain assurance criterion* (COMSAC). The COMSAC attempts to identify the element, if any, that contributes to a low value of MSAC. The COMSAC is calculated over a set of modal strain pairs, undelaminated versus delaminated. The two modal strains correspond to the same modal vector, but the set of modal strain pairs represents all modes of interest in a given frequency range (number of modes, N). For the sets of modal strains that are compared, there is a value of COMSAC computed for each element modal strain. COMSAC is defined as follows

$$\text{COMSAC}_{ml} = \frac{\left| \sum_{k=1}^{N} \varepsilon_{ml}^{rk} \left(\varepsilon_{ml}^{rk} \right)_{del} \right|^2}{\sum_{k=1}^{N} \left(\varepsilon_{ml}^{rk} \right)^2 \sum_{k=1}^{N} \left(\varepsilon_{ml}^{rk} \right)_{del}^2} \tag{4.2.2}$$

where, ε_{ml}^{rk} is the strain corresponding to the *k*th mode of vibration in the *ml*th element of the undelaminated structure while $\left(\varepsilon_{ml}^{rk} \right)_{del}$ is the similar strain in the delaminated structure. In the above equation is assumed that there is a match for every modal strain in

the two sets. Only those strains that match between the two sets are included in the computation.

A third damage index is developed by modifying the existing gapped smoothing technique (Ratcliffe and Bagaria, 1998) shown in Eqs. 4.1.2-3. First, extension is made to a two dimensional search procedure over the area of a plate and second, the polynomial coefficients are determined using the inplane strains rather than curvature. As shown before when using strains, the Laplace's difference equation is bypassed thereby eliminating an important source of errors. Also, the strains contain by far much more information than classical curvature because they are computed using the entire displacement field functions. By contrast, the curvature computation is based only on the out of plane displacements.

Strains are also a more accurate measure from an experimental point of view. It is easier to measure inplane strains from the free response or the forced response of a structure than to measure curvature from the frequency response functions. As shown in the work by Ratcliffe and Bagaria (1998), the experimental modal curvature is so noisy that even the curvature of the first mode is difficult to identify. In their work, the relative error in experimental curvature is reported to be on the order of 50-70% which can definitely obscure the effect of delamination. By comparison, the modal strains can be easily measured within an accuracy of 5-10%.

The procedure developed here locally fits a bicubic polynomial to one of the inplane strains. As shown in Fig. 4.1, the index m in x direction and l in the y direction are not included in the computation of the bicubic.
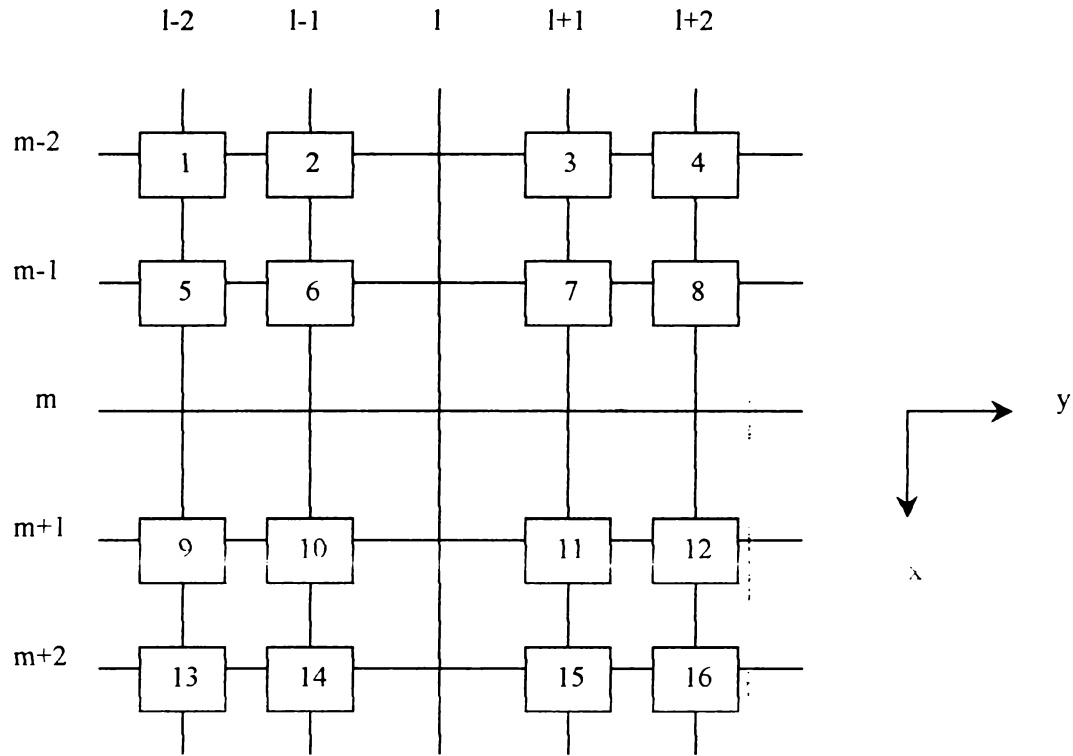
Figure 4.1.   Mesh for bidimensional gapped smoothing procedure

The gapped polynomial, calculated for the *(m,l)* component of the inplane strain is the product of two cubics, one for direction x and the other for y direction. This is defined as follows.

$$
\begin{aligned}
p(x, y) = {} & c_0 + c_1 x + c_2 y + c_3 x^2 + c_4 xy + c_5 y^2 + c_6 x^3 + c_7 x^2 y + c_8 xy^2 \\
& + c_9 y^3 + c_{10} x^3 y + c_{11} x^2 y^2 + c_{12} xy^3 + c_{13} x^3 y^2 + c_{14} x^2 y^3 + c_{15} x^3 y^3
\end{aligned}
\tag{4.2.3}
$$

The coefficients c_0, c_1,...,c_{15} are calculated using the strains $\varepsilon^{rk}_{m-2,l-2}$, $\varepsilon^{rk}_{m-2,l-1}$,..., $\varepsilon^{rk}_{m+2,l+2}$ of the 16 neighbors of *ml*th element (Fig. (4.1)). It must be noted that five elements with either a subscript *m* or *l* are not included in the calculation of the polynomial coefficients. This results in a system of 16 equations with 16 unknowns.

$$p(x_i, y_j) = \varepsilon_{ij}^{rk}, \qquad i = m-2, m-1, m+1, m+2, \qquad j = l-2, l-1, l+1, l+2 \qquad (4.2.4)$$

The damage index d_{ml} for the mlth element is calculated from the polynomial and the corresponding strain, as follows.

$$d_{m,l} = \left[p(x_m, y_l) - \varepsilon_{ml}^{rk} \right]^2 \qquad (4.2.5)$$

This is computed for each element, except the elements on two outermost rows on each side of the plate that do not have a complete set of neighbors. Note that the procedure described above do not require un undamaged reference. The method operates solely on the computed or measured strains of the damaged structure. Eliminating the need for an undamaged reference implies that the strain distribution for the undamaged structure is smooth and continuous. This also implies that the structure has no stiffness discontinuities. For structures with discontinuities for example, smart composite plates with surface bonded or embedded actuators and sensors, the method can be improved by comparing the damage index determined for the delaminated structure with that obtained from an undelaminated one.

A fourth measure of delamination is also proposed. This procedure eliminates the need for smooth and continuous strain distribution and is therefore applicable to the detection of delaminations in a smart composite plate. However, an undamaged reference is necessary. The inplane modal strains of the delaminated structure are compared with those of a similar healthy structure. The difference in modal strains is squared to diminish the small numerical errors or experimental noise. The new damage index is defines as follows

$$\delta_{ml} = \left[\varepsilon_{ml}^{rk} - \left(\varepsilon_{ml}^{rk} \right)_{del} \right]^2 \qquad (4.2.6)$$

where subscript *ml* refers to the element under investigation, subscript *r* is the number of vibration mode for which the modal strain is computed and k=1,2,6 refers to the appropriate strains. The damage index uses strains ε_1 and ε_2 for bending mode shapes and ε_6 for torsional mode shapes. Usually the modal strain corresponding to the first mode of vibration or a few lower modes is sufficient to properly identify the damaged zone.

As shown by Chattopadhyay et al. (1998) the delamination detection methods based on modal strain are more reliable than those based on classical mode shapes. A comparison of all of the methods described, for practical cases of composite and smart composite plates with delaminations is presented in the next chapter. The higher order theory and the continuity conditions presented in chapters 2 and 3 are used in the modeling of delamination. The finite element procedure discussed in chapter 3 is used to discretize composite plates with actuators and delaminations.

5.   Numerical Results

The finite element implementation of the developed theory must be correlated with other approaches to ensure its validity and accuracy. In this chapter, validations of the higher order theory applied to composite and adaptive structures in the presence of delaminations are presented. Comparisons are made with published experimental data and results obtained using the commercial finite element code NASTRAN. Next, results obtained using the present theory are presented to study the influence of delaminations and piezoelectric actuation on composite. The results from the higher order theory are also compared with those obtained using the classical laminate theory and the first order shear deformation theory for a wide range of plate thickness. Finally, the damage in the structure is characterized using the damage indices discussed in chapter 4.

5.1   Validation

5.1.1   Undelaminated Cantilever Composite Plate

In this section the results obtained using the developed higher order based technique, implemented using the finite element method, is compared with those obtained using NASTRAN (Chattopadhyay et al, 1998-1999). Numerical results are presented for a Graphite/Epoxy $[0^{o}/90^{o}]_{2s}$ composite strip plate with material properties E_1=134.4 GPa, E_2=10.3 GPa, G_{12}=G_{13}=5GPa and v_{12}=v_{12}=0.33. The plate dimensions are such that length a=0.127 m, width b=0.0127 m and total thickness h=0.001016 m (Fig. 5.1). A

15x4 finite element mesh is used to generate the inertia and stiffness matrices with the degree of accuracy required for the modes considered.
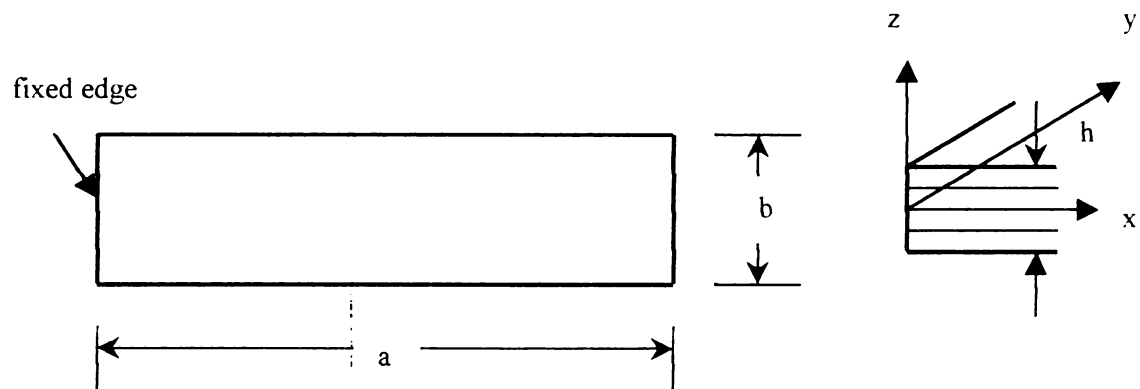
Figure. 5.1. Composite plate geometry

The results are presented in Table 5.1 where the first 10 natural frequencies obtained using the current approach are compared with NASTRAN results. Both CHEXA 3D elements and CQUAD 2D elements are used in NASTRAN modeling. The results from the current approach are very close to NASTRAN 3D results, the largest difference in natural frequencies being less than 3%. As expected all the natural frequencies obtained from the current approach are slightly greater than NASTRAN 3D results. This is due to the fact that the present theory is still a 2D plate theory leading to slightly stiffer numerical model compared to NASTRAN 3D model which uses a full three dimensional elasticity approach. The results based CQUAD elements, however are based on a first order theory and produces worse results than the proposed higher order theory. For example, the third and eighth natural frequencies are 5% and 6% smaller than the corresponding 3D solutions. However, the trend is not consistent and some natural

frequencies are greater than NASTRAN 3D solutions (the first and fourth) while other frequencies are smaller. For example, overall, the total error between the NASTRAN 3D and 2D approaches is two times larger than the total error between NASTRAN 3D and the present model. This proves the accuracy of the higher order theory over a large frequency domain, 0-4600Hz.

It is important to note that the computational effort associated with NASTRAN 3D modeling is much larger compared to the higher order theory. This is because a 3D mesh is necessary to model elements in each layer of the composite. The complexity increases with increase the number of plies since larger global matrices are obtained when the number of plies is large. By contrast, using the present theory, the calculation of the plate element properties is independent of the number of plies. The associated modeling time and CPU time for generating element matrices for a larger number of plies, using the present approach, is a small fraction of the total CPU time required in the calculations of the dynamic properties of the plate such as natural frequencies and mode shapes.

Table 5.1   Natural frequencies for a cantilever plate (Hz)

Mode no.	Present theory	NASTRAN 3D	NASTRAN 2D
1	82.116	81.878	81.94
2	513.34	511.45	509.38
3	610.33	597.31	567.33
4	877.54	860.85	863.47
5	1431.8	1428.1	1412.9
6	1888.8	1839.1	1746.64
7	2790.9	2790.8	2735.71
8	3329.4	3234.1	3050.1
9	4581.1	4580.1	4457.3
10	4717.3	4600.0	4535.1

5.1.2   Cantilever Composite Plates with Delaminations

In this section the influence of delaminations on first natural frequency of composite delaminated plates is studied. The results from the current theory are compared with published experimental results and NASTRAN 3D approach. The test articles are cantilever plates with geometry and material properties similar to one used in the previous section. Each plate has a through-the-width delamination of varying length (β). The delamination is placed at different laminae interfaces, at a distance z_d measured

from the laminate midplane as shown in Fig. 5.2. The center of delamination coincides, in all cases, with the center of the plate.

The finite element implementation accounts for different thicknesses and stacking sequences of regions with and without delamination. A 5x4 mesh is used to model each zone of the plate, both undelaminated ends and the two top and bottom sublaminates. The mesh density used can accurately model the important modes of vibration including a few bending modes, torsion modes and lateral bending modes. Also, some local sublaminates modes, appearing in cases with larger delamination are modeled appropriately.
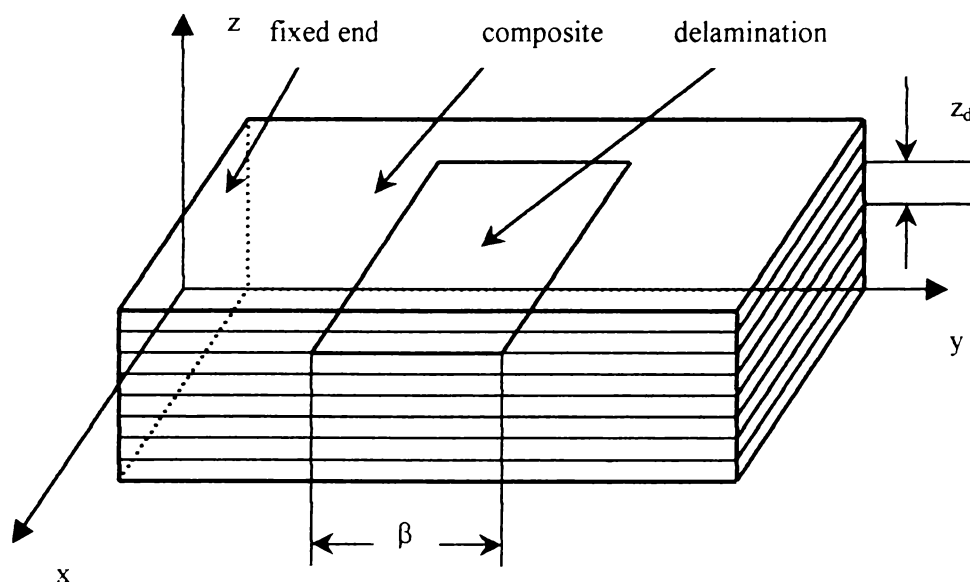
Figure. 5.2. Composite plate with delamination
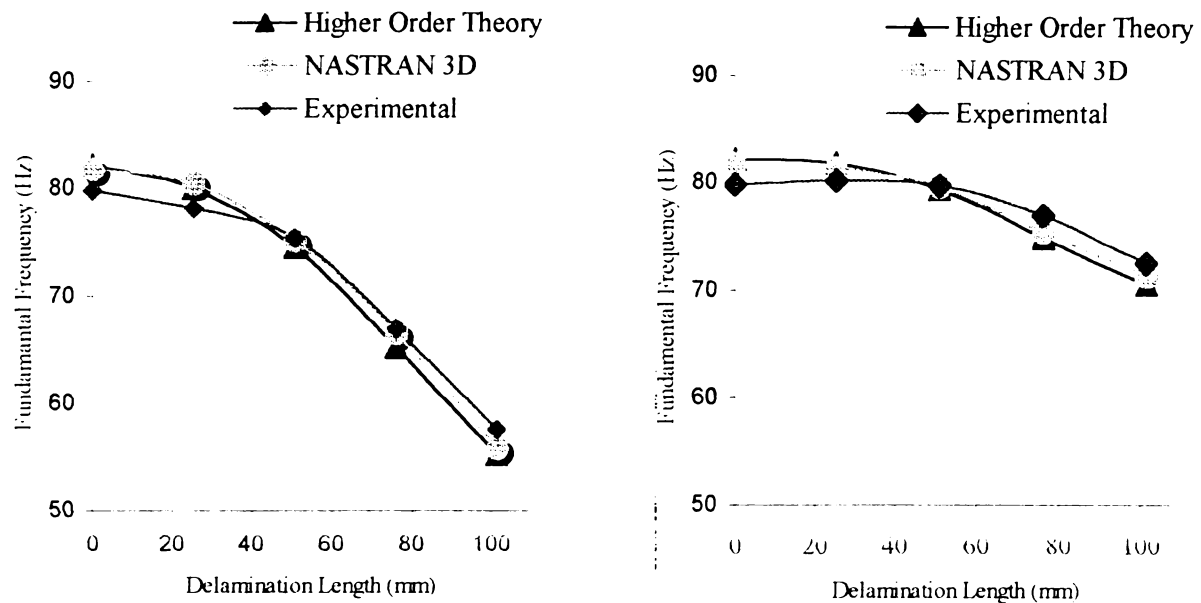
a. Midplane delamination, $z_d=0$.   b. Off midplane delamination, $z_d=0.279$ mm

Figure 5.3. Comparison of first natural frequency variation with delamination length.

The results from both the current higher order theory and NASTRAN 3D are compared with experimental results obtained by Shen and Grady (1991). As seen in Fig. 5.3 there is a very good agreement between the current approach and NASTRAN model over the entire range of delamination length, (β=0-100 mm). This proves that the higher order theory and the continuity conditions at the delamination lateral boundary as implemented in chapter 3 are very effective in modeling composites with delaminations. Both NASTRAN and higher order theory results slightly deviate from the experimental results, particularly in the case without delamination (β=0) or for small delamination lengths. The largest deviation is smaller than 3% which can be attribute to both experimental errors on one hand and modeling and numerical errors on the other hand.

Overall, the accuracy obtained using the higher order theory, with and without delaminations, allows the introduction of further complexity such as actuation. In section 5.3 smart composite plates with and without delaminations will be investigated. It must be noted the NASTRAN 3D computation expenses with modeling in the presence of delamination, is quite large compared to the higher order theory.

5.2   Thick Composite Plates

In this section the current implementation of the higher order theory is compared with results using other existing approaches. Numerical results from the present theory are presented along with results from the classical laminate theory and the first order theory to asses the importance of accurately modeling the transverse shear effects. Two parametric studies are presented. In the first study, the variation of natural frequencies with plate thickness is studied using all the three theories. The ratio a/h is varied between 125 representing a very thin laminate to 10 representing a very thick laminate. In the second study, for a thick composite plate, a midplane delamination of variable length β is introduced. The variation of natural frequencies with β is presented using all three theories.

5.2.1   Variation of Natural Frequencies with a/h

Plates as shown in Fig. 5.1 are considered as test articles. The inplane dimensions and material properties are the same as in section 5.1.1, while the thickness h is a variable

parameter. A 15x4 mesh is used to generate the natural frequencies in all three theories. The variation of the first two natural frequencies, corresponding to the first two bending modes, are shown in Fig. 5.4 a and b. The third natural frequency, corresponding to the first twisting mode, is presented in Fig. 5.4 c.

As expected, the agreement between all theories is good for thin plates. However, significant differences between the classical theory and the other theories occur for thicker plates with smaller a/h ratio. This is due to the fact that classical theory does not consider transverse shear effects and therefore cannot accurately describe the dynamics of thicker composites. The first order theory, introduces transverse shear deformation through a constant distribution of the strain through the thickness. Therefore, the transverse shear effects are not modeled accurately. The higher order theory, which uses the same number unknowns as the first order theory, allows for a quadratic variation in transverse shear deformation and consequently produces a more realistic lower stiffness model.

As seen in Figure 5.4 a, the first natural frequency is highly overestimated by the classical theory, especially for thick plates while the first order and the higher order theories are in good agreement. Larger differences between the theories are observed in Figs 5.4 b and c, for the second bending natural frequency and the first torsional natural frequency, respectively. Even the first order theory overpredicts these frequencies. The natural frequencies from the higher order theory are smaller, as expected, because the transverse shear deformation is better approximated in this theory.

The results obtained indicate that it is necessary to include an accurate description of the transverse shear stresses which is important in composites due to the large ratio between the directional material properties, Young's moduli and shear moduli. The transverse shear effects increase with plate thickness, resulting in larger deviations between theories as a/h reduces. Therefore, the present theory is applicable to plate of moderately large thickness.
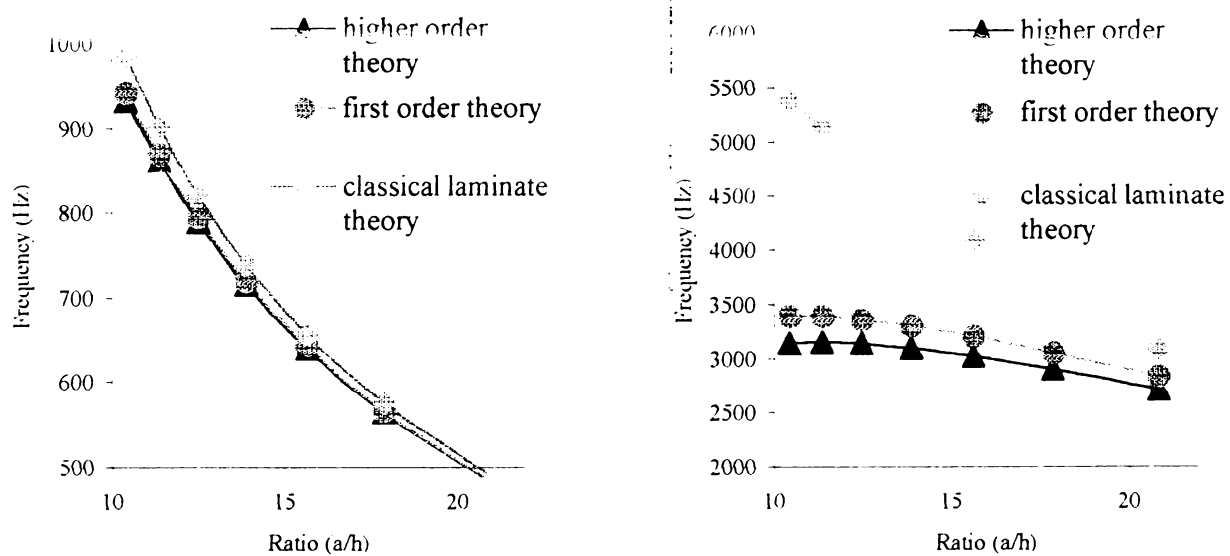
a. First bending natural frequency. b. Second bending natural frequency.

Figure 5.4. Variation of first three natural frequencies with a/h.
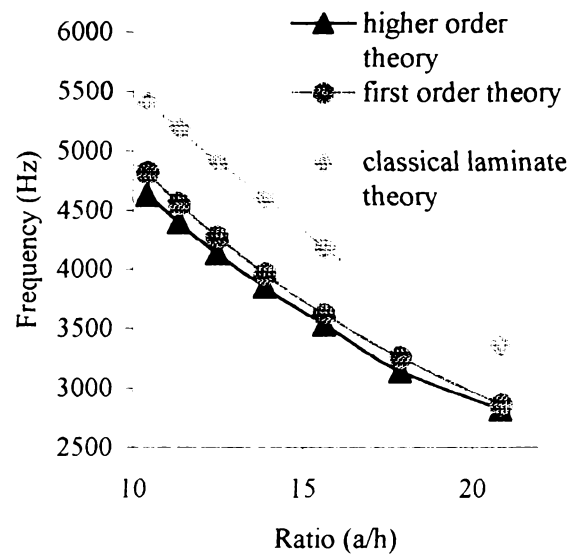
c. First torsional frequency

Figure 5.4. cont.

5.2.2 Delaminated Thick Composite Plates

In this section the effect of midplane through-the-width delaminations on thick composite plates is investigated. It is assumed that a single delamination of variable length β is located symmetrically with respect to plate length. The normalized delamination length varies between 0%, (undelaminated plates), and 90% of the total length of the plate (Figure 5.2). The inplane dimensions and material properties are the same as in section 5.1.1.

A 5x4 mesh is used to model the undelaminated zones and the two sublaminates, above and below the delamination interface. The continuity conditions, introduced chapter 3 are employed at the delamination lateral boundary. The same three theories are employed in the evaluation of the first two natural bending frequencies and the first torsion frequency for laminates with various delamination lengths. It must be noted that

for these thick plates, the importance of shear deformation is particularly important in the thicker undelaminated zones.

Figures 5.5 a-c present the variations of plate natural frequencies with changes in the delamination length β. The first order theory slightly overestimates the values of the first natural frequency, while the classical theory shows significant deviation (Fig. 5.5 a). The differences are more evident in higher natural frequencies (Figs 5.5 b-c). The higher order theory once again yields the smallest value because of a more accurate representation of the transverse shear deformation. It is seen that the transverse shear effect becomes larger as the delamination length reduces. This can be explained as follows. For short delamination length, the global dynamics of the plate is determined mainly by the total laminate thickness. Therefore, transverse shear effects are dominant in these cases. For relatively longer lengths, the dynamics of each thinner sublaminate become prevalent thereby reducing the transverse effect.
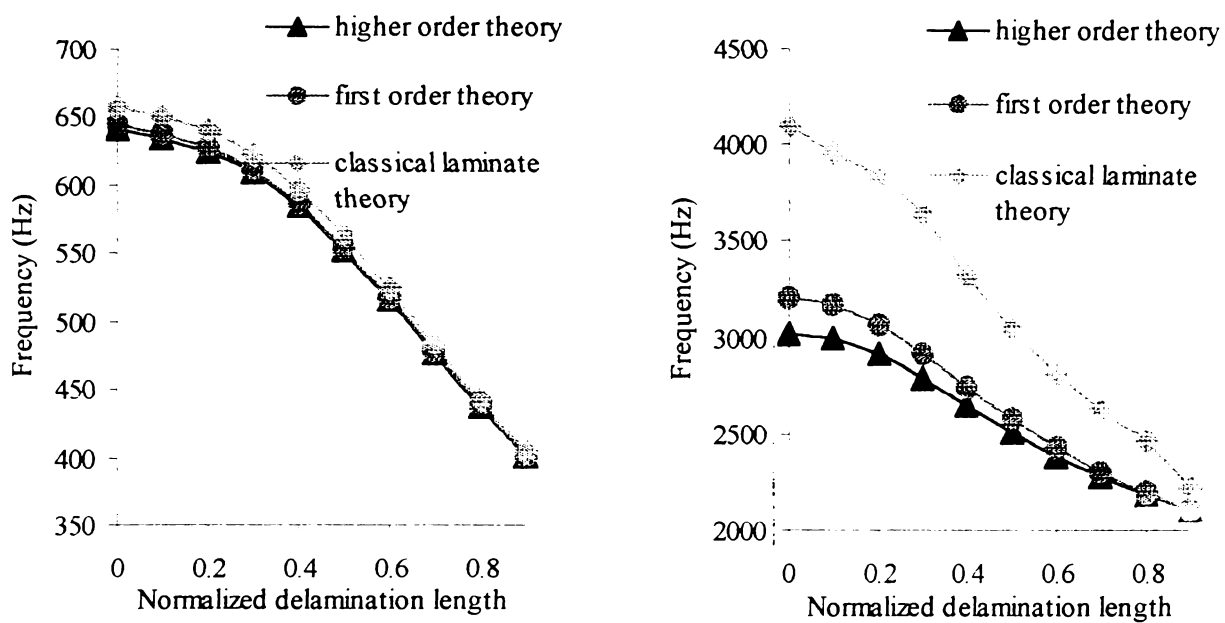
a. First bending natural frequency.

b. Second bending natural frequency.
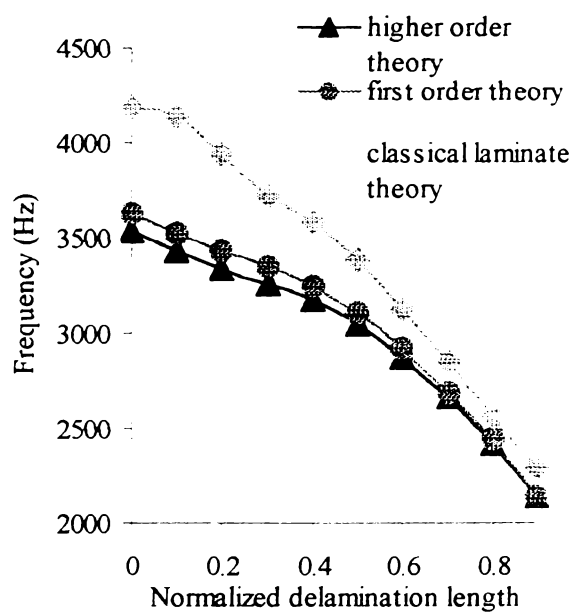
c. First torsion natural frequency.

Figure 5.5. Variation of natural frequencies with delamination length.

5.3   Strain Characterization of Delaminated Smart Composites

The modeling technique developed in chapters 2 and 3 is employed to analyze the effect of delaminations on a composite plate with piezoelectric actuators. The analysis uses the refined displacement field which carefully accounts for both the presence of distributed actuators and delaminations. Independent displacement fields are used in each zone where a change in thickness due to delamination or surfaces bonded actuators modifies the geometry and/or the material properties. The effect of delamination is investigated under both static and dynamic conditions. Piezoelectric forces computed in chapters 2-3 are used to produce static deflection of smart composite plates. The analysis is implemented using the finite element method. Numerical results presented indicate significant changes in mechanical parameters due to a small delamination.

5.3.1   Static Results

The test article is a graphite/epoxy cantilever smart composite plate with three pairs of surface bonded actuators. The composite substrate has eight plies with stacking sequence $[0^{o}/90^{o}/45^{o}/-45^{o}]_{s}$ and material properties , E_{1}=134.4 GPa, E_{2}=10.3 GPa, v_{12}=0.33, G_{12}= G_{13}=5 GPa, G_{23}=2 GPa, ρ=1477 Kg/m^{3}. Delaminations are introduced between the fourth and the fifth plate layers (Figs. 5.6 and 5.7). The length of the plate is a=0.127 m, the width is b=0.0508 m and the total thickness h=0.001016 m. Two additional PZT layers accounts for actuators in bimorph configuration. The material properties of piezoelectric material are E=63 GPa, v=0.33, G=24.2 GPa, ρ=7600 Kg/m^{3},

$d_{12}=254\text{x}10^{-12}$ m/V. The piezoelectric actuator pairs have dimensions of $L_p=0.0254$ m, $h_p=0.000254$ m and $b_p=0.0127$ m, located as shown in Fig.5.7.
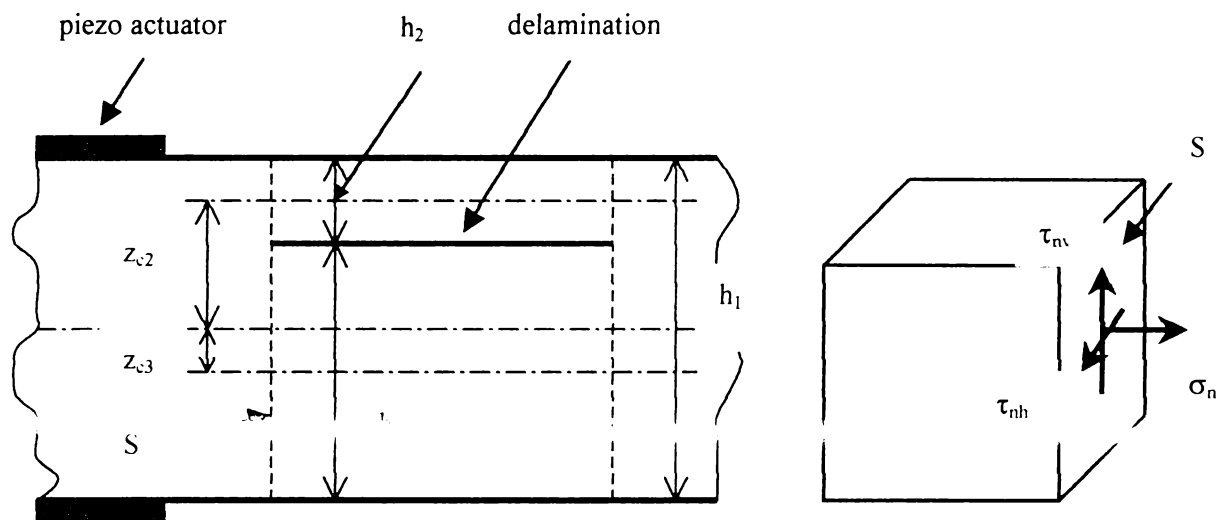
Figure 5.6. Laminate cross section and stresses on S.

Numerical results are presented for a smart composite plate with one end clamped and others free. The delamination is located at a distance of 0.0381 m from the clamped end and has a length $\beta=0.00127$ m. It must be noted that in this example the delamination lies in a region which is not covered with PZT actuators. A global 25x4 mesh is used to model the smart composite plate while local 5x4 meshes are used for the two top and bottom sublaminates.

The effect of static actuation on normal strain distributions for plates without and with delamination is presented next. The normal strains are influenced by the presence of delamination only in the delamination region (Figures. 5.8 a and b). The presence of the normal strain ε_2 (in the width direction) in this zone is due to the camber of the plate under static actuation while the longitudinal strain ε_1 is due to Poisson's effect. As seen

from these figures, there is a large jump in the strains between the regions with and without actuators. This is due to the concentrated nature of the induced strain and the change in thickness between the plate regions with and without surface bonded actuators.
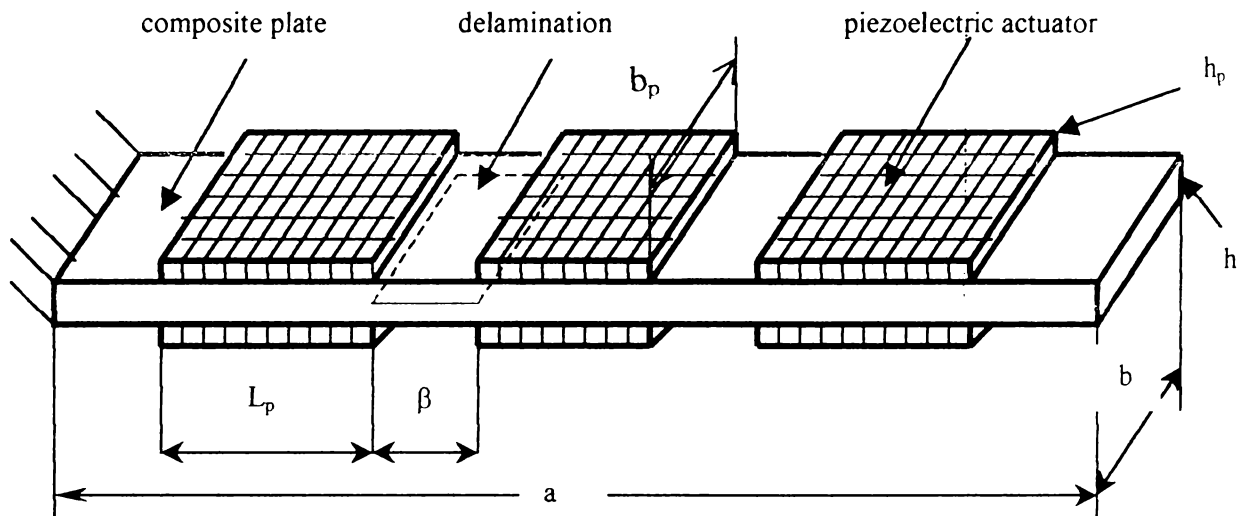
Figure 5.7. Delaminated plate with piezoelectric actuators

Because the delamination lies outside the region covered by the actuators the actuation generalized forces are not affected by the presence of delamination. Also, the delamination region is free of any external force.

a. Normal strain ε_1 – static actuation.   b. Normal strain ε_2 – static actuation.
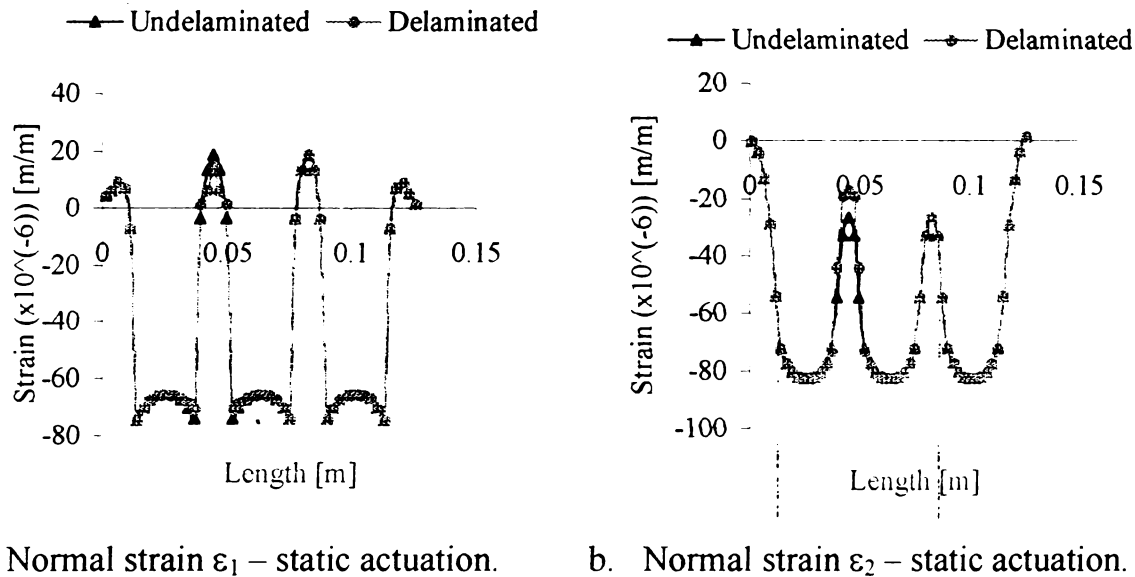
Figure 5.8.   Strain distribution (without and with delamination).

5.3.2   Dynamic Results

The same delaminated smart composite plate model, as in previous section, is used to determine the influence of delaminations in dynamic properties. The changes in mode shapes and dynamic modal strain are computed in an attempt to identify the important differences between healthy and damaged structures. Therefore, a 50x4 mesh is used in the finite element implementation. This mesh density allows for a very good characterization of bending and torsion mode shapes and the associated derived variables such as strains and stresses. The strain results are presented for points belonging to the plate longitudinal axis of symmetry.

Figures 5.9 a and b present comparisons between the first two mode shapes for the undelaminated and the delaminated plate, respectively. For a small delamination, as in Fig.5.7, the difference between the mode shapes is insignificant. In addition, this

difference extends over a very large zone. Also, the maximum difference does not occur at the middle of the delamination region. This makes it difficult to use the mode shapes for locating delaminations.
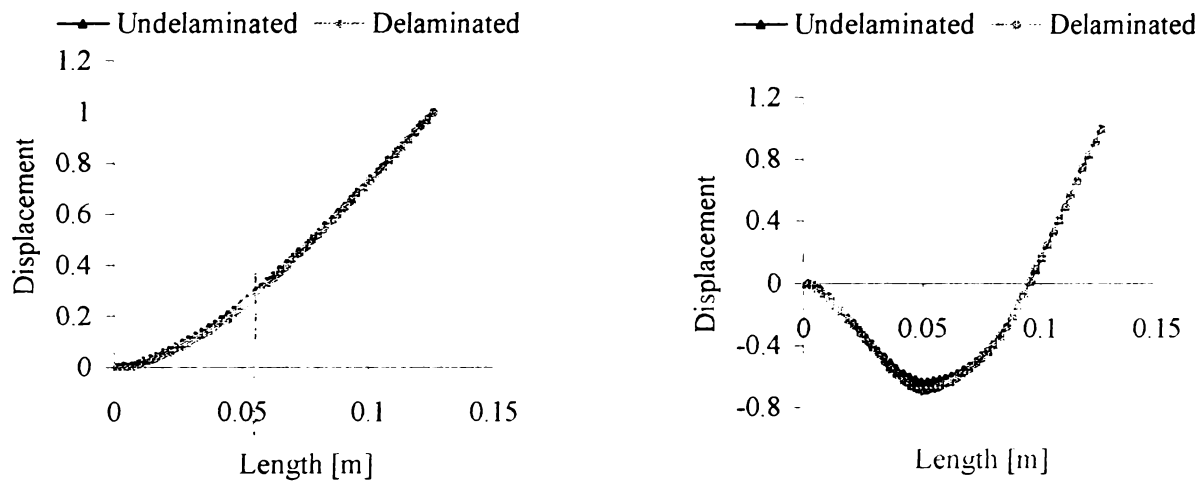
a. Out of plane displacement-first mode   b. Out of plane displacement-second mode

Figure 5.9.   First two bending mode shapes (without and with delamination).

Figures 5.10 and 5.11 present the normal strains ε_1 and ε_2 corresponding to the first two bending modes for the undelaminated and the delaminated plate, respectively. As seen from these figures very significant changes are observed in strains for cases without delamination and with delamination. The changes are concentrated in the region of delamination. Therefore, if a sensor is placed on the top of this region, the measured strain from this sensor will provide a strong indication of the presence of delamination. However if in the absence of a sensor in that particular location, the influence of delamination on strains will be very hard to detect.
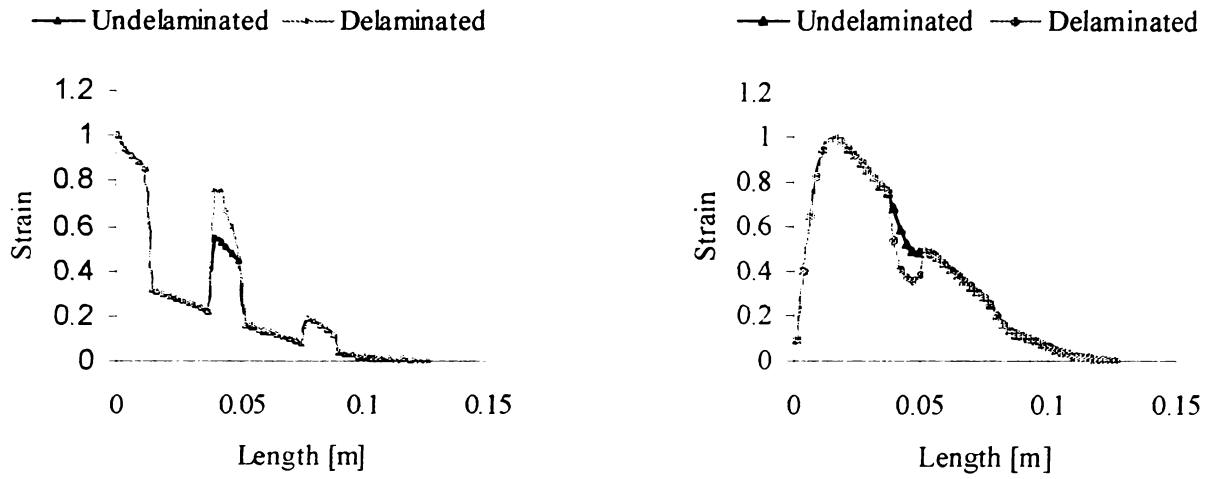
a. Normal strain ε_1.

b. Normal strain ε_2.

Figure 5.10.   Modal strain distribution, first mode of vibration.
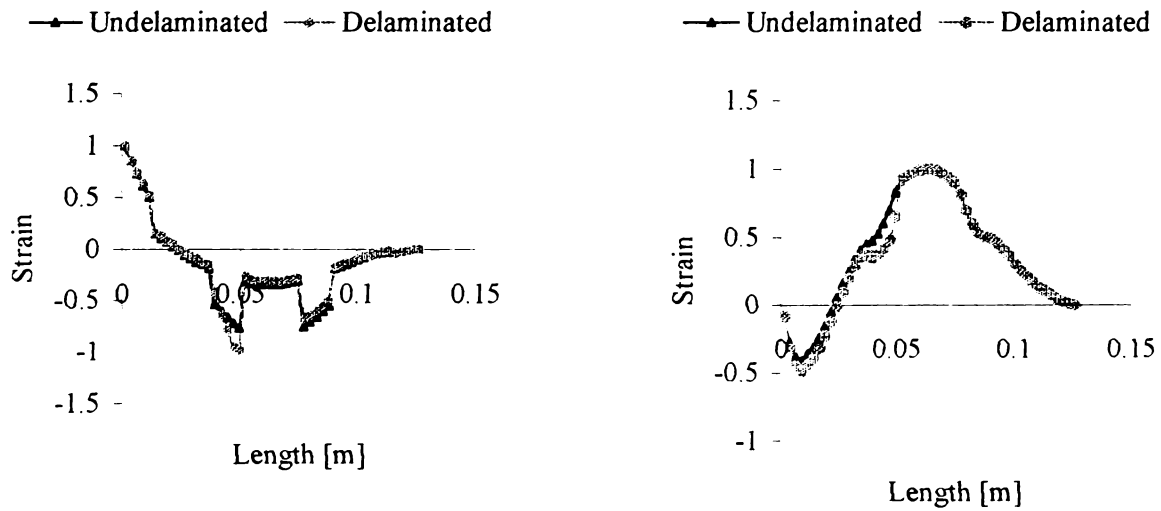
a. Normal strain ε_1.

b. Normal strain ε_2.

Figure 5.11. Modal strain distribution, second mode of vibration.

5.4   Damage Detection Results

Composite and smart composite plates with single or multiple delaminations are analyzed in this section. Various sizes and locations of delaminations are considered. Numerical investigation is conducted to search for significant differences in modal strains corresponding to various mode shapes of composite structures. Therefore, a postprocessing of data, resulting from the finite element analysis, is required. The postprocessor was written and designed to compute the derived variables such as strains from the primary variables obtained from the finite element processor. It is also able to extract and plot the out of plane displacement mode shapes and all the associated inplane strains.

Both composite and smart composite plates are analyzed. The smart composite plates, even in the absence of delamination, behave differently from their composite counterparts. The influence of thickness and material property changes, on active actuated zones, complicates the analysis particularly if delaminations and actuators are present in the same zone of the plate. Care must be taken to differentiate between the strain variation due to piezo actuators and delamination influence.

Finally, for each case presented in this section, multiple characterizations of damage are used in an attempt to identify the position and extension of delaminated zone. For this purpose the damage indices introduced in the previous chapter are employed. A processor for damage indices was implemented. Since in experiments, data are contaminated with noise, the results from the finite element postprocessor are perturbed

with random noise. The damage indices are recomputed for data with noise and their robustness is measured with respect to noise ratio.

5.4.1 Composite Plates

In this section the higher order theory is used to compute mode shapes, modal strains and damage indices of delaminated composite laminate. The geometry of the test structure is shown in Fig. 5.12. This laminate consists of eight plies, each with thickness 1.27 mm and stacking sequence $[0°/90°/0°/90°]_s$. First, a single delamination is introduced between the fourth and the fifth plies. The length of delamination is one third of the length of the plate as shown in Fig. 5.13 a. Then, two delaminations, assumed to be symmetrically placed with respect to the ends of the plate, are considered (Fig. 5.13 b). The material properties of the laminate are as follows: E_1=60 GPa, E_2=25 GPa, G_{12}= G_{13}=12 GPa, G_{23}=4.8 GPa, ρ=1500 Kg/m^3. The inplane dimensions are a=0.2 m and b=0.053 m corresponding to a length to thickness ratio of 20.

<u>Single Delamination</u>: For this case (Fig. 5.13 a), the mode shapes and modal strains are obtained using a 15x4 global mesh while each sublaminate is modeled using a 5x4 mesh. This meshsize was determined from a trade-off study conducted between accuracy and CPU time requirements. Also for the gapped smoothing technique index, this mesh is at the lower limit in the y direction. With four elements per width the above index is computed using gapping in x direction only and smoothing in both x and y directions. The other indices are computed as discussed in chapter 4.

The sequence of computations is as follows. First, the healthy structure is discretized using the global mesh. A finite element processing is performed and the nodal variables, u_0, α, v_0, β, w_0, $w_{0,x}$, $w_{0,y}$, $w_{0,xy}$ are calculated at each of the 550 nodes of the global mesh. At this stage, the postprocessor extracts the out of plane displacement mode shapes. Then the postprocessor converts the displacement variables into strains and plots the modal strains associated with the various mode of vibrations.
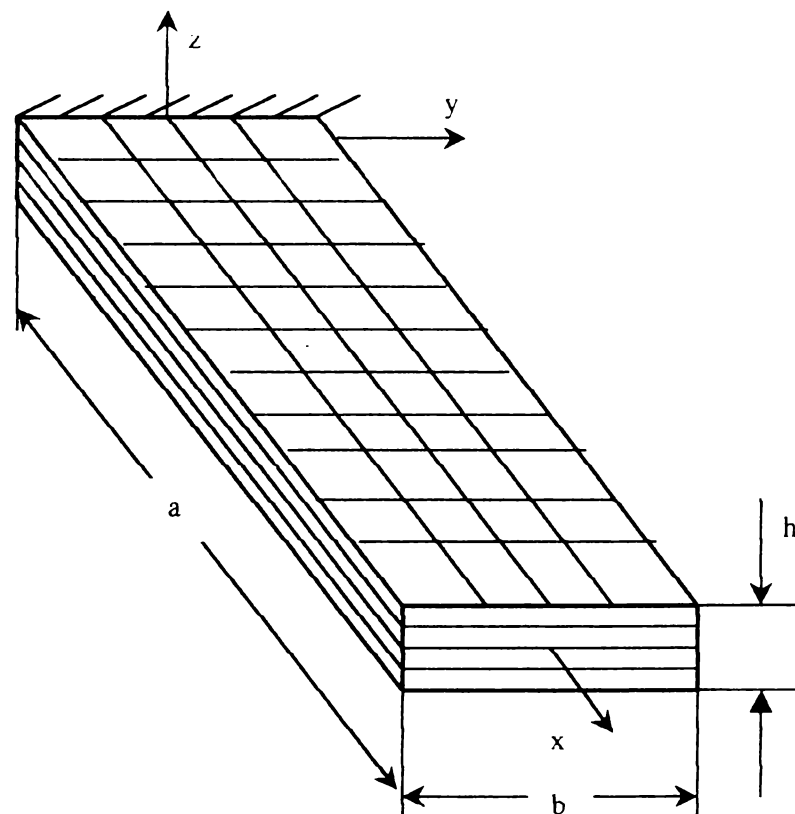
Figure 5.12. Healthy composite plate.

When delamination is analyzed, the process is somewhat different. First, two sets of elements and nodes are assigned to the top and bottom delaminated sublaminates. A connectivity table takes care of the position of each element, node and material properties

in the mesh. Even the finite element processor is different. The elements with nodes on delamination lateral boundary, S (Fig. 5.13 a) are transformed and those node variables are related to the nodes in the healthy laminate zone as shown in chapters 2 and 3. This process occurs during the finite element assembly stage. It was pointed out in chapter 3 that this approach allows for significant savings in both memory requirements and CPU processing time. The obtained time saving is on the order 40-80% depending on delamination geometry. In Fig. 5.13, indices l and m corresponds to the global mesh and are used to generate the mesh and the element connectivity table. The natural frequencies and mode shapes are calculated next. The delaminated element displacements are than converted back to the local system of node displacements for those nodes being on S. The postprocessor then computes the modal strains and the results are obtained. The damage index processor is then invoked and the indices are plotted. As discussed before, in this last stage a random perturbation of finite element results is allowed to account for noise. The robustness of each damage index can then be checked.

For the case shown in Fig 5.13 a, the first three mode shapes are computed. In Figs. 5.14 (a-c) the modes of the undamaged plate are shown while in Figs. 5.15 (a-c) the modes of the delaminated plates are presented. Insignificant changes between the two cases are observed which do not allow for damage identification. Moreover if a 5% random noise is used to perturb the data the small changes are hidden by the perturbation. This further proves that the mode shape approach does not allow a correct detection of delamination position and size.

a. Single delamination

b. Two delaminations.
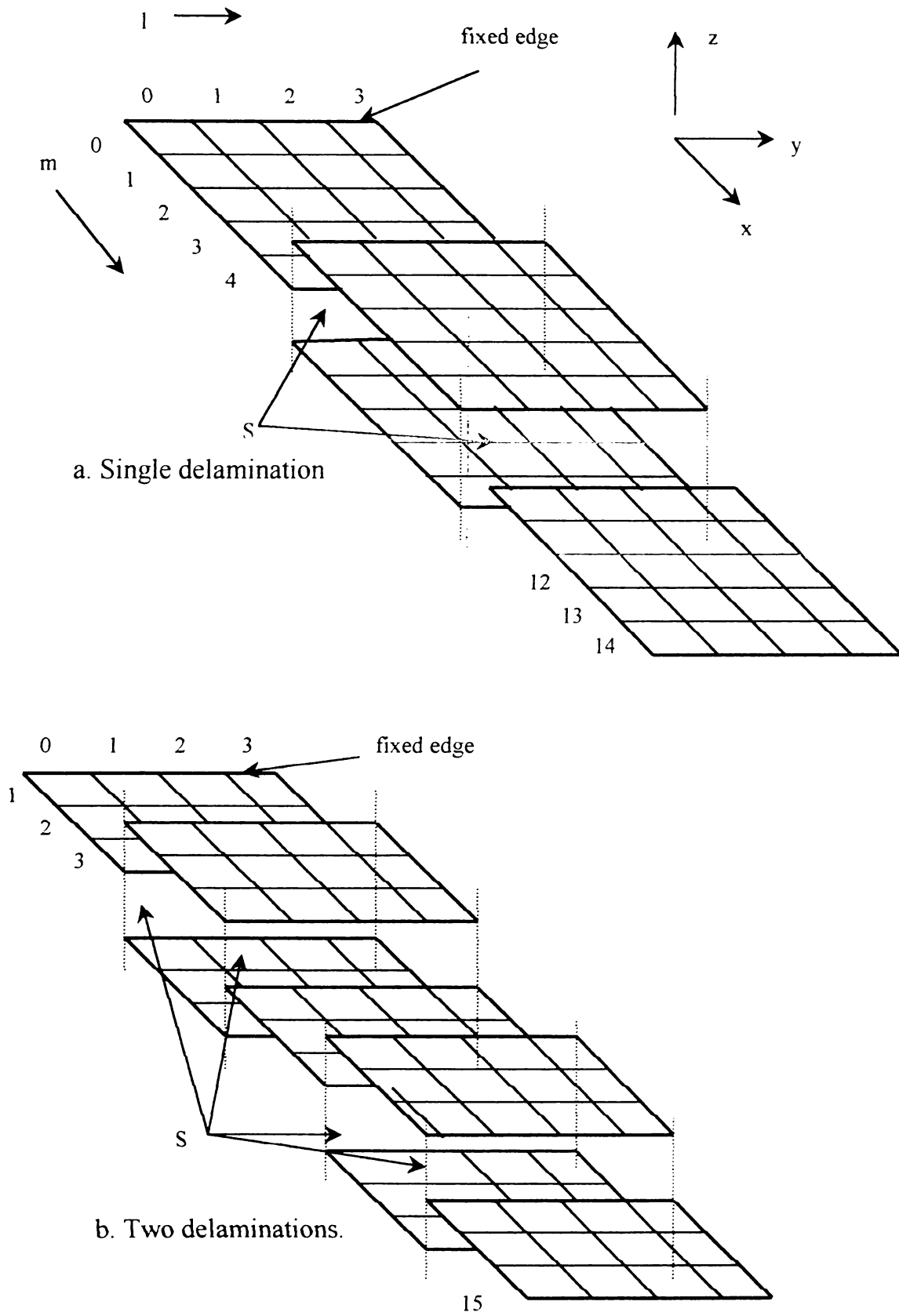
Figure 5.13. Delaminated plates, finite element meshes.
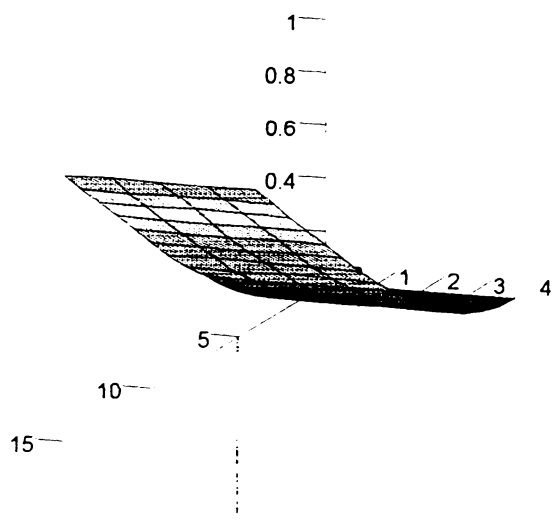
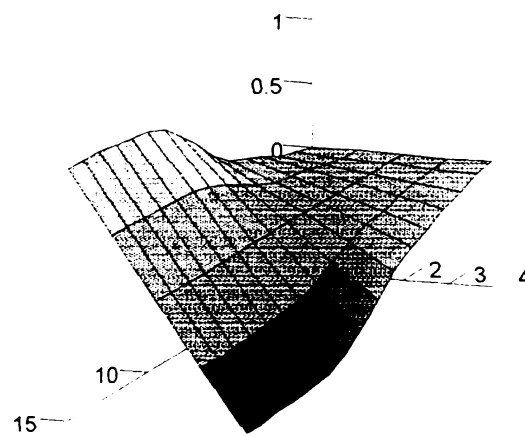a. First bending.
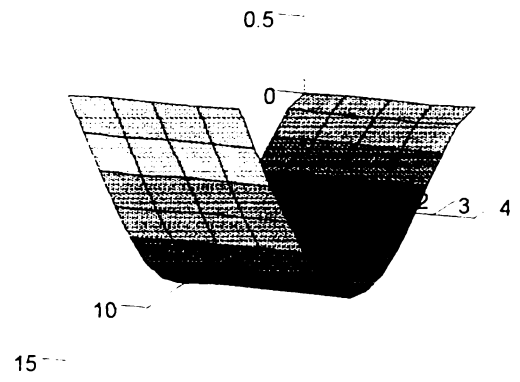
b. Second bending.
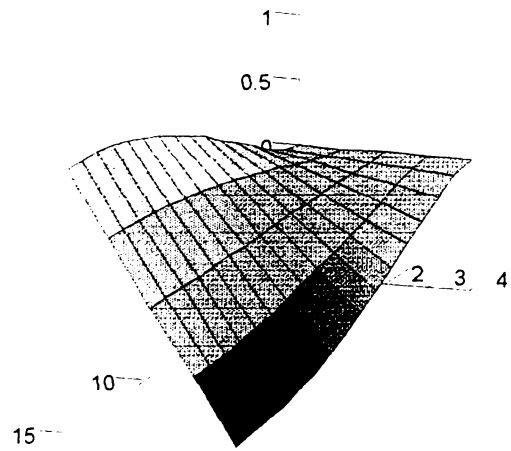
First twist.

Figure 5.14.   First three modes of vibration, undamaged structure.
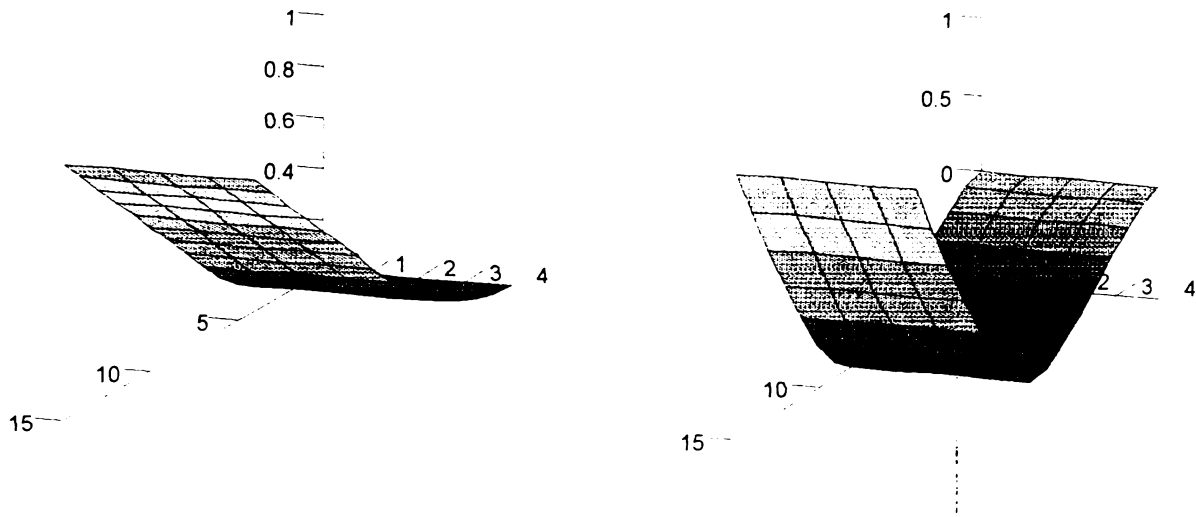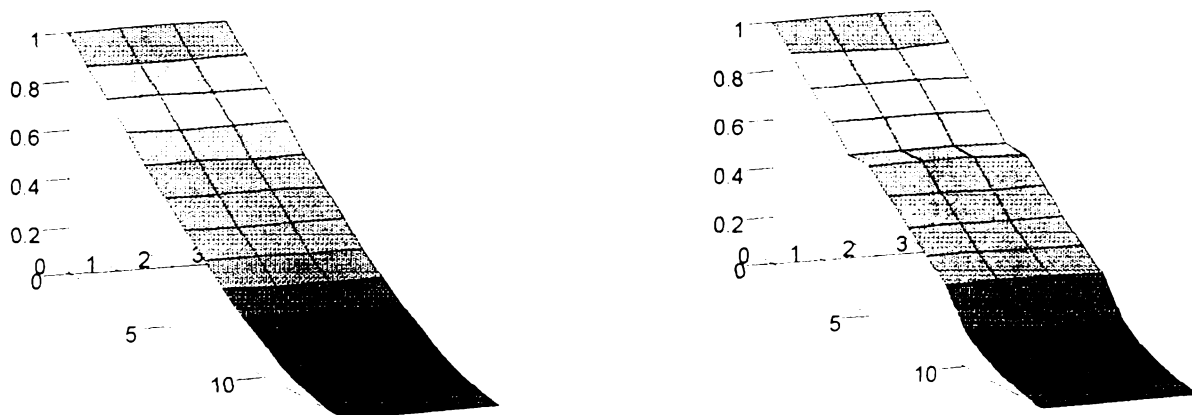
a. First bending

b. Second bending

c. First twist

Fig. 5.15 First three modes of vibration for a single delamination.

Next, the modal strains are computed from the eigenvectors of both the healthy and the damaged structures. The best computation accuracy is obtained when computing the strains at the centroid of each element or at the Gauss points of one order less quadrature method. In this work the centroids are used. The distributions of the strain ε_1 corresponding to the first bending mode, without and with delaminations are presented in Figs. 5.16 a and b, respectively. Very noticeable changes are observed between the two cases. The strain in the damaged plate is significantly different over the entire delamination zone compared to the undamaged reference. This deviation forms the basis for the damage detection techniques presented in chapter 4.

a. Without delamination.   b. With delamination

Figure 5.16. Modal strain ε_1, first bending mode.

Figures 5.17 a and b present the modal strain ε_2 for the first bending mode. The changes in strain, although noticeable, are not as significant as in ε_1. This is due to the fact that for this beam like type bending mode, important changes occur in the longitudinal strain. Naturally, the changes in inplane strain, ε_6, are even less important since no inplane deformation is produced by the first bending mode in the healthy plate. However, due to the cross coupling between the displacements in the presence of delamination, some inplane shear deformation is generated. The inplane shear strain distributions for this mode are not shown here.
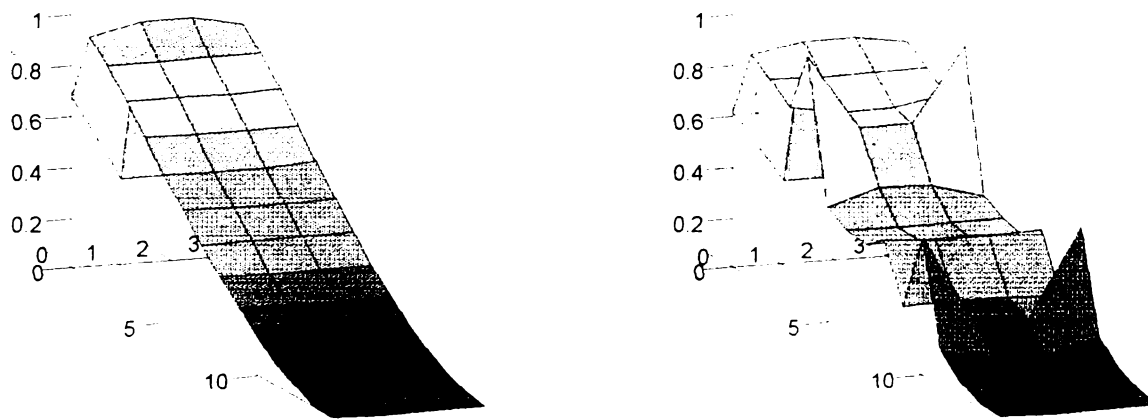
a. Without delamination.   b. With delamination.

Figure 5.17. Modal strain ε_2, first bending mode.

However, this information can be used as an indicator of delamination if the twist modes are analyzed. The modal strain distributions, for the first twist mode, of both

undelaminated and delaminated plates are presented in Figs. 5.18 a and b respectively. Important changes are observed indicating the inplane shear (ε_6) is an appropriate measure of delamination when considering twist deformation. More important, the inplane shear deformation for the delaminated plate significantly deviates from its healthy reference only in the delaminated zone (elements with m=5,6,...,9 and l=1,2,3,4 in Fig. 5.13 a). This deviation is due to a smaller twist stiffness when delamination is introduced in the structure. The two sublaminates in the delaminated zone do not have the same capacity to resist twist as the undelaminated reference. A structure with reduced stiffness to twist, exhibits a different shear deformation distribution. The coupling between the various displacement degrees of freedom affects the overall behavior of inplane shear modal strain over the plate surface.
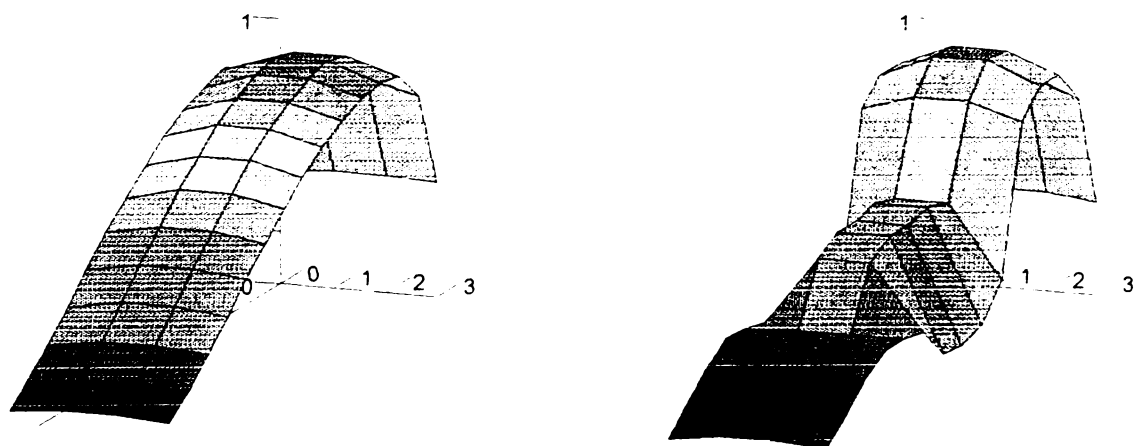
a. Without delamination.   b. With delamination.

Figure 5.18. Modal strain ε_6, first twist mode.

Depending on plate geometry, material properties, boundary conditions and delamination position and size one or more modal strains must be considered. For practical cases, the bending, twist, camber and inplane modes interlace and some modal strains can be more useful than the others. However, only a few lower modes can be accurately measured in experimental work therefore attention is restricted to those modes. The higher modes are also affected by larger errors even in the finite element implementation.

The damage indices introduced in chapter 4 are now used in an attempt to identify delaminations. In the case of a plate with a single delamination shown in Fig. 5.13 a, all four indices are calculated. Both MSAC and COMSAC, (Fig. 5.19), fail to identify the presence of delamination. For example, considering the longitudinal strain ε_1, MSAC gives a value of 0.992 which can suggest a very good correlation between the healthy and the damaged cases. This is explained as follows. The modal strains are computed for the same structure, therefore the strain distributions are in good agreement over a large area of the plate. From a damage detection point of view this index is not reliable. The COMSAC is computed taking into account different modal strains for different modes of vibration. For example, when considering the longitudinal strains for the first three mode pairs of healthy and damaged structures COMSAC exhibits the behavior shown in Fig. 5.19. The shape of COMSAC index surface exhibits irrelevant and inconsistent variations. Moreover, some of the largest jumps occur out of the delaminated zone. Neither MSAC or COMSAC are therefore appropriate as damage detection criteria. However, it must be noted when considering the classical mode shapes, the differences

between the delaminated and undelaminated cases are even smaller. Also, it must be noted that the two classical indices, MAC and COMAC produce even less significant results (Pandey et al., 1991).
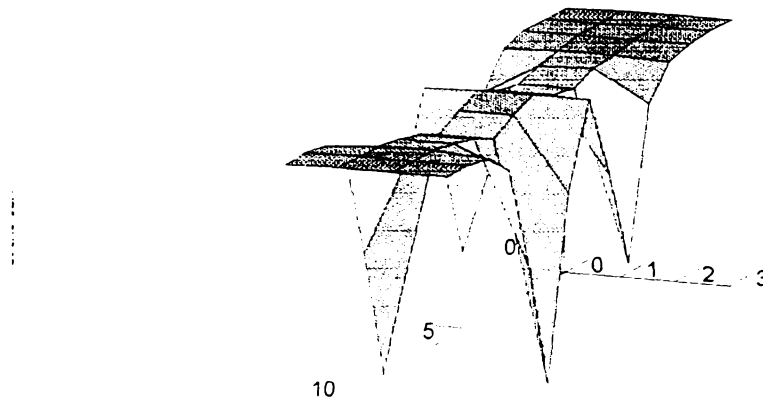

Figure 5.19. COMSAC index representation.

The other two damage indices introduced in chapter 4 are now used to characterize delaminations. First, the index derived from the gapped smoothing technique is computed and plotted over the area of the plate. The strain distribution shown in Fig. 5.16 is used here. As seen in Fig. 5.20 (a) this index shows the presence of the damage in the plate. However, for elements with m = 6, 7, 8, the value of the index is very small. Besides, elements with m = 3, 4 or m=10, 11, 12 are incorectly shown as delaminated. It must be noted that this index uses information from the damaged structure only. Using a healthy plate reference, the damage prediction can be improved as shown in Fig. 5.20 (b). Even so, elements with m=4 or m=10 are incorrectly shown as belonging to the

delamination zone. Therefore, this index artificially increases the size of the delaminated zone. This is due to the fact that the smoothing technique that uses neighboring elements in computing the damage index. Thus, the contribution of delaminated elements is artificially distributed to some neighboring undelaminated elements.
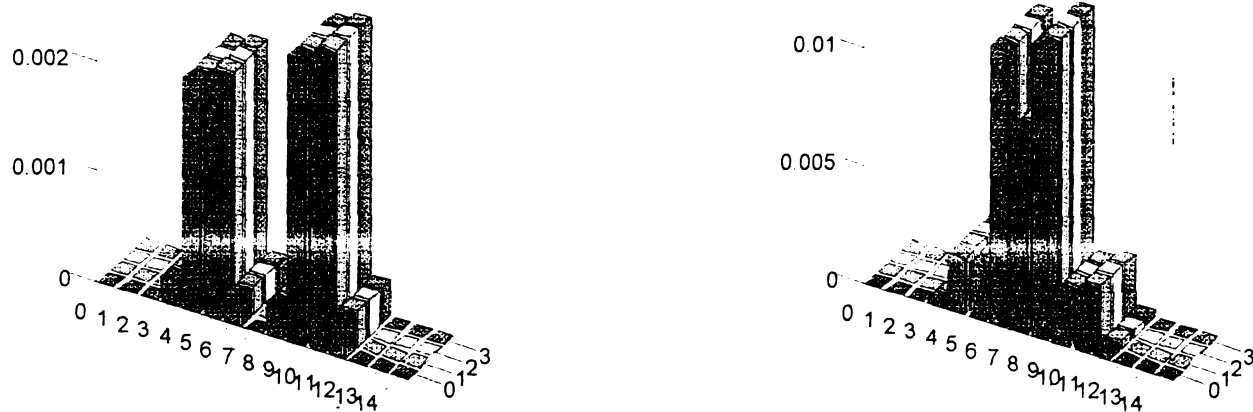
a. Gapped index, without reference.   b. Gapped index with healthy reference.

Figure 5.20. Gapped smoothing technique index.

The new damage index defined in Eq. 4.2.6 is computed next. This damage index calculated using longitudinal modal strains (Fig. 5.16), is presented in Fig. 5.21. It is observed that it precisely indicates the delamination position and size (elements with m=5,6,..,9 and l=1,2,3,4). None of the healthy zone neighbors are included in the damaged zone prediction. This damage index can also be used in experimental work when the appropriate modal strain distribution is measured.
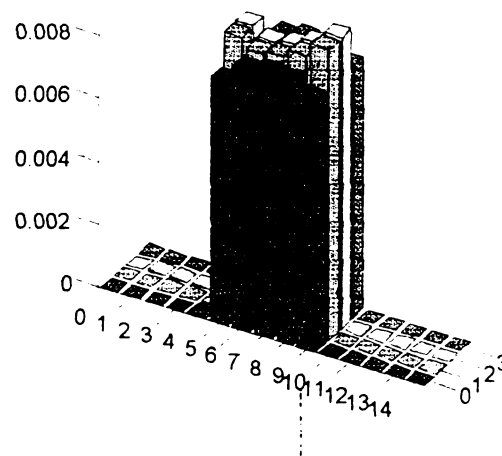
Figure 5.21. Damage index defined in Eq. 4.2.6.

Next, the robustness of the last two indices is assessed. It is known that both numerical results and experimental data are affected by errors. To simulate errors and to check the reliability of the damage indices in the presence of noise, numerical data obtained from the finite element postprocessor are perturbed with random noise. This study takes into consideration absolute random perturbation in the range 0-5 percent from the maximum value of strain. The worst case scenario is shown in Fig. 5.22. A 5% random noise almost diffuses the influence of delamination in the longitudinal modal strain for the first mode of vibration. In this case, the MSAC and COMSAC indices again give erroneous indications. For example the value of MSAC is 0.993 which can lead to the incorrect conclusion that no difference exists between the damaged and undamaged structures.

The other two indices are now tested in the presence of noise. First the gapped smoothing technique is used for the delaminated case. Figure 5.23 (a) shows the values of

this index without using an undelaminated reference. While showing that damage is present, this index again overestimates the extent of delamination. Elements next to the delaminated area are affected once again by those in the delaminated area. When an undelaminated reference is used, as in Fig. 5.23 (b), the accuracy is improved However, an error of 7% in delamination position detection occurs implying a shift of one element along x direction. The index in Fig. 5.23 (b) is however reliable and robust to data noise.

a. Without delamination.   b. With delamination.
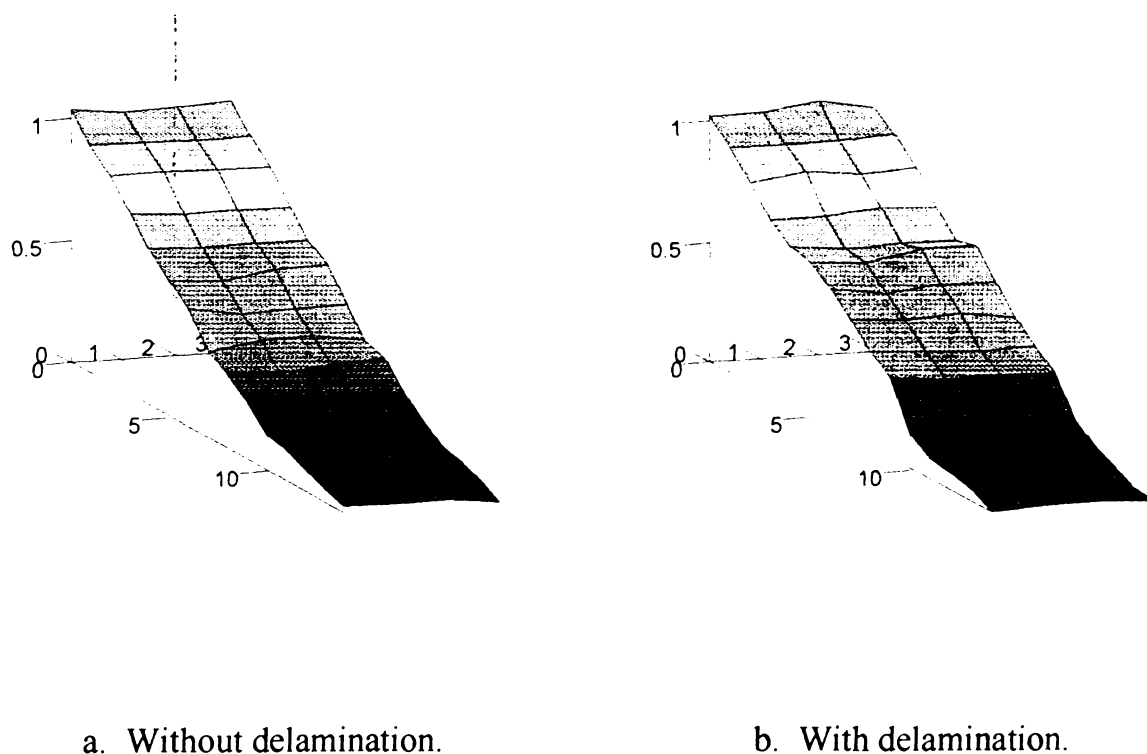
Figure 5.22.   Modal strain ε_1, first bending mode (5% noise).

The most effective and robust index is again that computed using Eq. (4.2.6). As shown in Fig. 5.24, the position and size of delamination is exactly determined. This index can be implemented easily in experimental work. Different methods of exciting the first mode of vibration, without much interference from other modes, can be utilized.

Data filtering can be applied if necessary. The strains can be measured, simply, using strain gauge techniques or piezoelectric sensors.
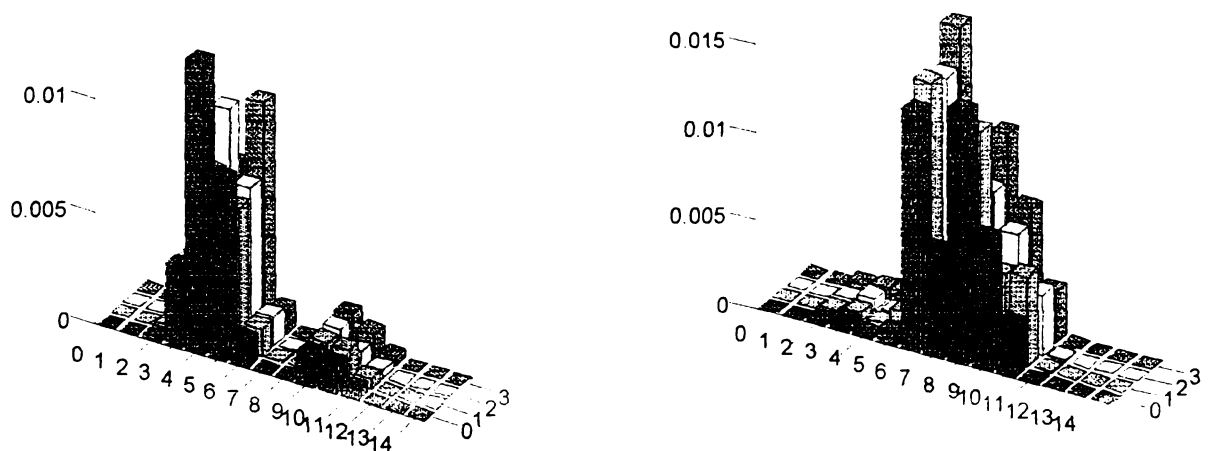
a. Gapped index, without reference.   b. Gapped index with healthy reference.

Figure 5.23. Gapped smoothing technique index (5% noise).
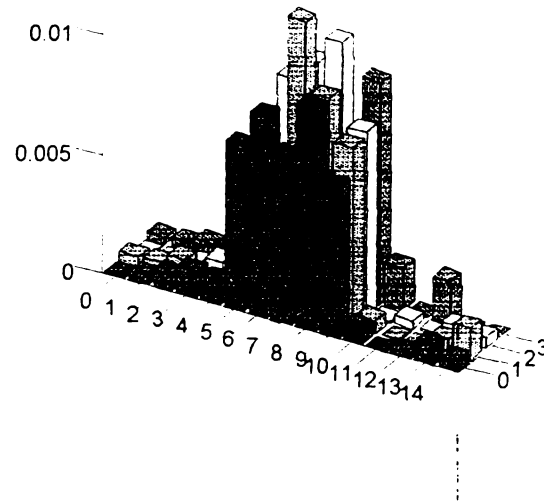
Figure 5.24.   Damage index defined in Eq. 4.2.6 (5% noise).

Multiple Delaminations

The case shown in Fig. 5.13 (b) is considered now. Two delaminations are assumed to be symmetrically placed with respect to the fixed edge and the free edge. In this case the mode shapes and modal strains are obtained using a 15x4 global mesh while each sublaminate is modeled using a 3x4 mesh. The finite element model consists of 105 plate elements with a total of 800 degrees of freedom. The implementation of the continuity conditions presented in chapters 2 and 3 allows for important savings in computation time. When compared to penalty approach or Lagrange multipliers method, the memory requirements and CPU time are almost half.

The most important changes between the healthy and the damaged structure appear once again in the longitudinal strain distribution as seen in Figs. 5.25 a and b. As expected, the delamination placed near the fixed edge (Fig. 5.13 b), produces a stronger

change in strain than the one placed near the free end. This behavior is because of imposing Dirichlet boundary conditions at the fixed end. The longitudinal strain corresponding to the first mode of vibration is maximum at the fixed end and any delamination influence is larger here (Fig. 5.25 b).
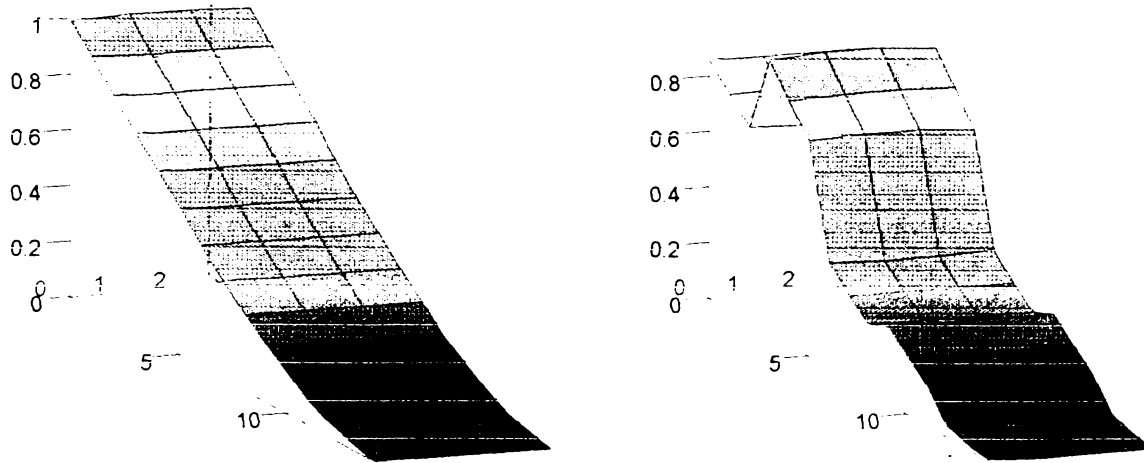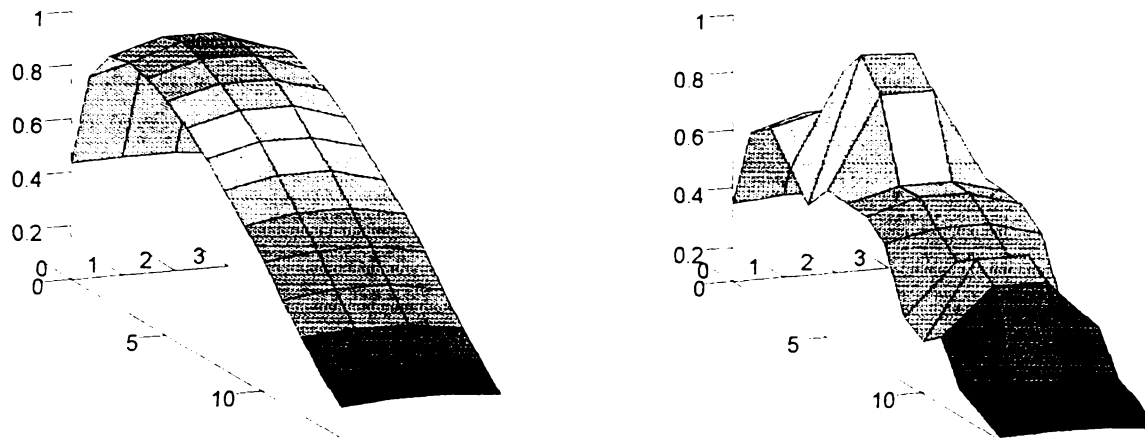

a. Without delaminations.   b. With delaminations.

Fig 5. 25 Modal strain ε_1, first bending mode.

Figures 5.26 a and b shows the inplane shear strain for the third mode of vibration which is a twist mode. Again, as for the longitudinal strain for the first mode of vibration, the changes due to delaminations are important only in the delaminated zones, that is for elements with m=3,4,5 and m=9,10,11 in the healthy mesh. The change in strain distribution shows that damage is present in the structure.

a. Without delaminations. b. With delaminations.

Figure 5.26 Modal strain ε_6, first twist mode.

As for a single delamination, the damage indices are used to characterize the influence of delaminations. Figures 5.27 a and b present the gapped smoothing technique index, without and with an undamaged reference, respectively. Both these indices show that damage is present in the structure. However, they fail to correctly identify the position and extent of delaminations. Therefore, they should be limited to a single delamination case and only for qualitative analysis.
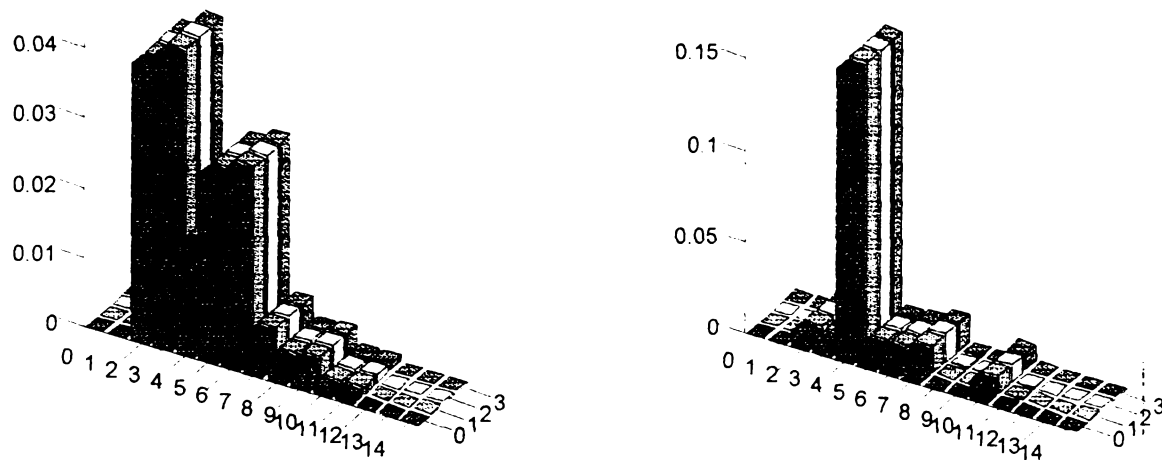
a. Gapped index, without reference.   b. Gapped index, with healthy reference.

Figure 5.27. Gapped smoothing technique index.

Next, the damage index based on Eq. 4.2.6 is computed. The result is shown in Fig. 5.28. The delaminated zone near the clamped end of the plate is precisely located. Elements with $m=3,4,5$ in the global mesh have a very high damage index compared to their neighbors. Also, for the delamination placed near the free end, elements with $m=9,10$ are correctly identified as belonging to the damaged zone. However, for $m=11$ the damage index is slightly larger than for $m=12$, in the healthy part of the plate. This is due to the fact that the delamination is very close to the free end and the longitudinal deformation is very small even without delaminations. Overall, this damage index is very accurate in delamination detection. It shows both delaminated zone locations. The extent

of delaminations placed in the zones with very small strains can be either overpredicted or underpredicted.
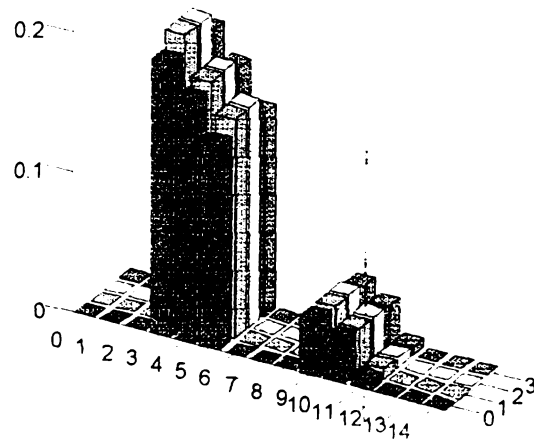
Figure 5.28. Damage index defined in Eq. 4.2.6.

Finally, the robustness of this damage index with respect to data errors is investigated. Random noise is assumed to perturb the distribution of longitudinal strain shown in Fig. 5.25. The damage index is computed for noise ratio up to 10% from the maximum values of strains. For the largest noise ratio the damage index (based on Eq. 4.2.6) is plotted in Fig. 5.29. As can be seen here, the delaminations are still correctly identified. The position and extent of the delaminated zone near the clamped end is also identified exactly. Because of its robustness in the presence of noise, this damage index can be successfully used in damage detection for multiple delamination case.
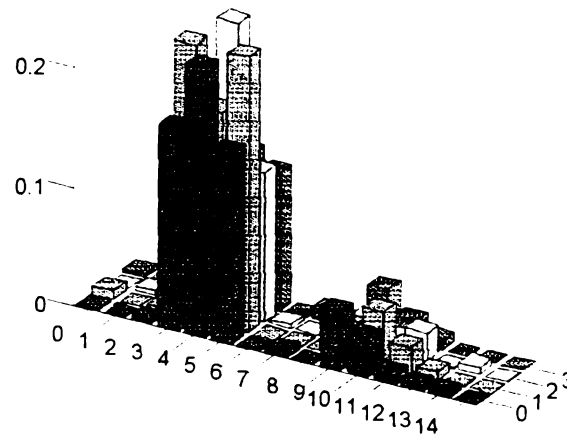
Figure 5.29. Damage index defined in Eq. 4.2.6 (10% noise).

5.4.2 Smart Composite Plates

In this section the higher order theory is employed to analyze delaminated composites with piezoelectric actuators. The problem becomes more complex because the zones where actuators are placed have different material properties. For surface bonded actuators, the thickness of active zones is also different compared to the composite substructure zones. Active forces induced by an applied electric field are also produced. These forces are used to control either the shape or the dynamic characteristics of the composite plate. In addition, further complexity is introduced when considering delaminations. Therefore, all combinations off zones without or with actuators and without or with delaminations must be considered. Different types of finite elements are used to implement the higher order theory for each zone. Also, active piezoelectric force vectors for elements with actuation are computed.

Table 5.2. Material properties for smart composite plates.

	E_1 (GPa)	E_2 (GPa)	ν_{12}	G_{12}, G_{13} (GPa)
Carbon-Epoxy AS/H3501	138	8.96	0.30	7.10
PZT	63	63	0.33	24.2

	G_{23} (GPa)	ρ (Kg/m^3)	$d_{03}(\times10^{-12}$ m/V)	
Carbon-Epoxy AS/H3501	2.9	1477	254	
PZT	24.2	7.6		

The test structure, shown in Fig. 5.30, is an adaptive composite plate with dimensions a=240 mm, b=135 mm and total thickness of composite zone h=3 mm. Four pairs of piezoelectric layers with length L_p=75 mm, width l_p=45 mm and thickness h_p=0.5 mm are assumed to be bonded to the plate surface. The material properties for both the composite substructure and the piezoelectric layers are shown in Table 5.1. The stacking sequence for this composite plate is $[90°,0°,45°,-45°,0°,90°]_s$. In the delaminated case a single through the width delamination of length β=45 mm is assumed to be placed between layers 7 and 8 of the composite plate. The numbering of layers starts with the bottom layer.
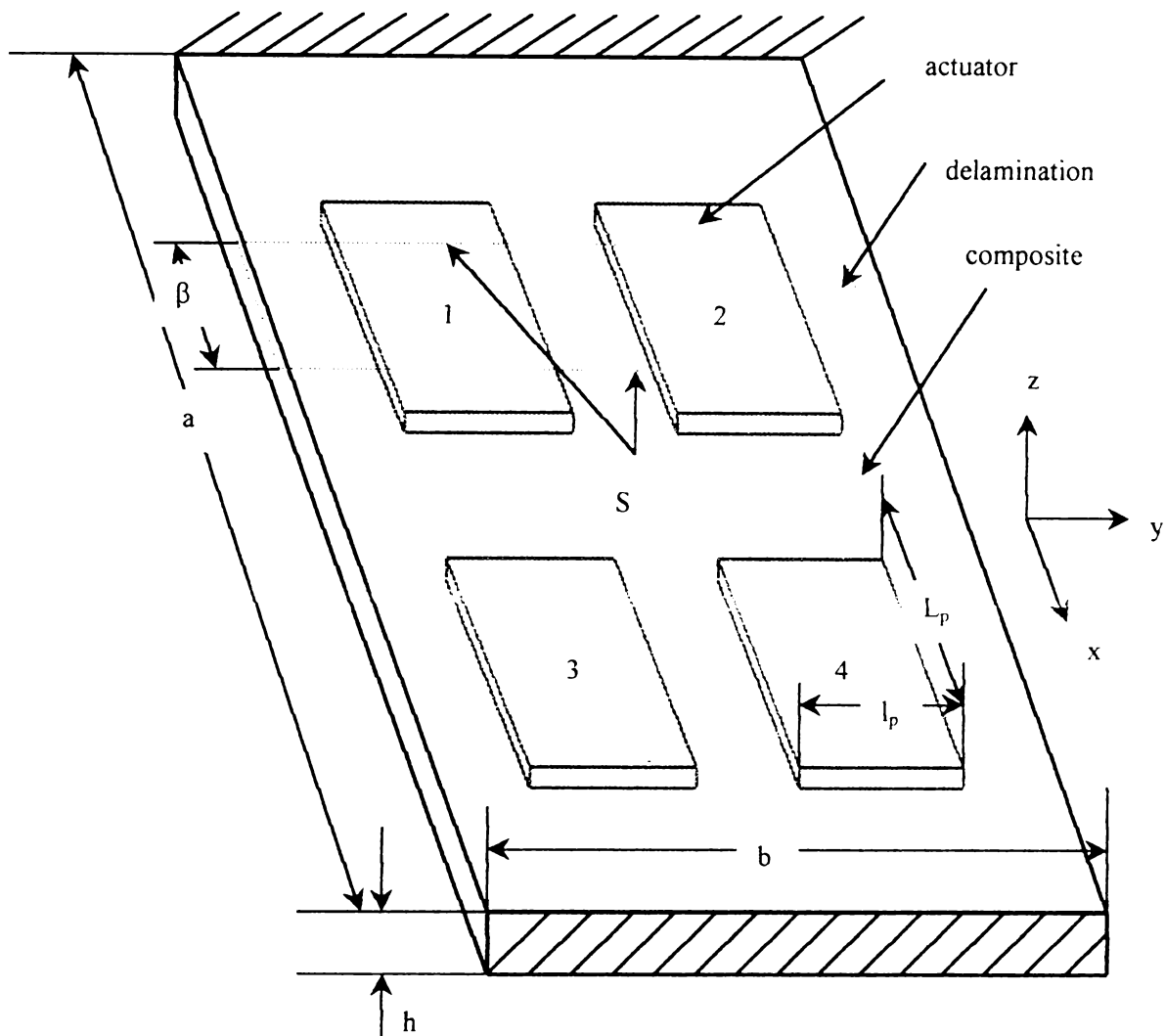
Figure 5.30.   Smart composite plate with delamination.

Actuator pairs 3 and 4 (Fig. 5.30) are modeled using the bimorph configuration. Due to the presence of delamination, only portions of actuator pairs 1 and 2 work in bimorph configuration. The actuator zones placed in the delaminated zone are individually modeled using the unimorph configuration for each sublaminate. The composite substructure in the delaminated zone is modeled as shown in the previous

section. Extra care is necessary when imposing the continuity conditions on S because the jumps in plate thickness in the delaminated zone requires different transformation matrices.

In the assembly process, the procedure accounts for six different types of plate elements. Two of them model the healthy composite zone and the healthy zone with piezo actuators. The other four correspond to the top and bottom sublaminates in the composite zones and in the active composite zones. When the postprocessor is called, the strains are computed from the local displacement of each element. The transformation matrices are used again to obtain the displacements in the local system of coordinates.

Figure 5.31 shows the first 10 mode shapes for the smart composite plate. As can be seen the bending, twist and camber modes interlace each other. The frequency range for these modes extends to 4500 Hz. As expected the mode shapes alone do not provide enough information for damage detection. Also, the frequency deviations between an undamaged reference and the delaminated smart composite plate do not exceed a few percent making it even the existence of damage in the smart composite plate difficult to predict. For composite plates, the change in natural frequencies with delamination length is also much more smaller compared to isotropic plates. For relatively small delaminations, these changes are within data errors. Therefore, that frequency changes and mode shapes cannot provide a reliable basis for delamination location in smart composite structures.
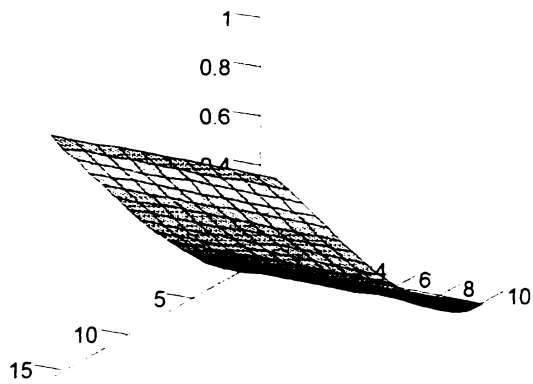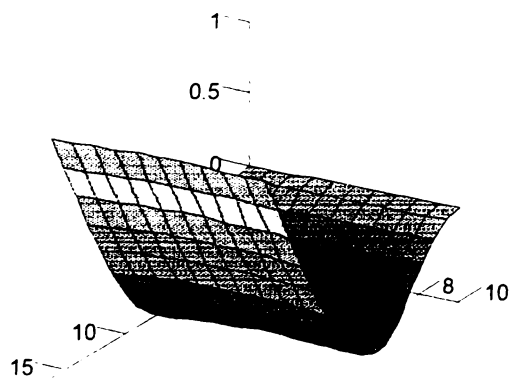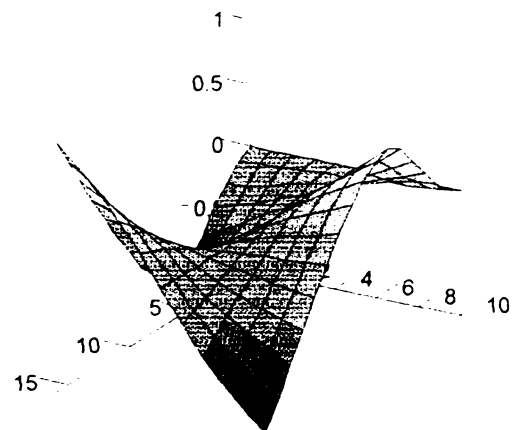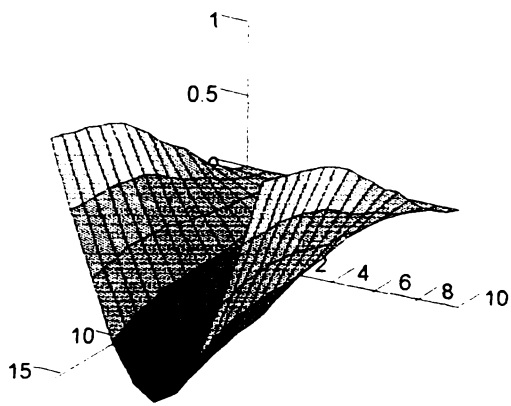
a. First bending.
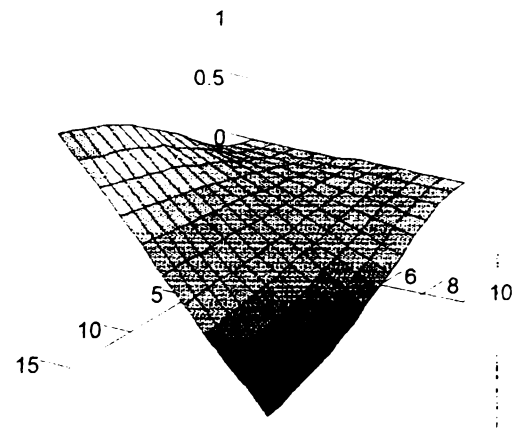
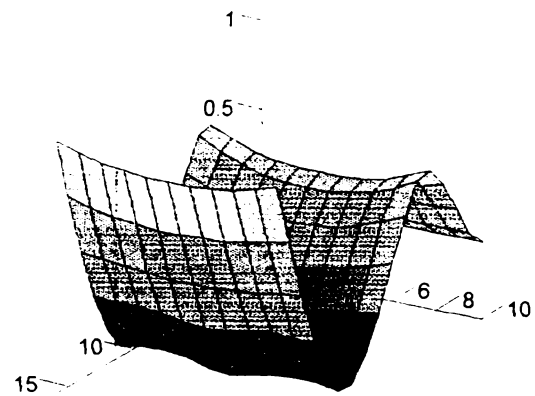b. First twist.

c. Second bending.
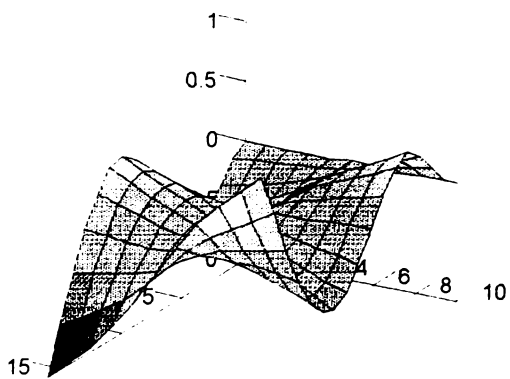
d. Second twist.

Fig. 5.31. First 10 modes of vibration of a smart composite plate.
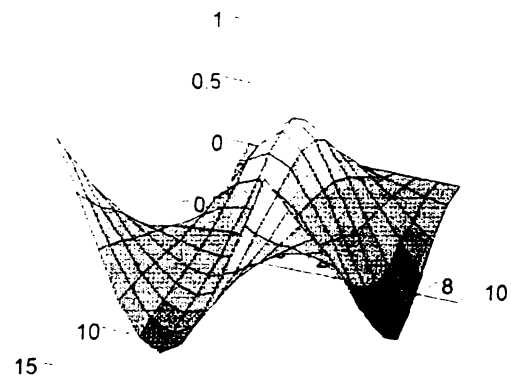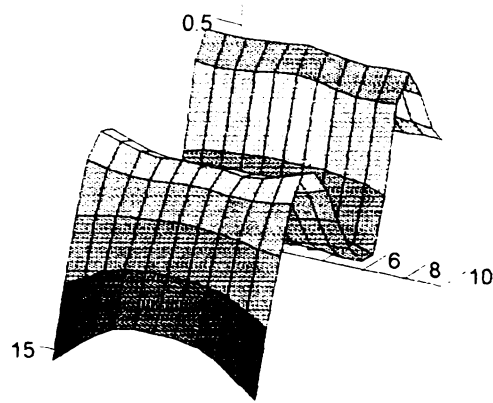
e. First camber.

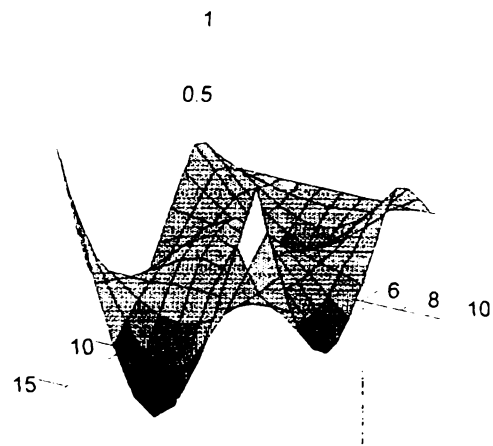f. Third bending.

g. Third twist.

h. Second camber.

Fig. 5.31 cont.

i. Fourth bending.   j. Third camber.

Fig. 5.31. cont.

Next, the strain distribution is computed. Figures 5.32 and 5.33 shows the distributions of ε_1 and ε_2 corresponding to the fundamental mode of vibration. As expected, these distributions exhibit more complex behavior than for composite plates without actuators. The presence of actuators lead to jumps in strains over the active zones. Neighboring elements, with and without piezoelectric actuators, undergo very different deformations due to jumps in material properties and thickness. In addition, the presence of delaminations leads to additional complexities. The global behavior of strain distribution for damaged smart composite plate is complicated and depends on plate geometry, material properties, boundary conditions and delamination location.
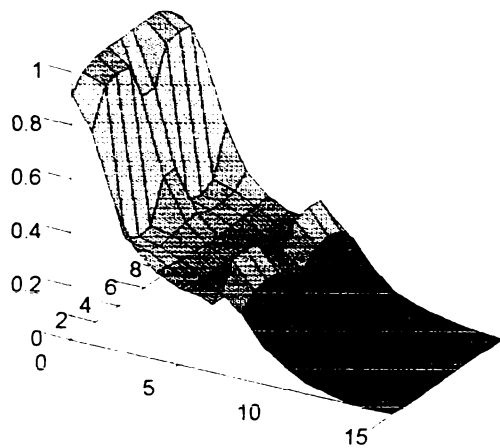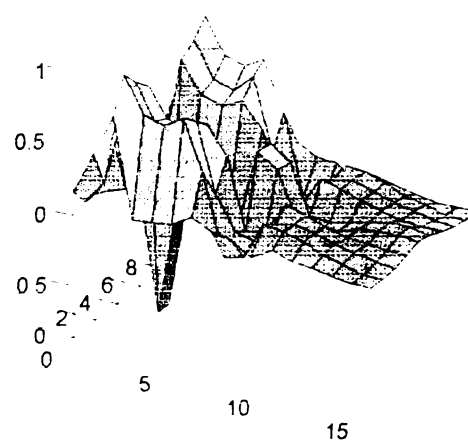
a. Without delamination.
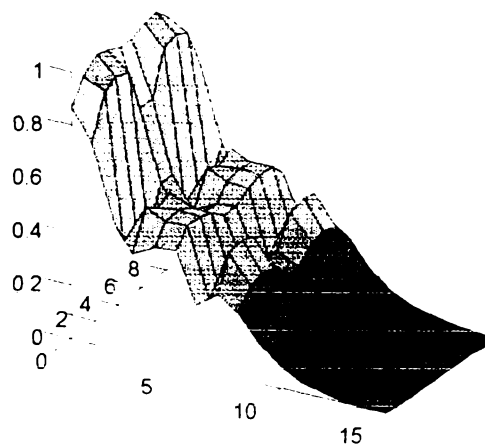
b. With delamination.

Fig. 5.32. Distribution of strain ε_1, first mode of vibration.
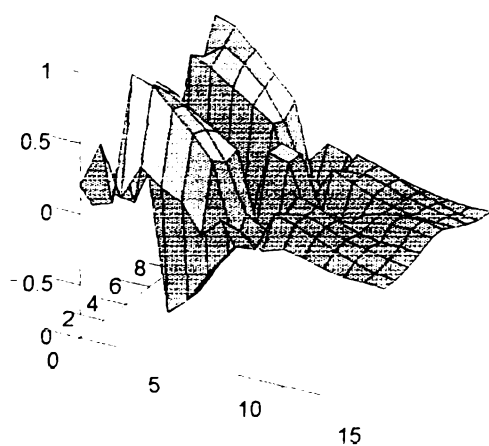
a. Without delamination.

b. With delamination.

Fig. 5.33. Distribution of strain ε_2, first mode of vibration.

However, unlike the mode shapes, the strain is again an appropriate measure of delamination presence. In figures 5.32 b and 5.33 b the strains shows extra jumps in the delaminated area when compared to the healthy cases shown in Fig. 5.32 a and 5.33 a respectively. Similar results were obtained when comparing other inplane strain distributions resulting from the finite element analysis. As mentioned before, the fist mode of vibration is most accurately determined in both numerical and experimental approaches. The corresponding strain is now used to compute the damage indices.
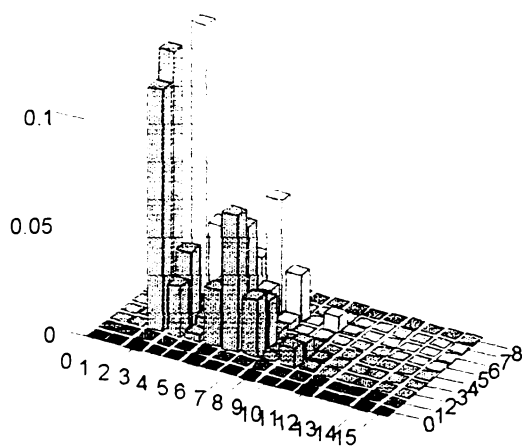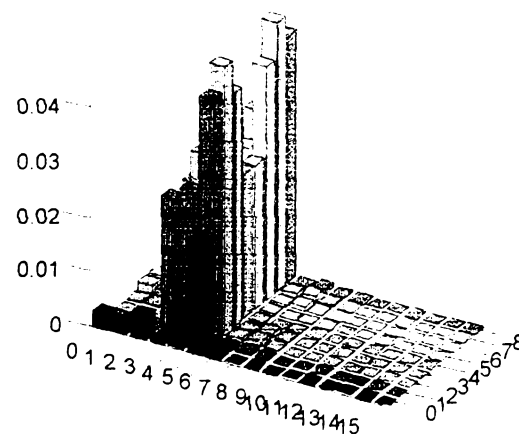

Fig. 5.34. Gapped index.

Fig. 5.35. Index defined in Eq. 4.2.6.

The index based on the gapped smoothing technique is only useful in showing the existence of some damage in the smart composite. As shown in Fig. 5.34, it fails to identify the delamination position and size. Even with an undamaged reference, due to

additional jumps in strain distribution, the accuracy is still unacceptable. By contrast, the new index (Eq. 4.2.6) is an excellent measure of delamination. As shown in Fig. 5.35 the position and size of delamination are both accurately predicted. This position corresponds to elements with numbers 3, 4 and 5 along x axis. Elements with numbers 0, 1, 2 and 6, 7,…,15 in the longitudinal direction belong to either the pure composite (no actuators) or active undamaged zones, while elements with numbers 3, 4 and 5 lie in the top and bottom delaminated sublaminates.

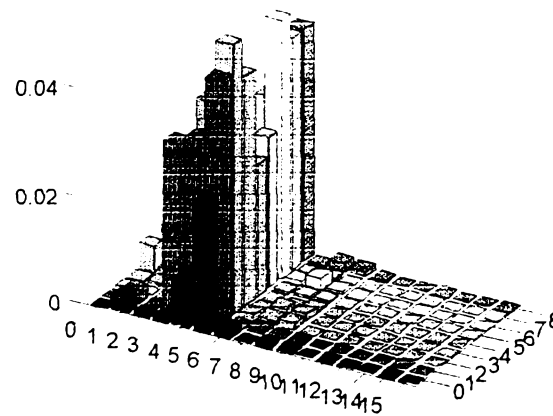

Fig. 5.36. Index defined in Eq. 4.2.6. (10% noise).

Finally, the robustness of the new damage index is verified. Noise is assumed to perturb the strain distribution. The damage index is now recalculated over the plate surface (Fig. 5.36). With 10% random noise affecting the data, the new damage index is still very accurate. The delaminated zone is completely identified. All the elements used

to model the damaged zone have very big values of the damage index when compared to the undamaged neighbors. In conclusion, the new index defined in Eq. 4.2.6 is a useful tool in delamination identification for complex structures such as smart composite plates. The efficiency and robustness of this index makes it a good choice in damage detection.

It must be noted that the sensitivity of the indices discussed above with delamination length has to be made. This study should show the size of smallest detectable delamination.

5.5   Concluding Remarks

A general frame work has been developed for the analysis of composite and smart composite plates in the presence of delaminations. A refined higher order theory has been used. It captures the shear deformation through the thickness of the composite plates while satisfying the stress free boundary conditions on the free surfaces, including the delamination interfaces. The higher order theory is implemented using the finite element method. New continuity conditions for the delaminated zones have been developed. Active piezoelectric forces have been computed using an induced strain approach. The results of the present theory are compared with published experimental results and numerical results obtained using NASTRAN. Comparisons of dynamic results obtained using the present theory with those obtained using the first order shear deformation theory and the classical laminate theory are made for thick plates in the presence of delaminations. The modal strains are used to compare plates with and without delaminations and with and without piezoelectric actuators. Strain based damage indices

delaminations and with and without piezoelectric actuators. Strain based damage indices are developed to identify the position and size of delaminations. A new damage index is developed in this work The following observations are made.

1) The developed theory correlates well with published experimental results and NASTRAN 3D solutions.

2) Implementation of the continuity conditions is consistent with the analytical model and reduces storage requirements and CPU time.

3) The natural frequencies are overestimated by both the classical and the first order theories compared to the present higher order theory in both undelaminated and delaminated plates. The deviations increase with plate thickness, due to increased transverse shear effects.

4) In a delaminated smart composite plate, under static piezoelectric actuation, the inplane strain is only locally influenced by the presence of delamination.

5) The classical mode shapes are not very sensitive to the presence of small delaminations.

6) The inplane modal strains have jumps in the region of delaminations.

7) The inplane modal strains also have jumps due to the presence of actuators. This induces additional complexity in delamination detection.

8) The new proposed damage index is more reliable and robust in locating delaminations in composite and smart composite structures.

References

1. Barbero, E. J. and Reddy, J. N., "Modeling of Delamination in Composite Laminates using a Layer-wise Plate Theory," *International Journal of Solids and Structures*, Vol. 28, No. 3, March 1991, pp. 373-388.

2. Cawley, P. and Adams, R. D., "A Vibration Technique for Nondestructive Testing of Fibre Composite Structures," *Journal of Composite Materials*, Vol. 13, No. 2, 1980, pp. 161-175.

3. Chandrashekhara, K., and Agarwal, A. N., "Active Vibration Control of Laminated Composite Plates Using Piezoelectric Devices: A Finite Element Approach," *Journal of Intelligent Material Systems and Structures*, Vol. 4, October 1993, pp. 496 – 508.

4. Chattopadhyay, A., Dragomir-Daescu, D., and Gu, H., "Dynamic Response of Smart Composites with Delaminations", *Proceedings of the International Workshop on Structural Health Monitoring*, Stanford, CA, September, 1997, pp. 729-740.

5. Chattopadhyay, A., Dragomir-Daescu, D., and Nam, C. H., "An Investigation of Delaminated Smart Composite Plates for Damage Detection," *Proceedings of the International Mechanical Engineering Congress and Exposition Winter Annual Meeting of ASME*, Anaheim, CA, December, 1998, pp. 257-268.

6. Chattopadhyay, A., and Gu, H., "A New Higher-Order Plate Theory in Modeling Delamination Buckling of Composite Laminates," *AIAA Journal*, Vol. 32, No. 8, August 1994, pp. 1709 – 1718.

7. Chattopadhyay, A., and Gu, H., "Elasticity Solutions for Delamination Buckling of Composite Plates", *Proceedings of the 37th AIAA ASME ASCE AHS ASC Structures, Structural Dynamics and Materials Conference and Adaptive Structures Forum*, Salt Lake City, UT, April, 1996, pp. 569-581.

8. Chattopadhyay, A., Radu, A. G., and Dragomir-Daescu, D., "Dynamic Instability of Delaminated Composite Plates Using a Higher Order Theory", submitted to *Computer Modeling and Simulation in Engineering*, 1999.

9. Chattopadhyay, A., and Seeley, C. E., "A Higher Order Theory for Modeling Composite Laminates with Induced Strain Actuators," *Composites*, Vol. 28B, 1997, pp. 143-152.

10. Chattopadhyay, A., and Seeley, C. E., "Experimental Investigation of Composites with Piezoelectric Actuation and Debonding," *Proceedings of the International Mechanical Engineering Congress and Exposition Winter Annual Meeting of ASME: Adaptive structures and Material Systems Symposium*, Dallas, TX, November, 1997, pp. 251-262.

11. Chattopadhyay, A., and Seeley, E. C., "Modeling of Adaptive Composites Including Debonding", *International Journal of Solids and Structures"*, 1998, (in press).

12. Crawley, E. F., and Anderson, E. H., "Detailed Models of Piezoelectric Actuation of Beams", *Proceedings of the 30th AIAA ASME ASCE AHS ASC Structures, Structural Dynamics and Materials Conference*, Mobile, AL, April, 1989, pp. 2000 – 2010.

13. Dragomir-Daescu, D., Chattopadhyay, A., and Gu, H., "Dynamics of Delaminated Composite Plates with Piezoelectric Actuators," *AIAA Journal*, in press.

14. Gu, H., and Chattopadhyay, A., "An Experimental Investigation of Delamination Buckling and Postbuckling of Composite Laminates," *Proceedings of the ASME International Mechanical Engineering Congress and Exposition*, Atlanta, GA, November, 1996, pp. 171-180.

15. Gummadi, L. N. B., and Hanagud, S., "Vibration Characteristics of Beams with Multiple Delaminations," *Proceedings of the 36th AIAA ASME ASCE AHS ASC Structures, Structural Dynamics and Materials Conference and Adaptive Structures Forum*, New Orleans, LA, April, 1995, pp. 140-150.

16. Harris, C. M., *Shock and Vibration Handbook*, McGraw-Hill, New York, 1996.

17. Keilers, C. H., and Chang F. K., "Identifying Delamination in Composite Beams Using Built-in Piezoelectrics: Part I – Experiments and Analysis; Part II An Identification Method," *Journal of Intelligent Material System and structures*, Vol. 5, No. 5, 1995, pp. 649-663.

18. Lew, J. S., "Using Transfer Function Parameter Changes for Damage detection of Structures," *AIAA Journal*, Vol. 33, No. 11, November, 1995, pp. 2189-2193.

19. Lew, J. S., "Transfer Function Parameter Changes Due to Structural Damage," *Proceedings of the 38th AIAA ASME ASCE AHS ASC Structures, Structural Dynamics, and Material Conference and Adaptive Structures Forum*, Reston, VA. 1997, pp. 1667-1674.

20. Mitchell, J. A., and Reddy, J. N., "A Refined Hybrid Plate Theory for Composite Laminates with Piezoelectric Laminae," *International Journal of Solids and Structures*, Vol. 32, No. 16, 1995, pp. 2345 – 2367.

21. Mujumdar, P. M., and Suryanarayan, S., "Flexural Vibrations of Beams with Delaminations,", *Journal of Sound and Vibration*, Vol 125, No. 3, 1998, pp. 441-461.

22. Pandey, A. K., Biswas, M., and Samman, M., "Damage Detection from Changes in Curvature Mode Shapes," *Journal of Sound and Vibration*, Vol. 145, No. 2, 1991, pp. 321-332.

23. Pavier, M. J., and Clarke, M. P., "A specialized Composite Plate Element for Problems of Delamination Buckling and Growth," *Composite structures*, Vol. 35, 1996, pp. 45-53.

24. Ratcliffe, C. P., and Bagaria, W. J., "Vibration Technique for Locating Delamination in a Composite Beam," *AIAA Journal*, Vol. 36, No. 6, June, 1998, pp. 1074-1077.

25. Reddy, J. N., *An Introduction to the Finite Element Method*, McGraw-Hill, 1993.

26. Reddy, J. N., "A Simple Higher-Order Theory for Laminated Composite Plates," *Journal of Applied Mechanics*, Vol. 51, December, 1984, pp. 745-752.

27. Robins, D. H., and Reddy, J. N., "Analysis of Piezoelectrically Actuated Beams Using a Layerwise Displacement Theory," *Computers and Structures*, Vol. 41, No. 2, 1993, pp. 265 – 279.

28. Robins, D. H., and Reddy, J. N., "Modeling of Thick Composites Using a Layerwise Laminate Theory," *International Journal for Numerical Methods in Engineering*, Vol. 36, 1993, pp. 655-677.

29. Seeley, C. E. *Analysis and optimization of Smart Composite structures Including Debonding*, Ph.D. Dissertation, Arizona State University, February, 1997.

30. Seeley, C. E., and Chattopadhyay, A. "Modeling Delaminations in Smart Composite Laminates," *Proceedings of the 37th AIAA ASME ASCE AHS ASC Structures, Structural Dynamics and Materials Conference and Adaptive Structures Forum*, Salt Lake City, UT, April, 1996, pp. 655-661.

31. Seeley, C. E ,and Chattopadhyay, A., "Delamination Modeling of Smart Composite Laminates: A Finite Element Approach", *Proceedings of the 38th AIAA ASME ASCE AHS ASC Structures, Structural Dynamics and Material Conference and Adaptive Structures Forum*, Kissimmee, Florida, April 7-11, 1997, pp. 1025-1037.

32. Shen, M. H., and Grady, J.E., "Free Vibration of Delaminated Beams", *Proceedings of 31st AIAA ASME ASCE AHS ASC Structures, Structural Dynamics and Material Conference*, Baltimore, MD, April, 1991, pp. 1361-1369.

33. Tracy, J. J., and Pardoen, G. C., "Effect of Delamination on The Natural Frequencies of Composite Laminates," *Journal of Composite Materials*, Vol. 23, December, 1989, pp. 1200-1215.

34. Vinson, J. R., *The Behavior of Structures Composed of Composite Materials*, Kluwer Academic Publishers, Dordrecht, 1987.

35. Williams, E. J., Messina, A., and Payne, B. S., "A Frequency-Change Correlation Approach to Damage Detection," *Proceeding of the 15th International Modal Analysis Conference*, Vol. 1, Society of Experimental Mechanics, Bethel, CT, 1997, pp. 652-657.

36. Yang, H. T. Y., and He, C. C., "Three-Dimensional Finite Element Analysis of Free Edge Stresses and Delamination of Composite Laminates," *Journal of Composite Materials*, Vol. 28, No.15, 1994, pp. 1394-1412.